EGG-TMI-7489
December 1986

INFORMAL REPORT

PATENT CLEARED

Idaho National Engineering Laboratory

Managed by the U.S. Department of Energy

TMI-2 ACCIDENT SCENARIO UPDATE

E. L. Tolman
J. P. Adams
J. L. Anderson
P. Kuan
R. K. McCardell
J. M. Broughton

Susan Chavez 10-22-92
Lewis Masson 2-19-92

EG&G Idaho

Work performed under DOE Contract No DE-AC07 76ID01570

EGG-TMI-7489

TMI-2 ACCIDENT SCENARIO UPDATE

E. L. Tolman
J. P. Adams
J. L. Anderson
P. Kuan
R. K. McCardell
J. M. Broughton

Published December 1986

EG&G Idaho, Inc.
Idaho Falls, Idaho 83415

Prepared for the
U.S. Department of Energy
Idaho Operations Office
Under DOE Contract No. DE AC07-76ID01570

ABSTRACT

This report summarizes the current best-estimate TMI-2 accident scenario describing the initial core heatup and degradation, continued degraded core heatup, and eventual core failure and migration of molten core materials into the reactor vessel lower plenum. Also included are discussions of fission product release, chemistry, and final postaccident distribution and inventory. The evidence indicates that the core damage and relocation occurred within 4 h of the accident initiation, after which the degraded reactor core was stable.

Development of the TMI-2 accident scenario is based on research conducted under the TMI-2 Accident Evaluation Program sponsored by the U.S. Department of Energy.

SUMMARY

Recent TMI-2 characterization and analysis have provided the basis for improved understanding of the accident scenario, including the core damage progression during the accident. Since questions remain to be answered concerning key points of the accident scenario, the scenario presented should be viewed as an interim interpretation of the accident. As the major unresolved questions are clarified, a final accident scenario will be documented.

The accident was initiated by cessation of secondary feedwater flow. The steam generator boiled dry, and the resultant reduction of primary-to-secondary heat exchange caused the primary coolant to heat up, surge into the pressurizer, and increase the primary system pressure. The pilot-operated relief valve (PORV) opened to relieve pressure but failed to close when the pressure decreased. The first 100 min of the accident can be characterized as a small break loss-of-coolant accident (LOCA) with resultant loss of primary coolant and decreasing pressure. It differed from the scenario expected during such a LOCA in that the pressurizer liquid level remained high. This was interpreted by the reactor operator as indicating that the reactor coolant system (RCS) was full of water when, in fact, the RCS was continually voiding. Up to 100 min, the core was covered with sufficient water to be cooled.

The reactor coolant pumps were turned off at 100 min, and core heatup was initiated as the water level stratified and decreased below the core top. By 150 min, a zircaloy-steam exothermic reaction was initiated, dramatically increasing the core heatup rate. As a result, zircaloy melting temperatures were exceeded, resulting in relocation of the molten zircaloy and some liquefied fuel to the lower core regions, solidifying near the coolant interface. This continued until 174 min, when a large region of consolidated, degraded core material existed in the lower, central regions of the core. Coolant flow through this consolidated material was probably negligible. The intact fuel rod stubs in the lower core region indicate that the lower 0.5 m of the core remained cool.

A reactor coolant pump was turned on briefly at 174 min, and coolant was pumped into the reactor vessel. The resultant thermal-mechanical forces generated from the rapid steam formation are believed to have shattered the oxidized fuel rod remnants in the upper regions of the core, forming a rubble bed on top of the consolidated core materials. The consolidated core materials continued to heatup during the next 50 min (174 to 224 min), even though coolant delivery to the reactor vessel from the pump transient and emergency core cooling injection is estimated to have covered the core by approximately 210 min. By 224 min, much of the consolidated region had reached temperatures sufficient to melt the U-Zr-O ternary mixture.

On-line TMI-2 data recorded during the accident indicate that the crust surrounding the consolidated core failed and some of the molten core material relocated to the lower plenum between 224 and 226 min. Based on the end-state core and core support assembly (CSA) configuration and supporting analysis of the degraded core heatup, it is believed that the crust failure occurred near the top of the molten core region in the southeast quadrant of the reactor vessel. Limited damage to the CSA occurred as the core material flowed to the lower plenum. Estimates of the maximum pressure vessel wall temperatures indicate that the melting point of stainless steel was not exceeded, even at the inside surface of the pressure vessel liner. The instrument assemblies, however, may have melted in the lower plenum above the vessel penetration weld. If this occurred, freezing of molten material is predicted to have plugged any holes in the instrument assembly tubes.

Important questions relative to core failure and relocation of the molten core material remain to be answered. Perhaps the most important of these is, what was the mechanism or mechanisms leading to failure of the crust surrounding the molten consolidated core? There appear to be several plausible failure mechanisms; however, an unequivocable answer to this question will require additional inspection of the core crust in the east quadrant and sample acquisition and examination of the crust material to determine its composition, material interactions, and physical and chemical

properties. Additional inspections of the core region in the east quadrant of the vessel are necessary to determine if the crust failure was localized or global in nature.

Another important question yet to be answered concerns the extent of damage to the reactor vessel. Additional inspection and sample examination data are necessary to adequately characterize the lower plenum debris and possible damage to the pressure vessel lower head and instrument tube penetrations.

Supporting analysis is necessary to interpret the data and improve our understanding of the formation of the degraded core and eventual failure of the supporting crust. Analysis is also needed to better estimate the interaction of the molten core material with the vessel coolant, formation of core debris, and long-term cooling of the degraded core materials, both within the original core boundaries and in the lower plenum.

The TMI-2 accident evaluation research is providing and will continue to provide crucial data to improve our understanding of severe accidents and for benchmarking severe accident analysis techniques and tools. Important research findings to date include:

- When the high-pressure injection was initiated as 200 min, core cooling resulted. However, the molten, consolidated core material continued to heat up, despite the presence of water surrounding the crust.

- There is no supporting evidence that a steam explosion occurred when the crust surrounding the consolidated molten core material failed, allowing approximately 10% of the total core mass to fall into the water-filled lower plenum.

- The presence of water in the lower plenum terminated the accident progression and prevented failure of the reactor vessel lower head.

- Fission product release from the fuel and the RCS is very sensitive to the volatility of the individual elements or chemical species. Release of the high-volatile fission products (iodine and cesium) was less than expected, especially of cesium, up to 20% of which was retained in the previously molten core material that relocated to the lower plenum. Retention of the medium- and low-volatile fission products in the reactor pressure vessel (RPV) was nearly complete, although significant amounts of antimony and ruthenium were released from the fuel and are believed to be bound to metallic structures in the reactor vessel.

ACKNOWLEDGMENTS

This report has been a team effort by the authors and represents a major milestone of the TMI-2 Accident Evaluation Program. Special recognition is extended to Doug Akers and Charles Olsen for their work in directing and performing the laboratory examination of the degraded core materials. Sid Langer and M. (Bud) Russell have compiled much of the fission product distribution information. Chris Allison is recognized for his work in directing the TMI-2 SCDAP analysis over the past two years; he has been a major contributor in interpreting the TMI-2 data and developing the core damage progression scenario.

Recent analysis by Robert Henry, Hans Fauske, Michael Epstein, Michael Hutcherson, and Marc Kenton, of Fauske and Associates, Inc., has improved our understanding of the reactor system thermal-hydraulic response and potential core failure mechanisms.

August (Gus) Cronenberg, of Engineering Science and Analysis, has provided the analytical basis for estimating the potential damage to the reactor vessel lower head and instrument penetrations.

A special thanks is extended to Nadine Wade, for her excellent support in editing and compiling the report.

CONTENTS

FIGURES

TABLES

ACRONYMS

AEP	Accident Evaluation Program
BWR	boiling water reactor
CSA	core support assembly
DOE	U.S. Department of Energy
EDS	Energy-dispersive X-ray spectroscopy
LOCA	loss-of-coolant accident
MUP	make-up purification
NRC	U.S. Nuclear Regulatory Commission
PBF	Power Burst Facility
PORV	pilot-operated relief valve
PWR	pressurized water reactor
RCS	reactor cooling system
RCP	reactor coolant pump
RPV	reactor pressure vessel
RTD	resistance temperature detector
SCDAP	Severe Core Damage Accident Package
SDS	submerged demineralizer system
SEM	scanning electron microscopy
SRM	source range monitor
SPND	self-powered neutron detector
TMI-2	Three Mile Island Unit No. 2

TMI-2 ACCIDENT SCENARIO UPDATE

1. INTRODUCTION

The March 1979 accident at the Three Mile Island Unit 2 (TMI-2) pressurized water reactor (PWR) was the most severe core damage accident that has ever occurred in a commercial PWR. An understanding of the accident scenario, including the dominant physical processes, can greatly aid PWR designers and operators to ensure that such an accident does not occur again. This report represents the current best-estimate accident scenario. It should be recognized that additional information will yet become available which may change and/or enhance our understanding of the accident. Thus, this is an interim report; finalization of the accident scenario will take place after all data on the plant have been gathered and analyzed.

Damage to the TMI-2 core was much more extensive than originally estimated. Inspection of the lower plenum regions shows that from 10 to 20 metric tons of previously molten core material currently reside on the bottom reactor vessel head. Inspection of the lower core region, completed in August 1986, implies that approximately 30% of the original core reached melting temperatures during the accident. Thus, the TMI-2 accident represents a unique research resource to improve our understanding of severe accidents and associated fission product behavior.

Since the accident, work has been underway to improve our understanding of the physical mechanisms that led to and controlled the core damage progression, fission product release from the fuel, and fission product transport and retention within the reactor cooling system (RCS) and other auxiliary piping systems. Initial core damage evaluation work[1] was performed without confirmatory evidence of the extent of core damage and limited understanding of the physical mechanisms controlling core degradation. Therefore, it is not surprising that the initial estimates of core damage were generally inaccurate. Over the past several years, however, an improved understanding of the mechanisms controlling core

degradation has been established through separate-effects and integral experiments, performed primarily under the auspices of the U.S. Nuclear Regulatory Commission (NRC). In addition, the end-state condition of the TMI-2 core is being measured as the reactor vessel is defueled.

The TMI-2 Accident Evaluation Program (AEP)[2] is being conducted by the Department of Energy (DOE) to:

- Understand the physical and chemical state of the TMI-2 core and related structures and the external influences which affected the accident,

- Understand what happened during the accident and to provide a qualified data base and standard problem of the TMI-2 accident to benchmark severe-accident analysis codes and methodologies,

- Understand the relationship between the phenomena and processes controlling the accident and the important severe accident/source term technical issues, and

- Assure that the results of the program are effectively transferred to the nuclear community.

Development of the TMI-2 accident scenario is the focal point of the AEP and involves integration of information from (a) TMI-2 reactor system measurements recorded during the accident; (b) the end-state characterization of the TMI-2 core, core support structures, and reactor vessel; and (c) independent experiments simulating fuel and fission product behavior during severe accidents. Analysis to interpret and integrate these data sources is crucial, since insufficient data exist from any single source to uniquely define the accident scenario. This "integration" process is shown schematically in Figure 1.

Previous scenario work[3] was based on the available data through mid-1985. Recent work in the following areas provides the basis for an improved understanding of the accident:

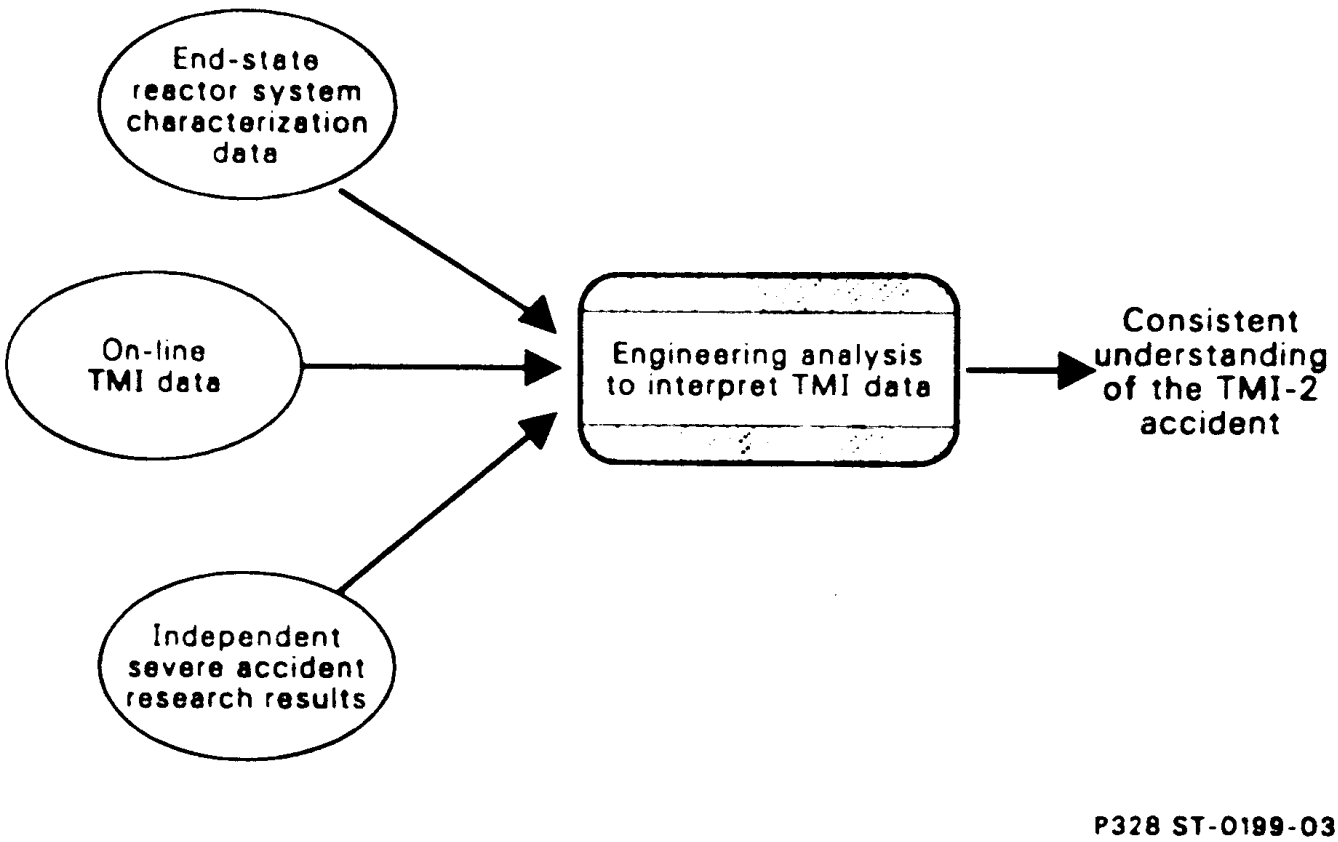

Figure 1. TMI-2 accident development methodology.

- Determination of damage to the lower core, core support assembly (CSA), and lower plenum region,

- Examination results from lower plenum debris samples,

- Defueling of the upper debris bed and intact fuel assemblies from the core periphery,

- Analysis of potential damage to the lower vessel head and the instrument penetration nozzles,

- Analysis to improve understanding of the degraded core heatup and the mechanisms which controlled core relocation,

- Analysis of the reactor system thermal-hydraulic response that includes RCS coolant inventory and core heat transfer rates,

- Improved interpretation of the source range monitor and in-core self-powered neutron detector responses.

The scenario for the TMI-2 accident is revised in this report based on the research results acquired since the original scenario was proposed. Important questions still remain to be answered, and these are identified and discussed.

The remainder of the report is organized into four major sections: (a) a summary of the known end-state conditions of the core and reactor vessel; (b) a development of the core damage progression during the first four hours of the accident; (c) a summary of the end-state distribution and inventory of important fission products, the limited information relative to transient release of fission products during the initial core heatup period, and important findings relative to fission product chemistry; and (d) important conclusions based on the TMI-2 research completed to date. Supporting detail is provided in Appendices A through G.

2. KNOWN CORE AND REACTOR VESSEL CONDITIONS

The known end-state conditions of the core and reactor vessel components are presented prior to developing the accident scenario, since these conditions must be consistent with the postulated scenario. A discussion of known core and reactor vessel conditions follows.

2.1 Damage to the Reactor Vessel Upper Plenum and Upper Fuel Assembly Grid Plate

The reactor vessel upper plenum assembly was removed as a unit and was found to be intact with little damage. Upper plenum structural temperatures and fission product deposition have been inferred from laboratory examination of two of the stainless steel control rod leadscrews which were removed from the H8 and B8 fuel assembly positions. Figure 2 is a schematic of the TMI-2 core, showing the location of the removed leadscrews. Major findings from the control rod leadscrew examinations[4,5] include:

- Initial visual inspection showed that the leadscrew section was undamaged and covered by a uniform dark coating, overlayed by orange deposits. The overlayed deposits appeared thicker on the upper thread surfaces. Gamma spectroscopy results indicated that 96% of the count rate was from ^{134}Cs and ^{137}Cs, with the remainder of the activity from ^{125}Sb and trace ^{60}Co. Radiological activity was greater in the higher (cooler) axial regions of the leadscrews than the lower (hotter) regions nearer to the core. The stainless steel microsctuctures indicate that the B8 position experienced slower cooling rates than the H8 position

- The axial temperature gradient along the H8 leadscrew ranged from 1255 K immediately above the core to 666 K at the elevation of the hot leg nozzle; and the axial temperature gradient along the B8 leadscrew ranged from 1033 K immediately above the core to

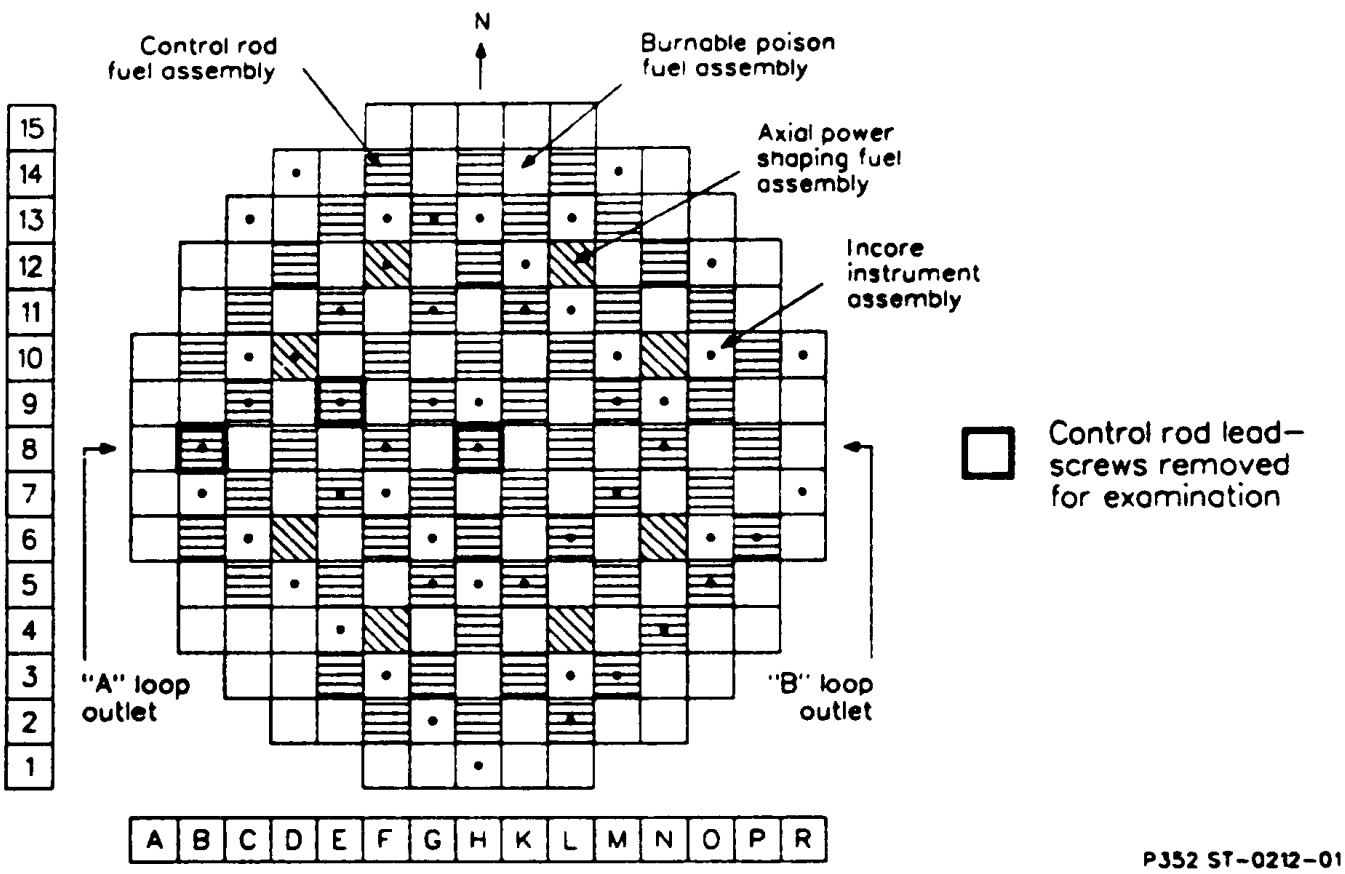

Figure 2. Location of TMI-2 control rod leadscrews removed for laboratory examination.

723 K at the elevation of the hot leg nozzle. The uncertainty in these temperature estimates, which are based on metallurgical measurement, is ± 50 K.

- Metallographic and scanning electron microscopy (SEM) examinations of longitudinal leadscrew cross sections revealed three distinct layers of surface deposits. The innermost layer next to the base metal was approximately 3 μm thick and was most likely a normally produced, in-service oxide layer. The next layer outward was porous in appearance and tightly adherent. Observed thickness of the adherent layer ranged from 10 to 90 μm, but was generally 40 to 50 μm. Silver-rich metal globules ranging from approximately 15 to 300 μm in size were bonded to the outside surface of the adherent layer of deposits. The adherent layer was covered with loosely adherent deposits which could be removed by vigorous brushing. Thickness of the loosely adherent layer ranged from 25 to 75 μm. Energy-dispersive X-ray spectroscopy (EDS) analysis indicated that the adherent layer was enriched in chromium and depleted in iron compared with the base metal.

  Chemistry/radiochemistry results indicated that no cesium penetration of the leadscrew base metal had occurred. Essentially no cesium activity remained after removal of the adherent deposit layer by an HNO_3/HF soak. Radiochemistry results showed that most of the ^{134}Cs and ^{137}Cs isotopes were contained in the adherent deposits, while most of the beta-emitting ^{90}Sr was present in the loosely adherent deposits. Results from chemical analysis showed higher levels of elements from fuel and control components present in the loosely adherent layer than in the adherent layer.

  Microchemical and X-ray diffraction examinations carried out at Argonne National Laboratory provided further information about the surface deposits. Auger analysis showed that the layers

contained uniformly distributed oxygen. Electron microprobe results indicated that the silver-rich globules contained indium (without cadmium) and were diffusion-bonded to the adherent layer. The adherent layer was found to have chromium and iron in the form of a spinel oxide and uranium and zirconium present only as oxides.

The damage to the upper fuel assembly grid was determined from video inspections performed after removal of the assembly from the reactor vessel. Damage to the grid structure was clearly observable on the lower surface. The axial damage (upward into the plenum region) has not been fully determined but apparently did not extend up to the top surface of this structure. Two major damage zones exist, as shown in Figure 3, and indicate the presence of multidimensional steam/gas flow within the reactor core during the period of high core temperatures. Within each damage zone, localized variations in damage are evident. For example, within the limited area above only one fuel assembly, localized ablation of the stainless steel structure is observed; however, grid structures adjacent to the ablated zone appear to be undamaged. Also, in some regions, the molten grid material appears to have a foamy-like, high-porosity texture which occurs when stainless steel oxidizes near the melting temperature. Previously molten material within a few inches of the foamy-like structure appears essentially unoxidized, suggesting that some of the hot gases exiting the core were oxygen deficient, probably high in hydrogen. Thus, the upper fuel assembly grid damage suggests that highly non-uniform flow patterns were present at the time of grid damage; and localized gas conditions (composition, flow rate, and temperature) varied significantly within the flow stream.

2.2 End-State Core Configuration

The reactor defueling work completed over the past three years and the recent inspection of the lower core regions during the core-boring operation have provided sufficient data to estimate the end-state core

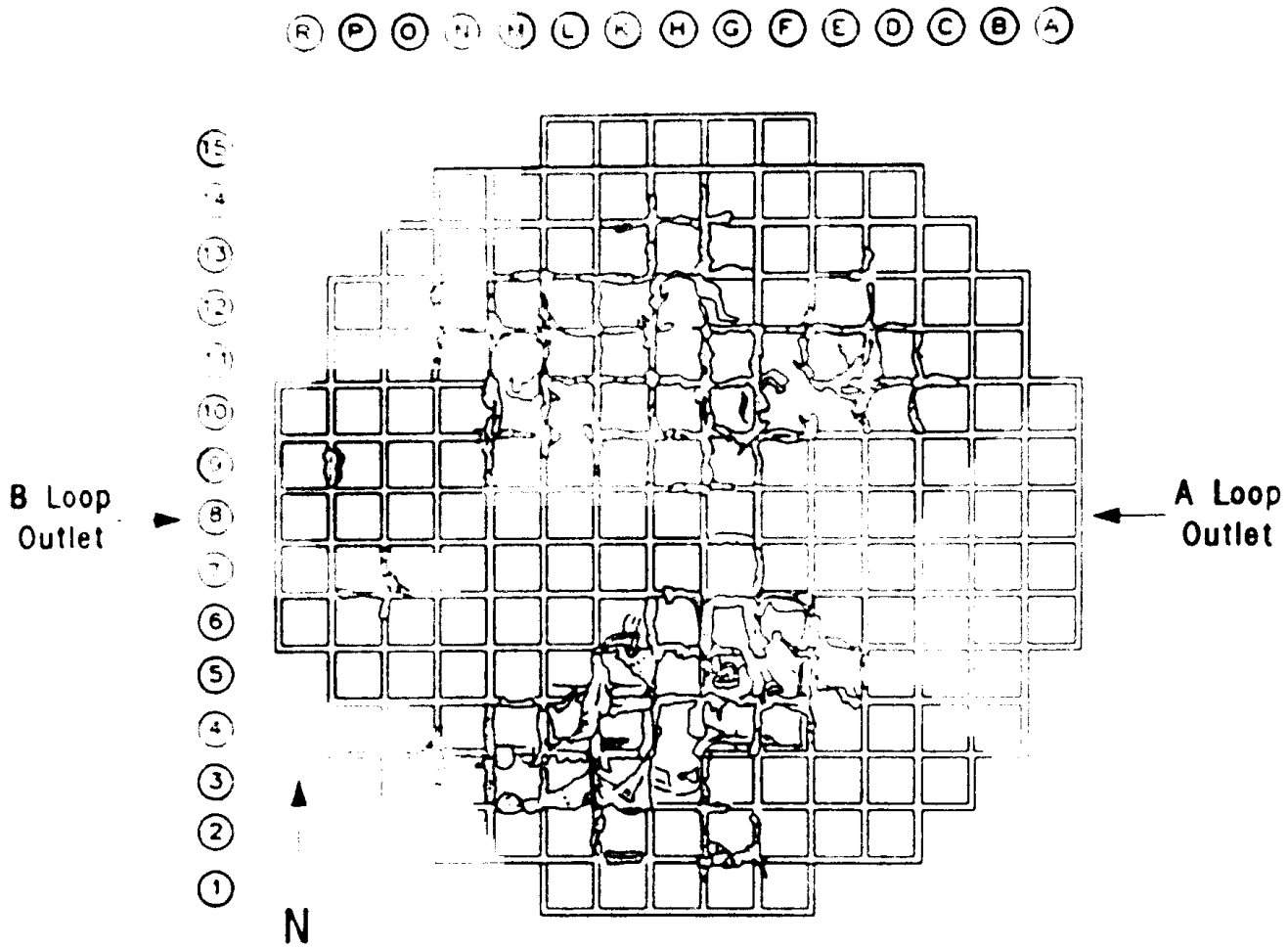

Figure 3. Damage map of the TMI-2 fuel assembly upper grid plate.

configuration with reasonable certainty. These data show four distinct regions within the original core volume, as shown in Figure 4 and described below:

1. A cavity existed at the top of the core with a volume of approximately 9.3 m^3.[6] The cavity volume represents approximately 26% of the original core volume and extends nearly across the full diameter of the upper core region. The average depth of the cavity is approximately 1.5 m; in places the maximum depth approaches 2 m. Standing fuel rod assemblies remained only on the core periphery, with no more than two of the 177 original fuel assemblies appearing to be totally intact. Only 42 fuel assemblies had full-length fuel rods intact.

2. A debris bed, ranging from 0.6 to 1.0 m in depth, rested on a solid crust that was located at about the core mid-plane. The debris bed has been sampled in eleven regions. Most of the particles examined contained regions of previously molten U-Zr-O, indicating peak temperatures of greater than 2200 K. Of these, many are previously molten $(U,Zr)O_2$, indicating peak temperatures greater than 2800 K. There are a few examples of previously molten material that are almost pure UO_2, indicating temperatures up to 3100 K. However, based on the relatively unstructured appearance observed for much of the fuel, even though there are attached regions of previously molten ceramics, much of the fuel probably remained at fairly low temperatures (<2000 K) or was exposed to high temperatures for only a short time. The detailed examination results have been reported,[7] and a summary of major findings is given in Appendix A.

   The contour of the upper surface of the debris bed was determined using acoustic topography[6] and is shown in Figure 5. The debris material was extensively probed to determine its depth,[8] and the probe data were used to make the contour map of the lower

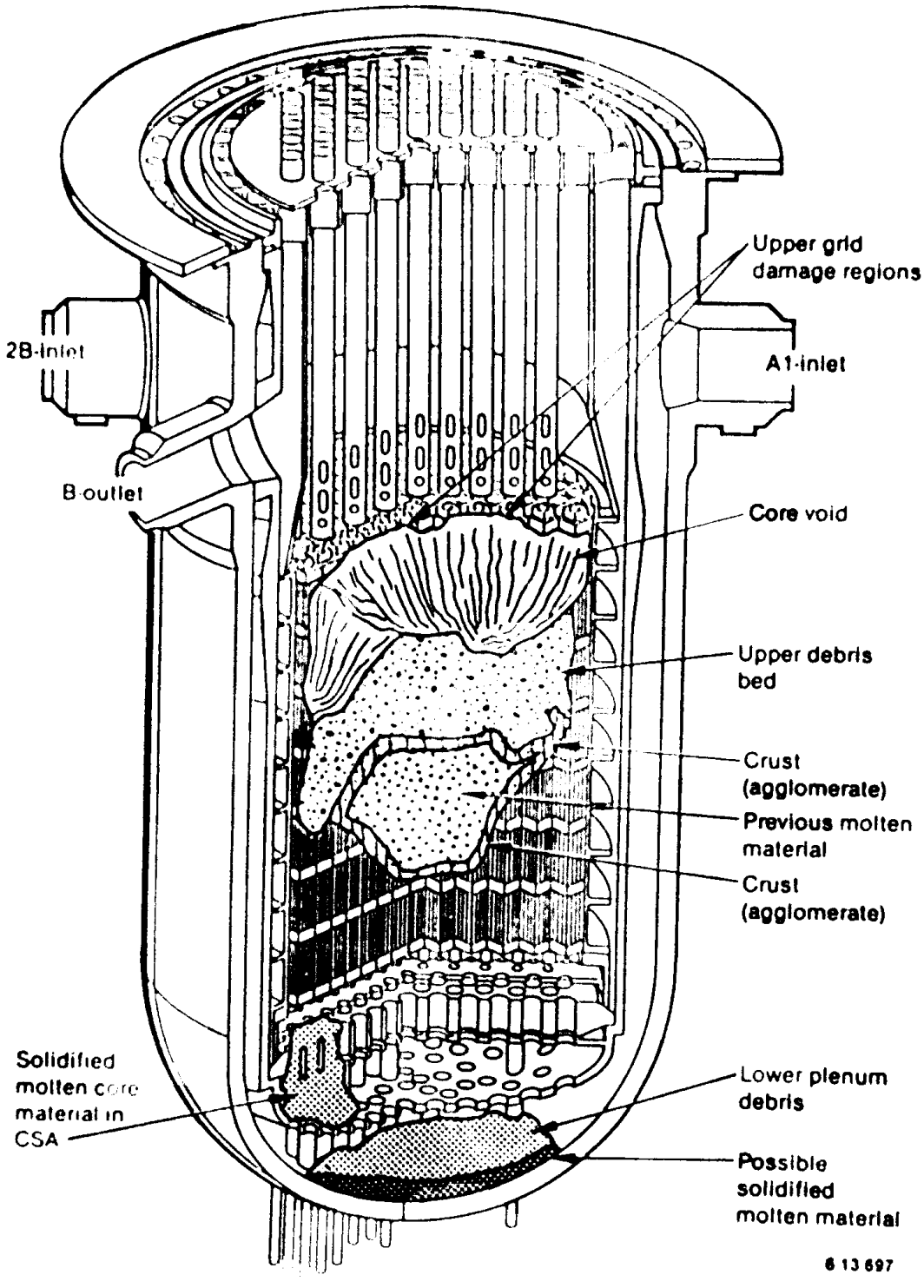

Figure 4. TMI-2 known end-state core configuration.

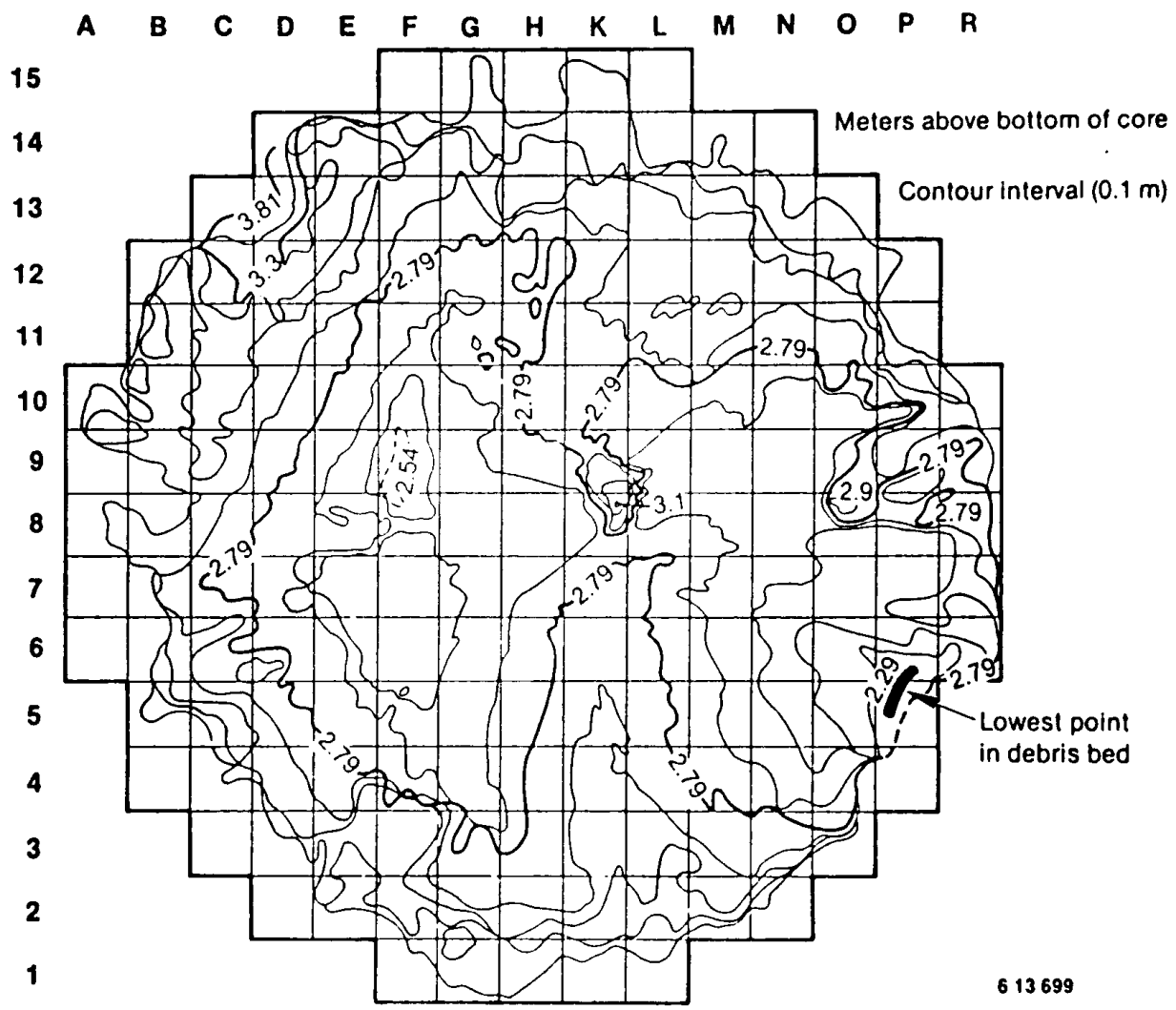

Figure 5. TMI-2 upper core debris top surface contour.

surface of the upper debris bed, which is also the top surface of the previously molten core region. This contour surface is shown in Figure 6.

3. A region containing previously molten core material in the lower half of the core was found during the core boring operation.[9] An overview of the core boring operation and a summary of core boring observations are presented in Appendix B. Two distinct regions containing previously molten core material were observed:

   a. A region of relocated previously molten material surrounding damaged but intact fuel pellets and/or partial fuel rods. Previously molten material in which some fuel rod structure is discernible (cladding and/or fuel pellets) is referred to as "agglomerate".

   b. A region that appears to have been uniformly molten with no remaining fuel rod structures evident is located in the center of the previously molten region. This material is referred to as "ceramic."

4. Standing fuel rod stubs extend upward from the bottom of the core to the interface with the solid, previously molten region. The core bore inspection data were used to contour map (axial elevations) the interface between the previously molten core material and the lower intact rod stubs. This interface contour map is shown in Figure 7.

The contour maps defining the upper debris bed region, molten core region (agglomerate and ceramic), and the lower standing fuel rod stubs allow core cross sections to be drawn showing the relative configurations of these regions. An example of these degraded core regions as they extend through the k row of fuel assemblies is shown in Figure 8. The crust-like material forming the bottom of the molten core region is funnel-shaped, with the lowest point (approximately 0.5 m from the bottom of the fuel)

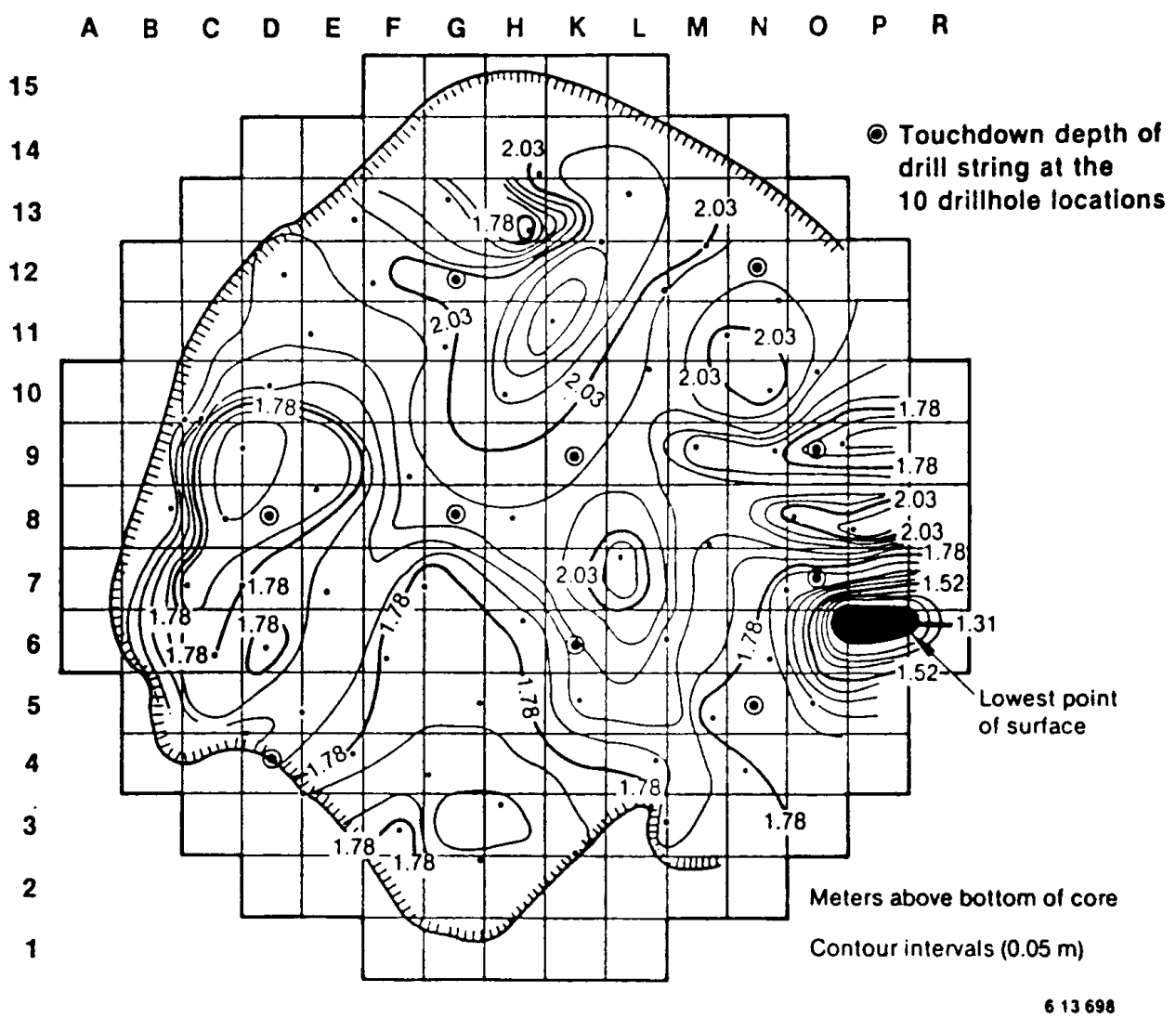

Figure 6. Contour map of the upper surface of the previously molten core region in TMI-2.

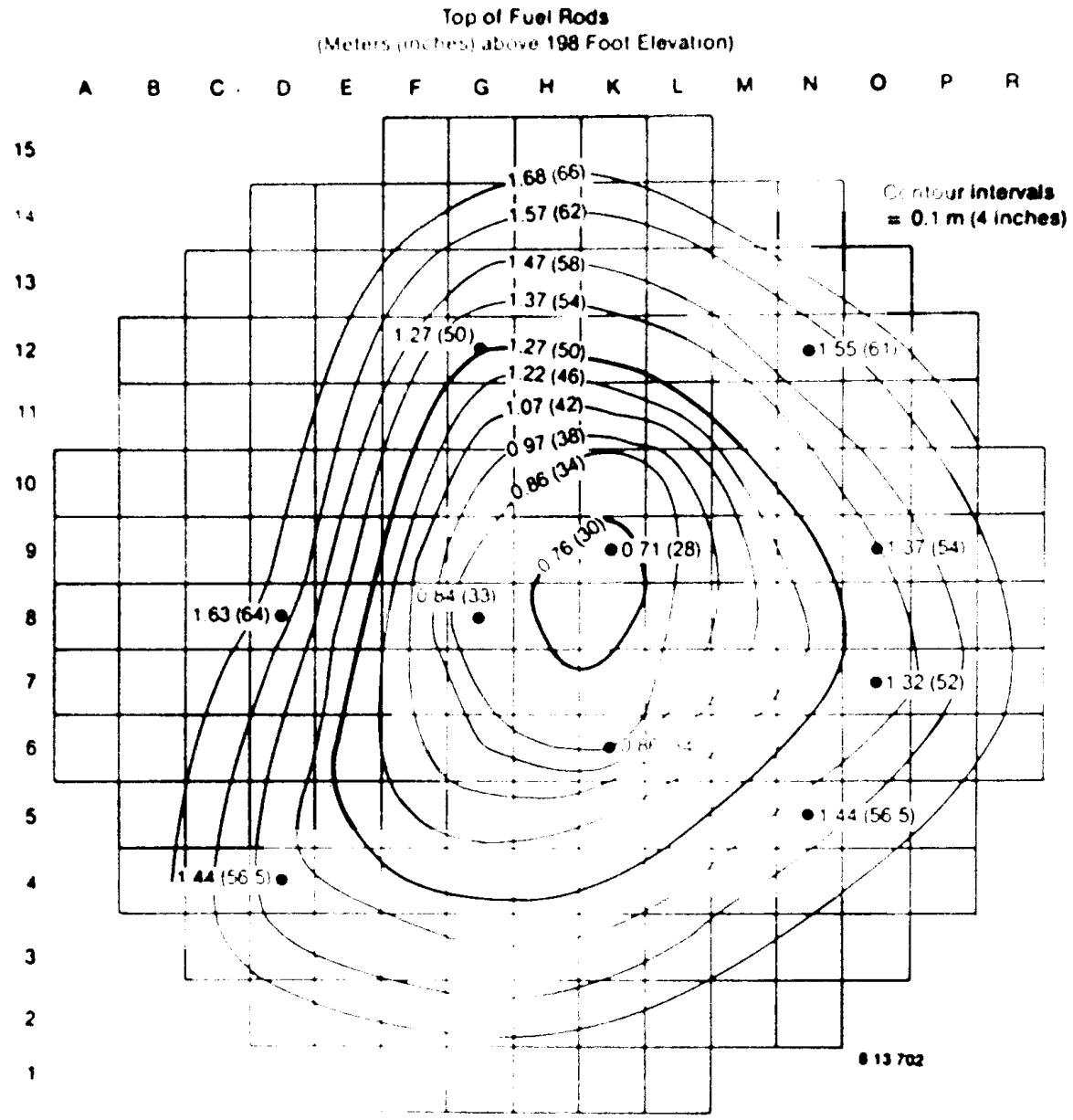

Figure 7. Contour map of the interface between the lower intact fuel rods and previously molten core materials (lower crust) in TMI 2.

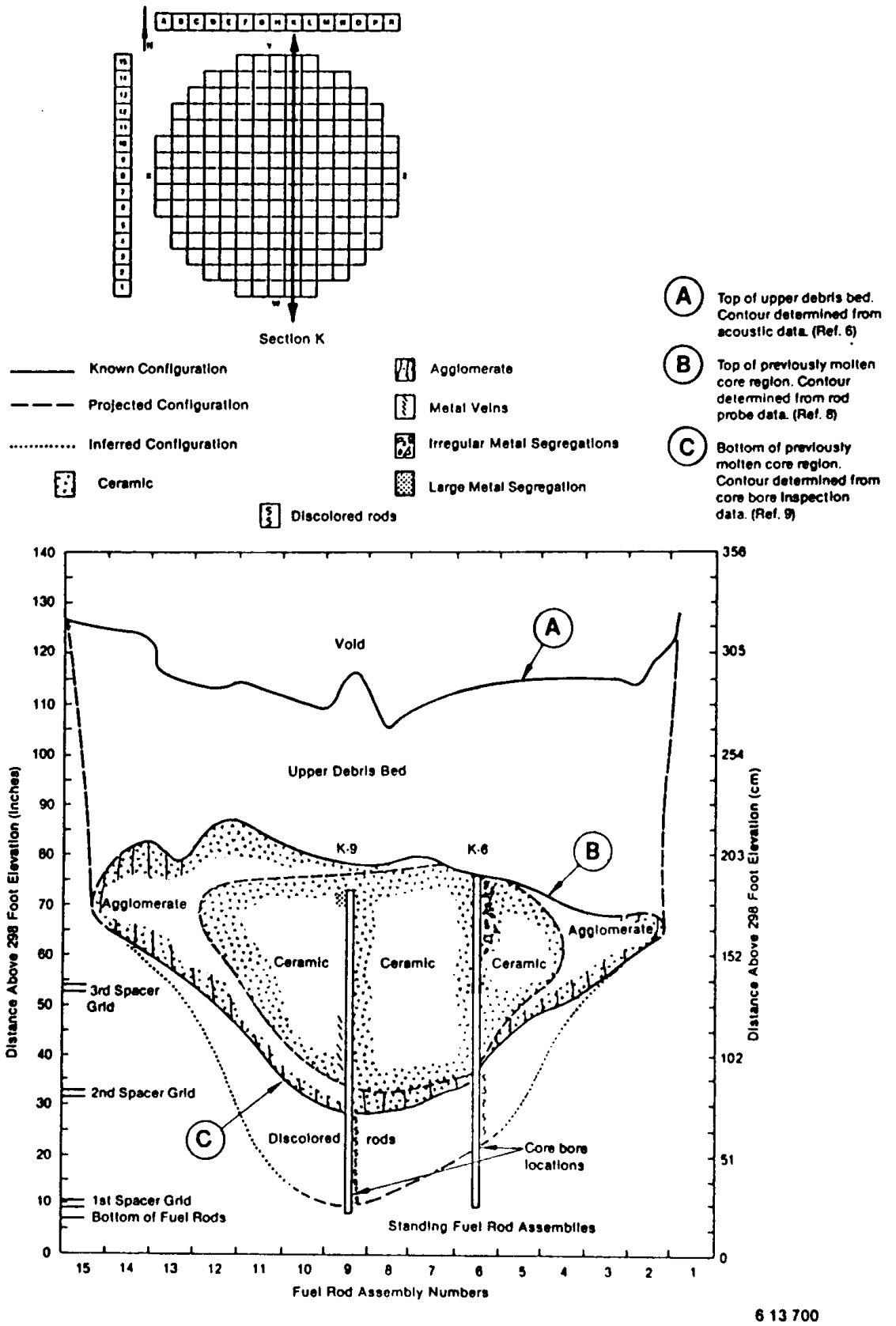

Figure 8. TMI-2 end-state core configuration through the K row of fuel assemblies.

near the center of the core. Near the core periphery, the elevation of the lower crust surface was found to be between 1 to 1.25 m from the bottom of the core. Additional core cross sections through fuel assembly rows B through P are presented in Appendix C.

2.3 Core Support Assembly Damage

The core bore visual inspections provided the first opportunity for assessment of possible damage to the CSA. Visual inspection of the CSA was performed by lowering a camera into each core bore hole. Approximately 50% of the CSA region was visible from the ten core bore locations, as illustrated by Figure 9. A description of the CSA configuration is found in Appendix D.

A small amount of fine, sandy material, most likely drilling debris, was visible at each of the central drill locations. However, there was essentially no previously molten core material or damage to the CSA directly beneath the central region of the core. Only at those locations in the east quadrant of the reactor vessel near the core periphery (N5, N12, 07, and 09) were significant quantities of previously molten core material visible in the CSA. The location and approximate orientation of the observed previously molten core material within the CSA region are shown in Figure 10. Even at these locations, the CSA did not appear to have been significantly damaged. However, the surface of the CSA near the previously molten material appeared to be discolored. This apparent discoloration may be due to surface oxidation caused by heating of the structure by the very high temperature molten ceramic material. The relocated core material in the CSA regions resembles the ceramic material observed in the core region and apparently froze as it flowed downward, thus resembling a "cascade" or "curtain." An enhanced video image showing the molten material to the north of core bore location N12 between the lower flow distributor plate and the grid forging is presented in Figure 11. A fuel rod shard produced by the drilling operation also appears in the foreground of Figure 11.

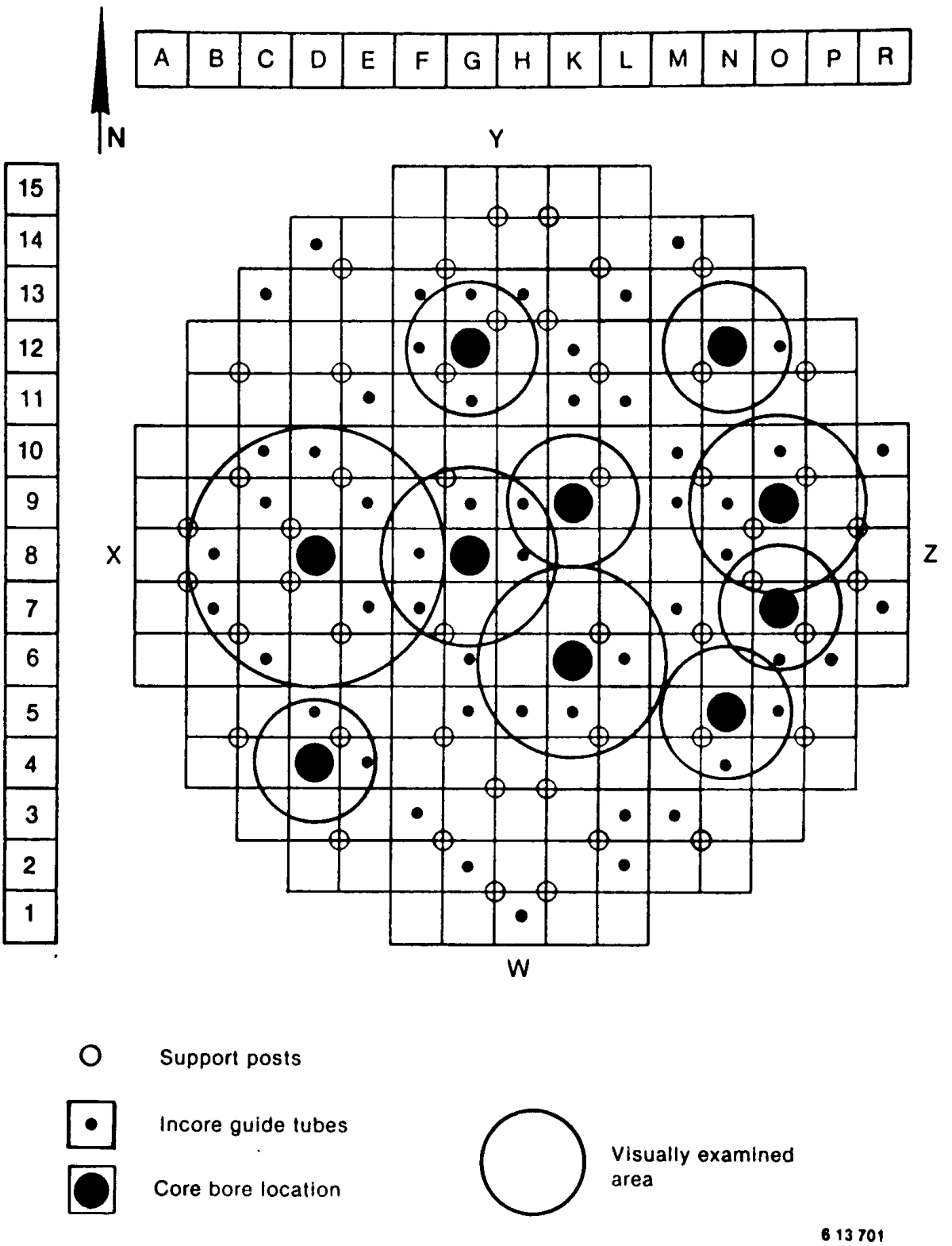

Figure 9. Approximate area of the TMI-2 CSA visible during the core bore inspections.

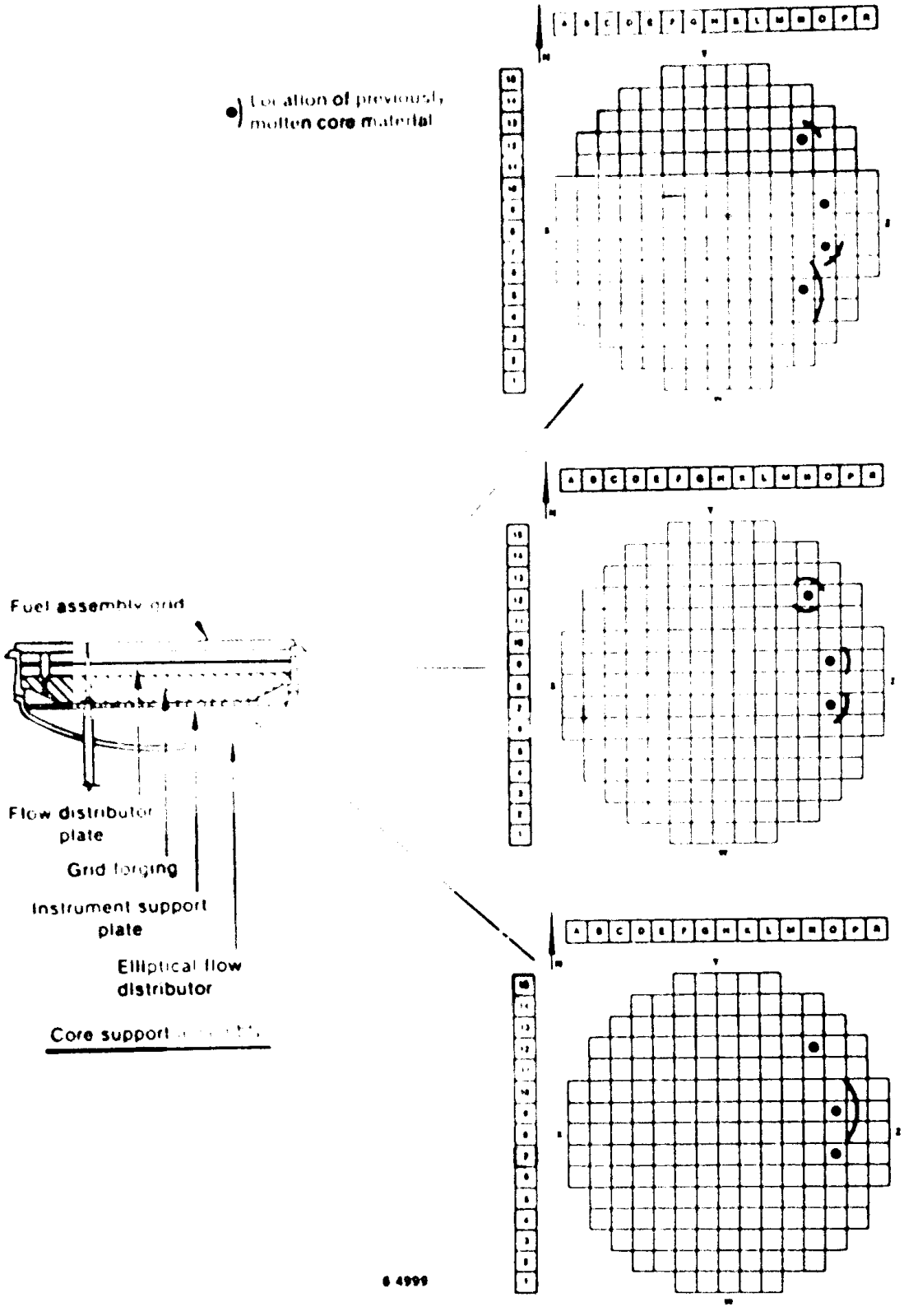

Figure 10. Locations and orientation of observed previously molten core material in the C A in TMI-2.

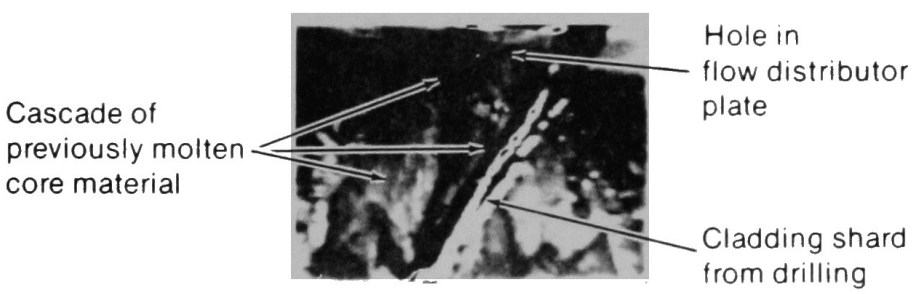

Figure 11. Cascade of TMI-2 previously molten core material in the CSA to the north of fuel assembly N12.

2.4 Reactor Vessel Lower Plenum

Visual inspection of the lower plenum has confirmed that previously molten core material now rests on the reactor vessel lower head. The debris particles have a wide range of sizes, ranging from solid, irregular-shaped pieces nearly 15 cm across to relatively fine, uniform particles less than 1.25 cm in diameter. An example of this debris near the periphery of the reactor vessel is shown in figure 12. The larger debris particles are generally located toward the periphery of the debris bed. An enhanced video image of the smaller debris particles near the center of the lower plenum is shown in figure 13. This example was obtained via the video inspections performed during the core boring operation.

Sampling of the lower plenum debris with the core bore machine was attempted at fuel assembly locations K9 and D4 by boring through the debris bed to within approximately 20 cm of the lower head. However, the material was not retained inside the core bore sampling unit. Subsequent visual inspection revealed that surrounding debris material had collapsed into the drill holes after the drill string was removed. Apparently the debris bed in the lower plenum readily fragments into relatively fine particles when subjected to sufficient mechanical stress. Core boring indicated that the required stress to fragment the debris into small particles is small, but it was not possible to accurately measure.

Data from the lower plenum inspections have been compiled and evaluated[10] to construct the contour map of the lower plenum debris bed shown in figure 14. From the configuration shown in figure 14, it is estimated that the debris bed contains between 10 and 20 metric tons of previously molten material. This is consistent with previous estimates that were based on neutron measurements made before visual access was available, suggesting that between 5 to 24 metric tons of fuel were present in the lower plenum.[11]

Selected debris particles retrieved from the lower plenum have been examined[12] The major findings from these examinations include:

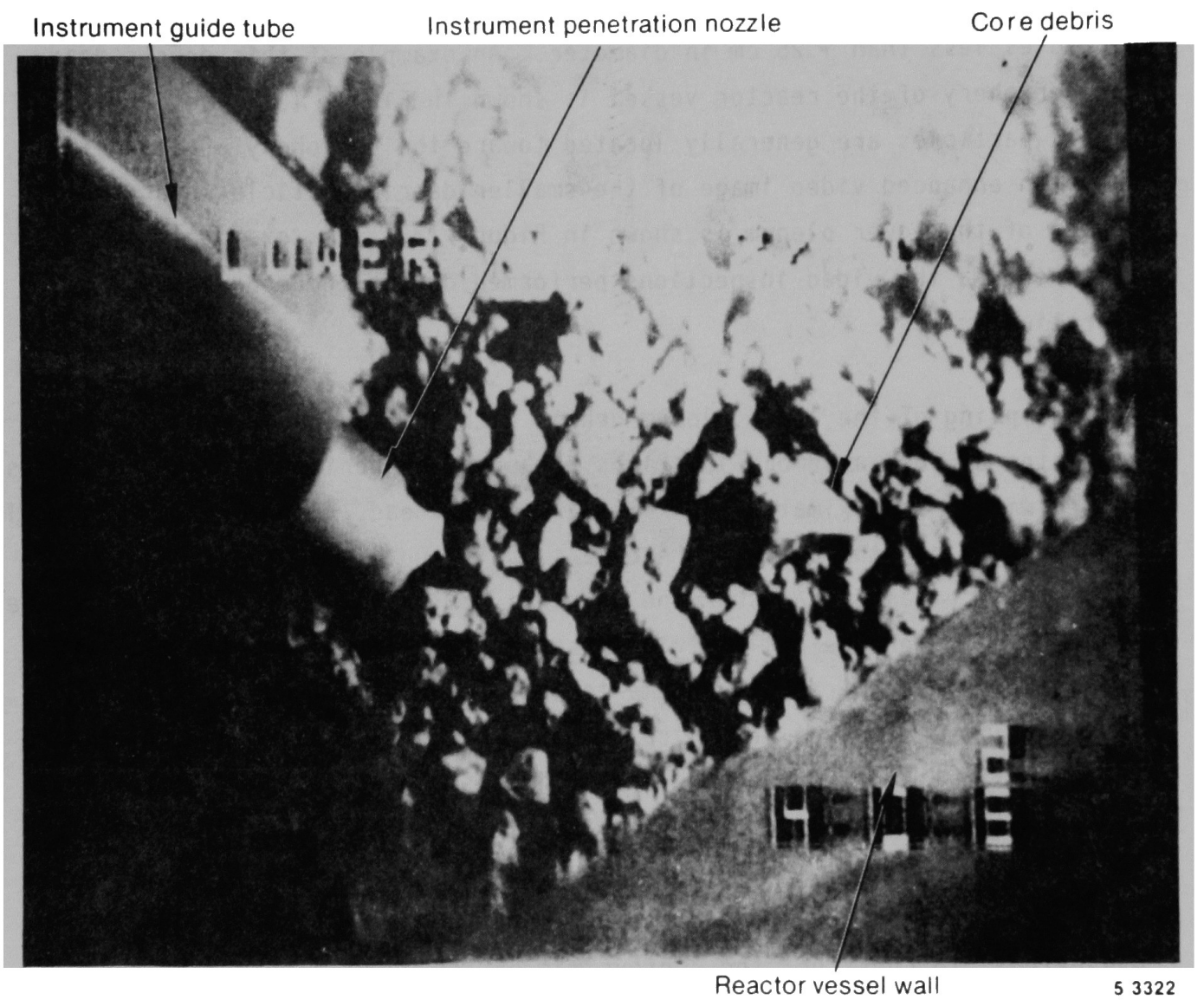

Figure 12. Debris particles in the TMI-2 lower plenum resting on the surface of the lower head.

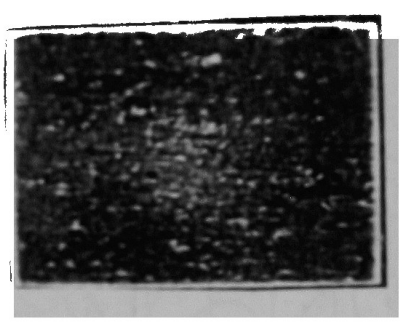

Figure 13. Fine particles (<0.5 in diameter) on the surface of the TMI-2 lower plenum debris bed.

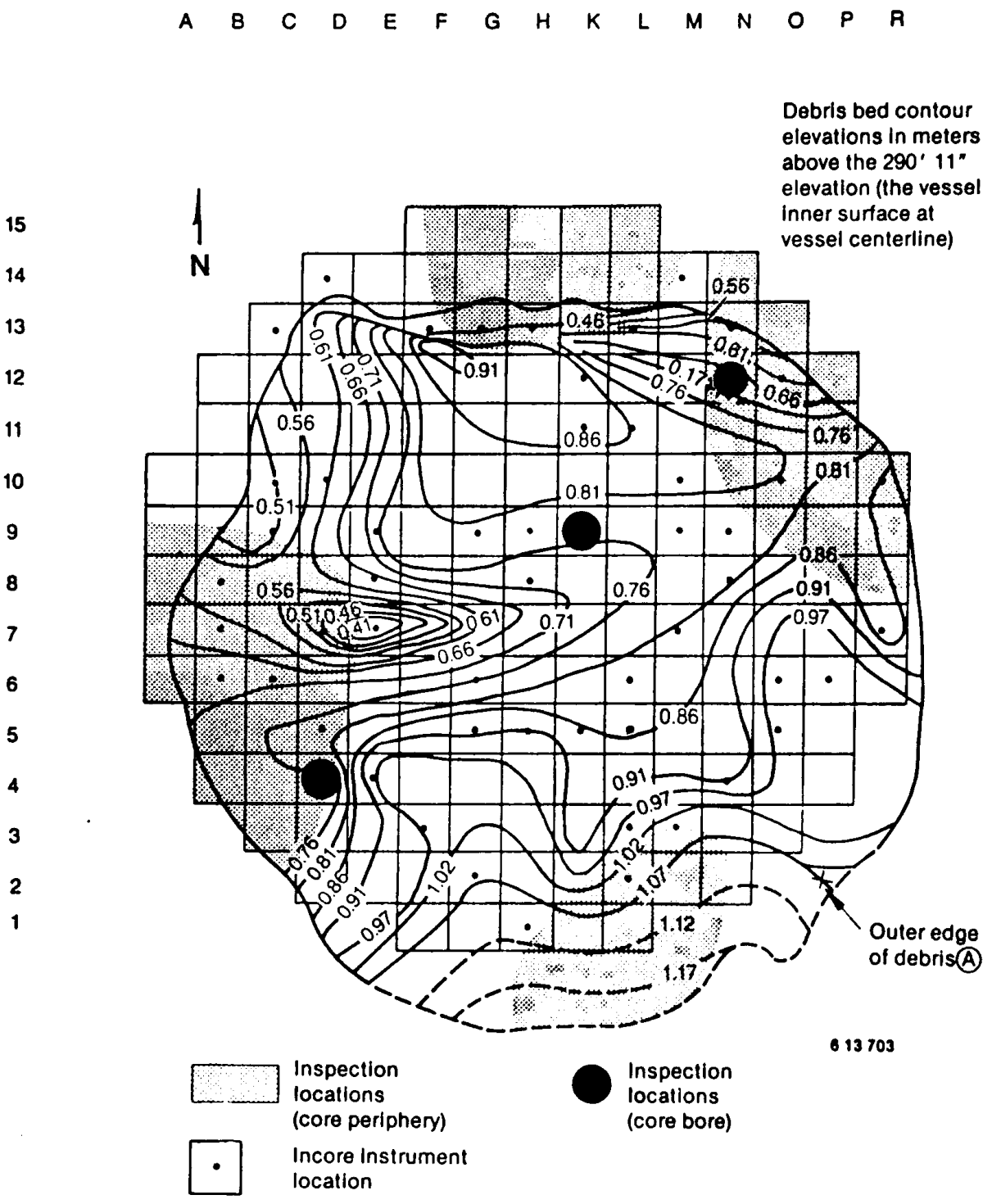

Figure 14. TMI-2 lower plenum debris bed configuration.

- Density of the previously molten material ranged from 6.6 to 8.1 g/cm^3. (The original density of the fuel pellets was ~10 g/cc.)

- Particle porosity varied from 5 to 40%.

- The material is composed mostly of UO_2 and ZrO_2 with small metallic inclusions composed primarily of Al_2O_3, FeO, Cr_2O_3, SiO_2, and NiO.

- The estimated peak temperature reached by the material is approximately 3100 K, which is basically equivalent to the melting point of UO_2.

- Cesium-134 was substantially retained (10 to 20%) in the previously molten material; retention of antimony and ruthenium was less than 10%; and europium and cerium were retained at nearly 100%.

2.5 Estimated Volumes and Masses of the Degraded Core Regions

Estimates have been made for the volumes and masses of the various core regions using the core cross sections presented in Appendix C, estimated densities of the degraded core material, and known densities of the intact fuel rods; Table 1 summarizes these estimates. The density of the consolidated (molten) core material is not known precisely; however, it was assumed to be identical to the lower plenum particles recently examined (7.25 g/cm^3). Based on the estimated mass remaining in the core region, approximately 16 metric tons of core material are estimated to be in the lower plenum region.

TABLE 1. ESTIMATED END-STATE CORE VOLUMES AND MASSES

Region	Estimated Volume (m^3)	Estimated Mass (kg)	Fraction of Total Core Mass
Original core	33.5	122,700	1.0
Upper core void	9.2	--	
Upper core debris	6.7	30,000	0.24
Molten zone	3.5	25,000	0.20
Standing rods	14.1	51,800	0.42
Lower plenum debris	4.5[a]	15,800	0.14

a. Obtained from estimated mass (15,800 kg), assumed debris packing fraction of 50%, and measured debris particle density of 7.25 g/cm^3.

3. ACCIDENT SCENARIO

This section integrates the known end-state core damage presented in the previous section with (a) data recorded during the accident, (b) results of analytical work to interpret the TMI-2 data, and (c) results of independent severe fuel damage experiments to develop a best-estimate scenario of core damage for the first four hours of the accident.

The accident is divided into four major time periods:

1. The loss-of-coolant period with the RCS pumps on from 0 to 100 min,

2. The initial core heatup and degradation period from 100 to 174 min,

3. The degraded core heatup period from 174 to 224 min, and

4. The period of core relocation from 224 to 230 min.

Although core heatup did not occur during the first 100 min, the RCS measurements have been extensively examined to (a) determine if the RCS hydraulic measurements (in particular, the pressurizer liquid level) are substantially valid indicators of RCS thermal-hydraulics, and (b) estimate the RCS inventory which is closely coupled to the start of core heatup after 100 min.

Details of the accident during each of the major time periods are discussed in the following sections.

3.1 Loss-of-Coolant Period with the RCS Pumps On (0 to 100 Min)

The first phase of the accident is defined to be from the turbine trip (defined as time zero) until the A-loop reactor coolant pumps (RCPs) were turned off at 100 min. (The B-loop RCPs were turned off earlier, at

73 min.) As far as can be determined, the core was covered with a two-phase mixture and remained cool as long as the RCPs were operating. Thus, the accident was a purely thermal-hydraulic transient during this time. This section presents a summary of the current understanding of the thermal-hydraulic state of the reactor during this time frame and is based on a detailed analysis of the pressurizer response[13] and the initial neutronic analysis to interpret the source range monitor (SRM) response.[14]

A schematic of the TMI-2 reactor coolant system (RCS) is shown in Figure 15, which illustrates the elevations of the various components (relative to sea level) and the locations of various RCS instrumentation. Of particular note are the locations of the hot and cold leg temperature measuring devices and the pressurizer surge line. There has been disagreement regarding the accuracy of the pressurizer liquid level measurement. However, based on the analysis presented in Reference 13, it is judged that the level measurement is a reliable indication of the liquid level within the pressurizer during the accident.

As the primary-to-secondary heat transfer degraded (in response to the termination of feedwater and the resulting decreasing secondary liquid level), more energy was being released from the core than was being removed from the RCS. This caused the RCS coolant to heat up and expand into the pressurizer, as shown in Figure 16 which presents a comparison of the RCS pressure and pressurizer liquid level. The RCS coolant expansion also resulted in an increase in the RCS pressure. The pressurizer liquid level and RCS pressure continued to increase until the pilot-operated relief valve (PORV) opened at an RCS pressure of 15.7 MPa (3 s) and the reactor scrammed on a high-pressure trip at 16.3 MPa (8 s). After reactor scram, more energy was being removed from the RCS through the PORV and the steam generators than was being generated in the core, which resulted in contraction of the RCS fluid. This resulted in a rapid decrease in the RCS pressure and the pressurizer level, which should have caused the PORV to close on decreasing RCS pressure. However, unknown to the operators, the PORV failed to close. The operators responded to the decreasing pressurizer liquid level by increasing the makeup flow to approximately

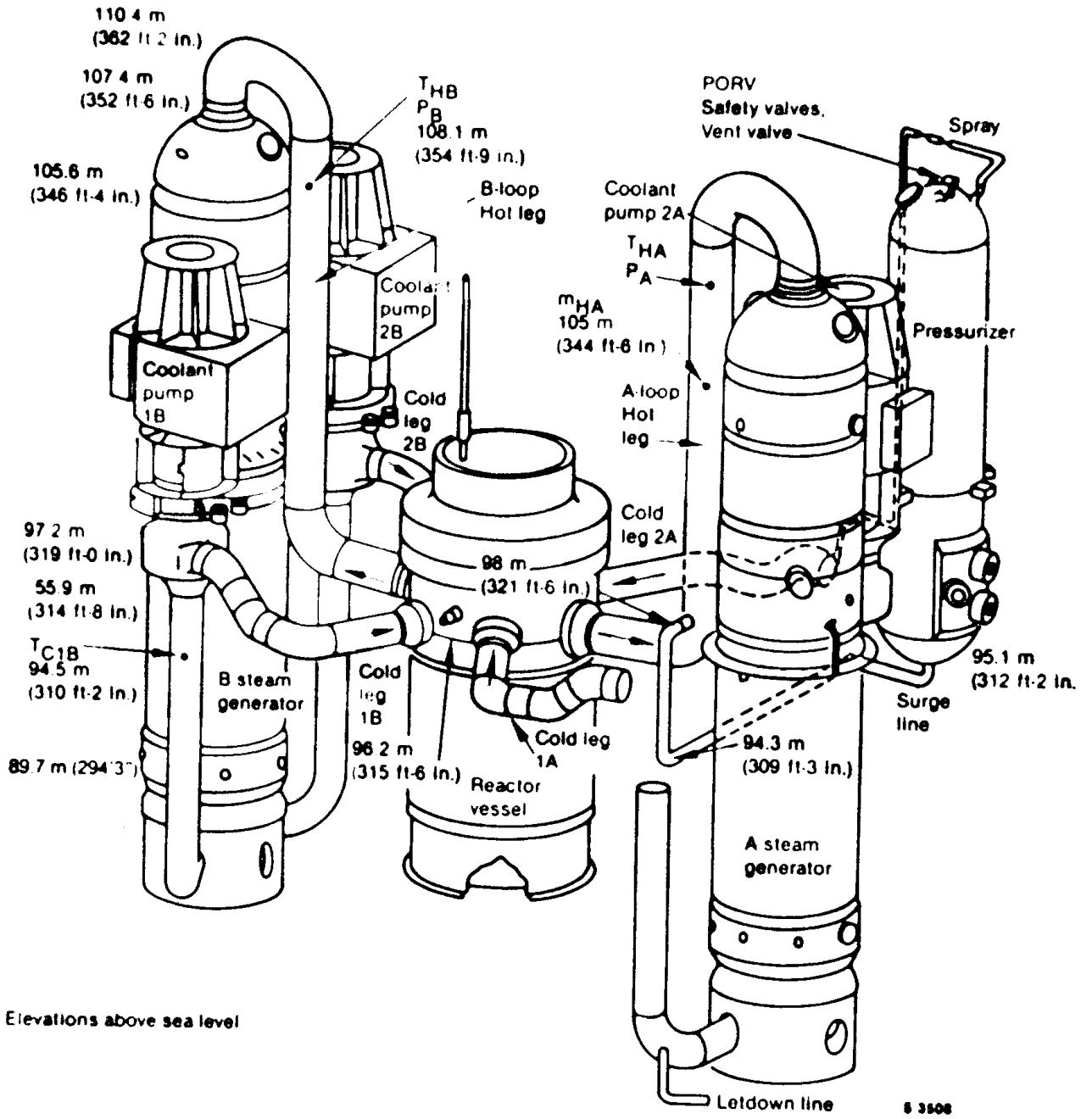

Figure 15. Isometric of the TMI-2 primary system.

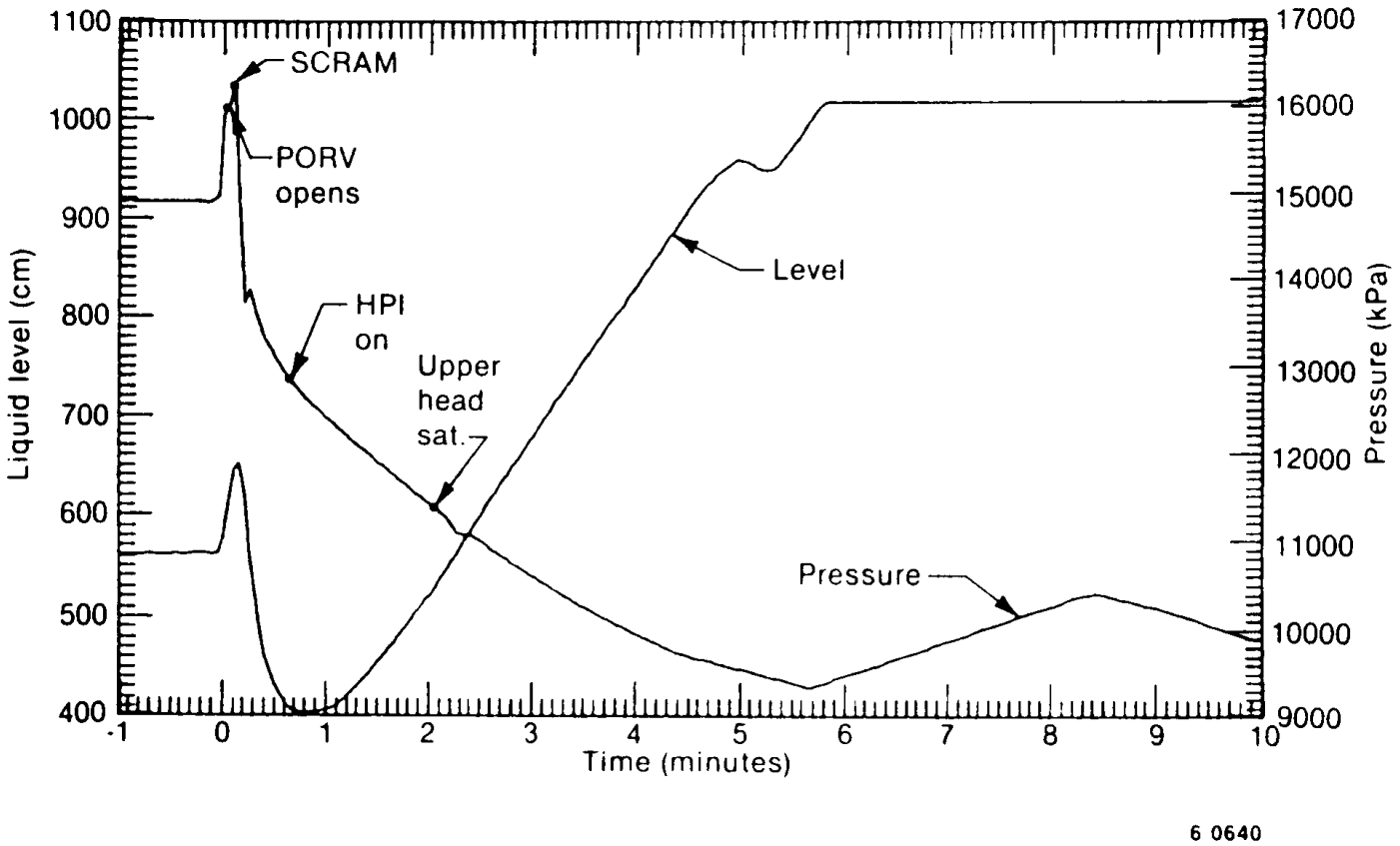

Figure 16. Comparison of TMI-2 pressurizer liquid level and primary system pressure (0 to 10 min).

30 l/s (41 s), which reversed the pressurizer level decrease. The RCS pressure decrease continued, however, reaching the saturation pressure of the coolant in the upper plenum at approximately 2 min and saturation pressure for the rest of the RCS at about 6 min.

The reduction in primary heat source due to the reactor scram caused the temperature differential from hot to cold leg to decrease from an initial 26 K to near zero by 1.5 min. This is illustrated in Figure 17, which compares the A-loop hot and cold leg fluid temperatures with the saturation temperature corresponding to the RCS pressure for the same time period. By 1.5 min, the secondary sides of the steam generators had dried out and primary-to-secondary heat transfer essentially ceased.

Cessation of heat transfer from the RCS eventually caused the RCS pressure to start to increase at approximately 5.7 min as the pressurizer filled and a much lower void fraction fluid started to flow out of the PORV. At 8 min, the operators opened the block valves, permitting auxiliary feedwater injection into the steam generator secondary sides. This restored primary-to-secondary heat transfer and started a gradual cooldown of the RCS.

Figure 18 shows the same measurements as Figure 17 (pressurizer level and RCS pressure) for the first 100 min of the transient. From approximately 20 min on, the RCS pressure remained nearly constant at 7 MPa. The pressurizer level, which was off-scale high at 6 min, came back on scale by 11 min and remained on scale, though very high, throughout the rest of this time period. The operators, responding to the high pressurizer liquid level, decreased makeup flow and increased letdown flow. This resulted in an increasing RCS void fraction but did little to affect the pressurizer liquid level which was responding to the pressure differential caused by continued flow through the still-open PORV. The RCPs in the B loop were turned off at 73 min due to low pump current and high vibration caused by pump cavitation.

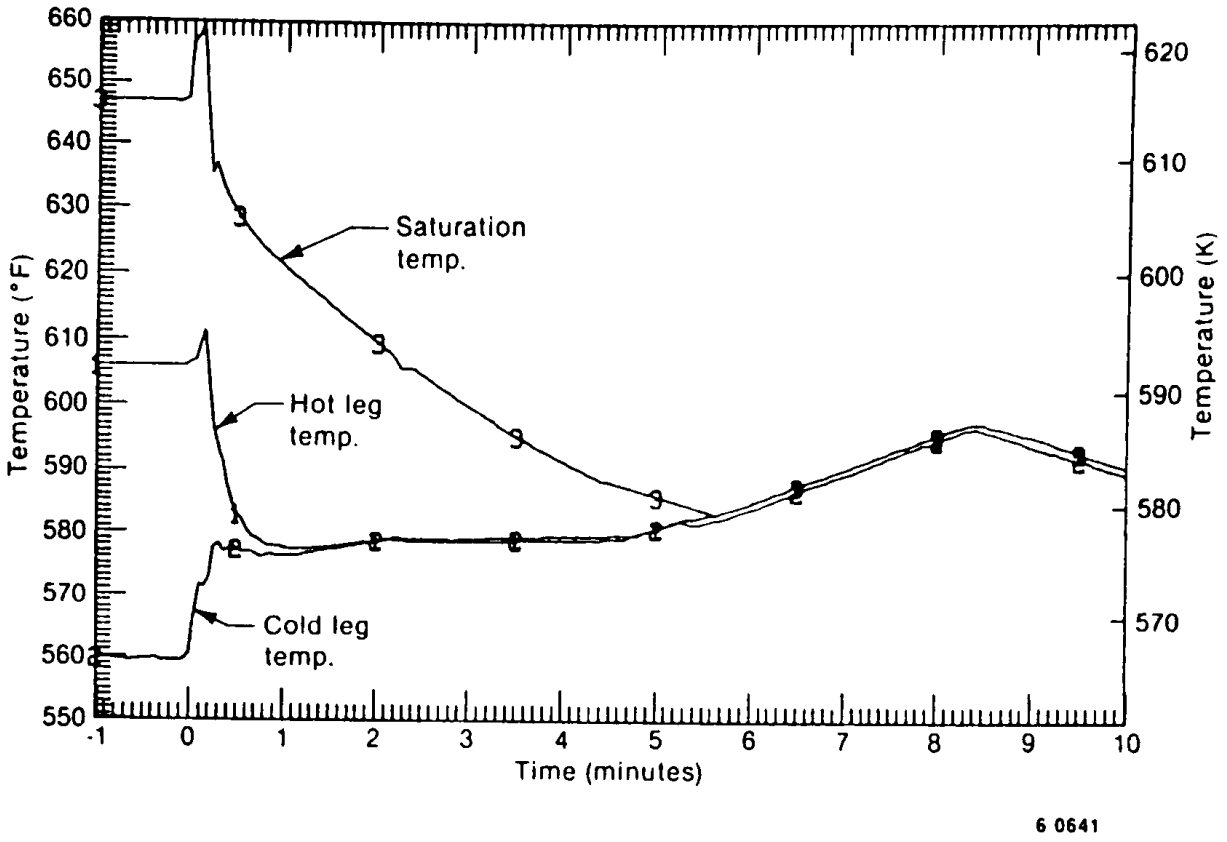

Figure 17. TMI-2 A-loop hot leg, cold leg, and saturation temperatures (0 to 10 min).

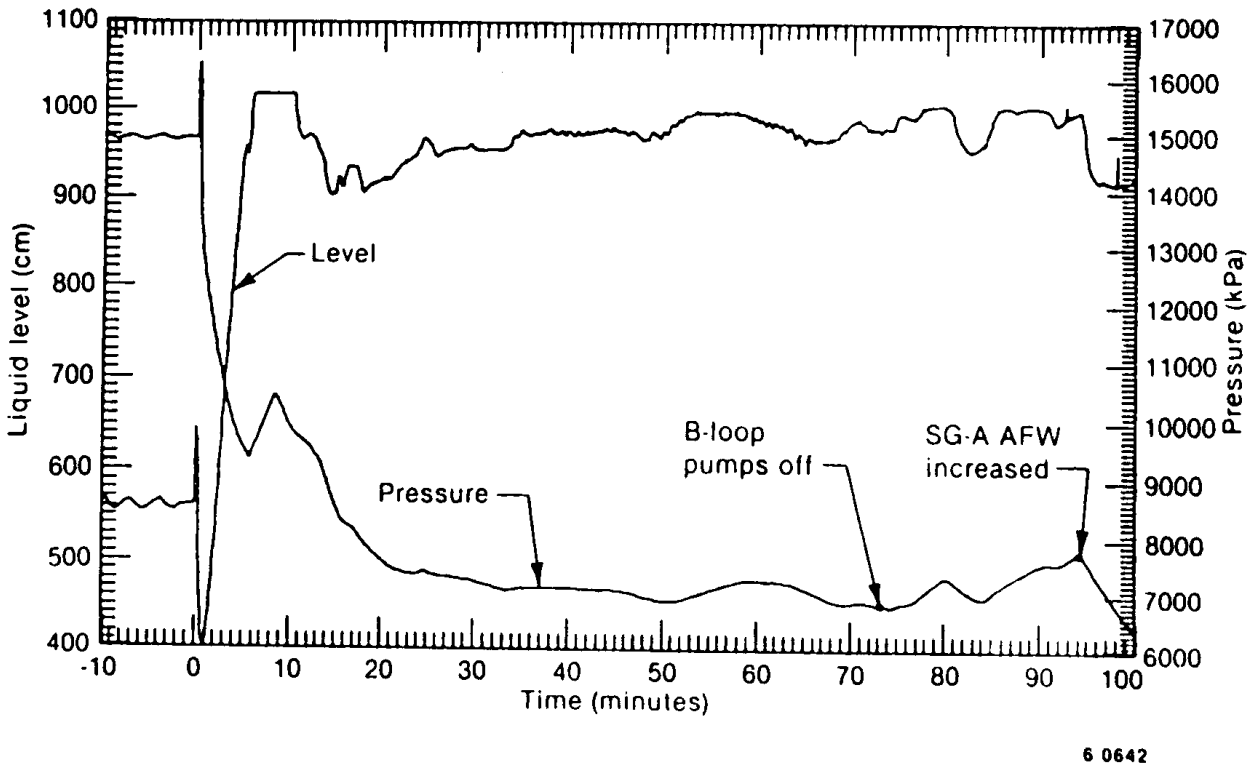

Figure 18. Comparison of TMI-2 pressurizer liquid level and primary system pressure (-10 to 100 min).

Though small, primary to-secondary heat transfer continued throughout this period. Figure 19 compares the hot and cold leg temperatures with primary and secondary saturation temperatures. The fluid temperatures remained relatively constant at approximately 560 K from 20 min on during this time period. Between 20 and 80 min, the primary temperatures closely followed the secondary saturation temperature. During this time period, a two-phase flow existed throughout the primary system. As mass continued to be lost from the RCS through the PORV and letdown, the void fraction of the two-phase flow increased. At about 85 min, feedwater injection into the A-loop steam generator was apparently terminated. By 92 min, the A-loop steam generator secondary had boiled dry, which resulted in a significant decrease in primary-to-secondary heat transfer. This is apparent in Figure 19, in which the primary temperatures began increasing above the secondary saturation temperature. At 95 min, the auxiliary feedwater flow was increased to the A-steam generator, increasing primary-to-secondary heat transfer and enhancing cooling of the RCS. The increased heat transfer resulted in condensation of steam, causing a decrease of the RCS pressure. The depressurization of the RCS resulted in a decrease of the pressurizer liquid level. This phase was ended when the RCPs in the A-loop were turned off at 100 min due to excessive vibration. The collapse of the liquid level in the reactor vessel to a level at or near the top of the core as a result of the RCP trip is inferred from indirect evidence. As coolant continued to be lost out of the RCS, the core started to uncover and heat up. (Superheated steam temperatures were recorded for the A-loop hot leg starting at approximately 112 min, an indication of core uncovery. Working backwards to 100 min, a liquid level near the top of the core, following pump trip, can be inferred from a coolant mass balance within the RCS.)

Knowledge of the RCS coolant makeup and letdown flows is crucial for accurate calculation of the thermal and hydraulic response of the plant during the accident, since the coolant inventory in the RCS and the timing and extent of core uncovery during the accident are directly affected. The results of a series of sensitivity calculations on the TMI-2 thermal hydraulics have been previously reported,[15] where the makeup flow

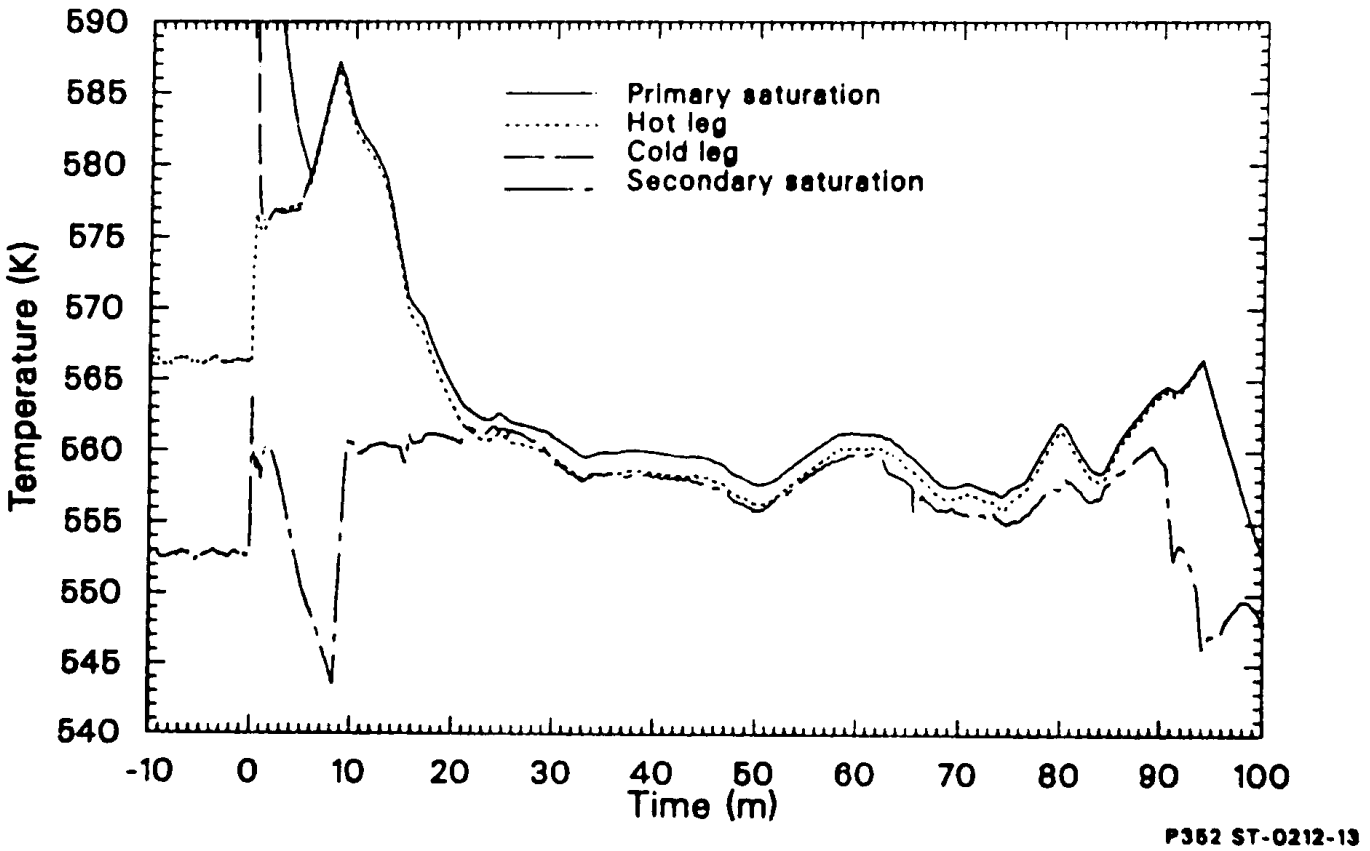

Figure 19. TMI-2 A-loop hot leg, cold leg, primary saturation, and secondary saturation temperatures (-10 to 100 min).

volume and history were varied. These calculations indicate that, for example, if the high pressure injection had been allowed to start up and run continuously from the start of the accident, the flow would have been sufficient to remove decay heat and prevent core damage regardless of emergency secondary feedwater injection delay.

The make-up injection flow rates were only recorded on the utility printer hourly log and represent a principal uncertainty in understanding the accident. An indirect indication of the liquid level in the reactor vessel is provided by an analysis of the SRM response during the accident. The SRM, a BF_3 neutron detector, was installed in the annulus between the reactor pressure vessel and the biological shield to provide a measurement of core power at very low power levels. The transducer has been determined to be sensitive to reactor vessel downcomer liquid level in that as the level decreases, neutron leakage increases due to reduced neutron moderation. Analysis of the SRM response during the accident was previously reported[14,16] and is summarized in Appendix E. On the basis of this analysis, it was concluded that homogeneous voiding occurred in the reactor vessel during the continuous pump operation, resulting in a void fraction of approximately 0.45 in the downcomer by the time the A-loop pumps were stopped

3.2 Initial Core Heatup and Degradation (100 to 174 Min)

After the final pump shutdown at 100 min, the water in the upper part of the primary cooling system drained into the reactor vessel. It is somewhat uncertain what the water level in the reactor vessel was at this time; but, as discussed in the previous section, it is judged to have been near the top of the core. The reactor vessel liquid level then continued to decrease due to boiling in the core region, loss through the PORV valve, and condensation in the steam generators (predominately the A-steam generator). The decreasing core liquid level led to core uncovery and subsequent core heatup sufficient to cause severe core degradation.

Data from selected TMI-2 plant instrumentation provide the basis for inferring core heatup versus time during this period. Analytical work was completed to bound the core heatup rate and provide the basis for interpreting the available plant data and defining a best-estimate core damage progression scenario. Details of the plant data interpretation and supporting analysis are provided in the following sections.

3.2.1 TMI Data Relative to Core Heatup and Degradation

Coolability of the reactor core is dependent on maintaining liquid in the core region to carry off the decay energy being generated in the fuel. As the core liquid level decreases, uncovering the core, transfer of the decay energy from the fuel decreases significantly and the fuel rods begin to heat up. Thus, knowledge of the core liquid level versus time is very important for estimating the timing of core heatup and the heatup rate. The source range monitor response (see Appendix E) provides the only time-dependent data to estimate core liquid levels; however, the data must be interpreted through neutronic analysis and accompanying assumptions relative to the core configuration and liquid distribution in the core and downcomer. The results of early analyses performed to estimate the bounds of core liquid level versus time are summarized in Figure 20.[14] Note from the figure that the initial core uncovery time is estimated to be in the range of 114 to 120 min and that minimum core liquid levels of approximately 0.5 to 1.0 m were predicted by 174 min. The initial source range monitor response included in Reference 16 assumed an intact core configuration throughout the accident and thus did not account for core material relocation.

Another data source relative to core liquid level and timing of the initial core heatup is the coolant temperature measured in the RCS hot legs. The A-loop hot leg temperature shown in Figure 21 indicates that the coolant temperature departs significantly from the RCS saturation temperature between 110 and 113 min, indicating that the core liquid level had fallen sufficiently by this time to allow the upper core region to exceed the RCS saturation temperature.

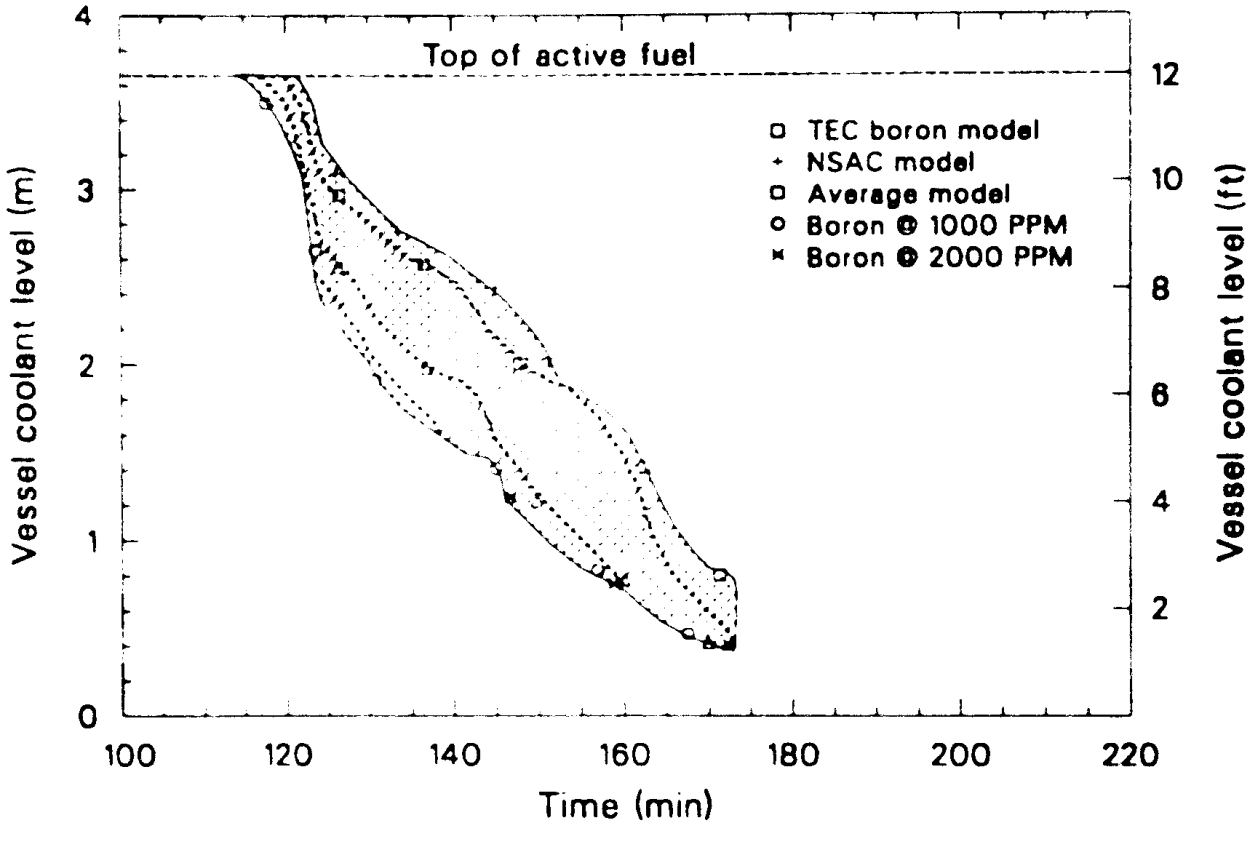

Figure 20. Bounding estimates of TMI-2 core liquid level versus time based on SRM data evaluation.

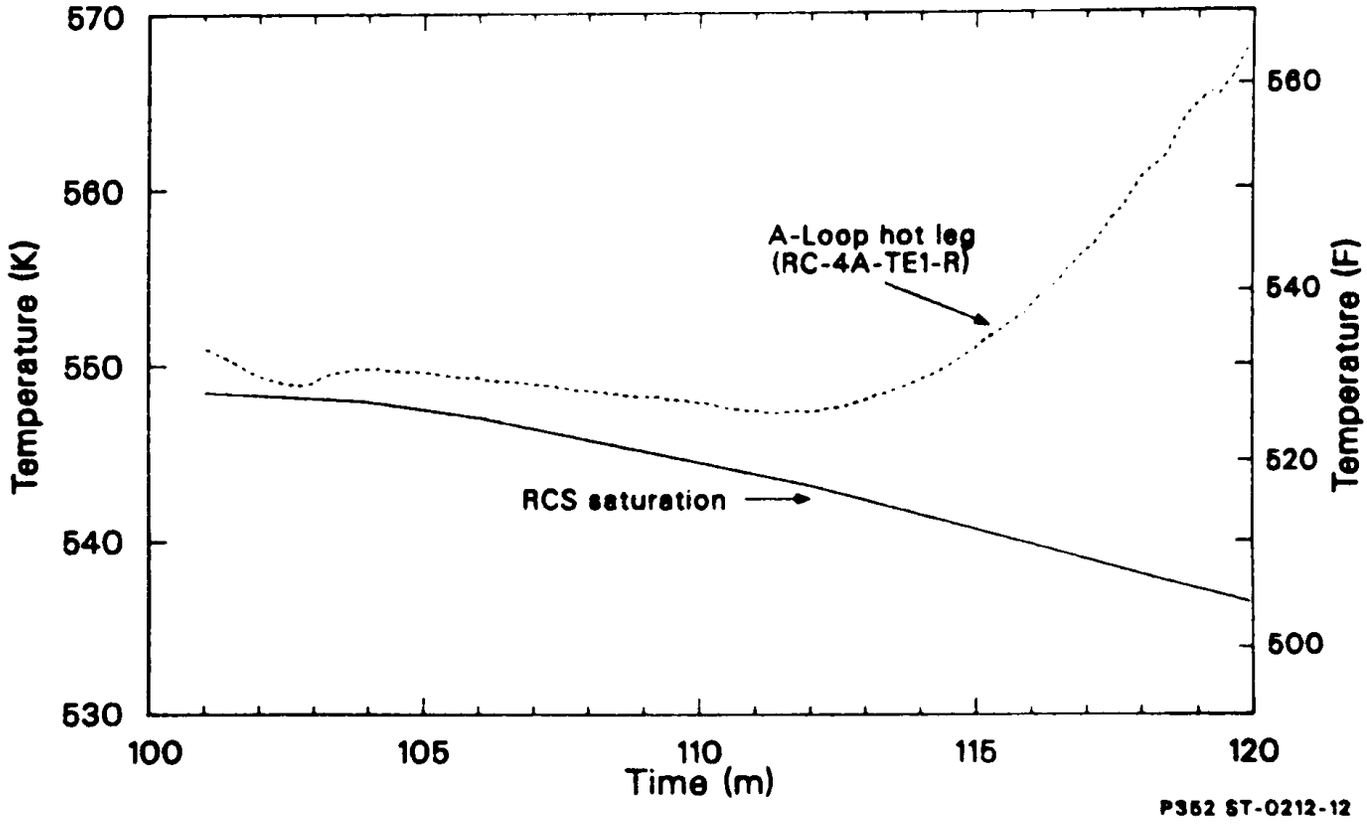

Figure 21. TMI-2 measured A-loop hot leg temperature.

The containment radiation monitors provide additional data relative to the core heatup. The response from the three containment radiation-measuring devices in the area adjacent to the reactor vessel increased significantly between 142-145 min, as shown in Figure 22. Core temperatures in excess of 1100 K are required to burst enough fuel rods to result in the measured increases in radiation levels. Actual fuel rod rupture times likely occurred several minutes earlier than the radiation monitor response. This is based on core-to-containment fission product transit times of between 3 to 5 min[14] estimated by correlating PORV opening times to the timing of increased containment radiation levels measured during later periods of the accident. Thus, the radiation measurements indicate that peak cladding temperatures of 1100 K within the core were achieved sometime between 137 and 142 min.

The in-core self powered neutron detectors (SPNDs) provide important data relative to the core heatup. (Appendix F summarizes the in-core instrument configuration.) Two major sources of SPND data are available; (a) the alarm system data, indicating when the instrument signals departed from the normal recording range (-20 to +1500 nA) and when they subsequently returned to the normal recording range, and (b) strip chart recorders that monitored the anomalous output signals from 18 selected SPNDs. An early interpretation of these data is summarized in References 14 and 16. More recent experiments to evaluate the SPND response under conditions simulating those during the accident and analysis to interpret the previous SPND data[17] have provided two important conclusions relative to the SPND behavior versus core heatup. These are:

1. As the SPND cables heat up, a negative current is generated at local temperatures of approximately 850 K, and

2. The polarity of the anomalous output current changes from negative to positive as the local temperatures exceed 1350 K. The generation of high positive output currents and change in output polarity were confirmed via SPND testing in the LOFT LP-FP-02 experiment,[18] and the high temperatures were

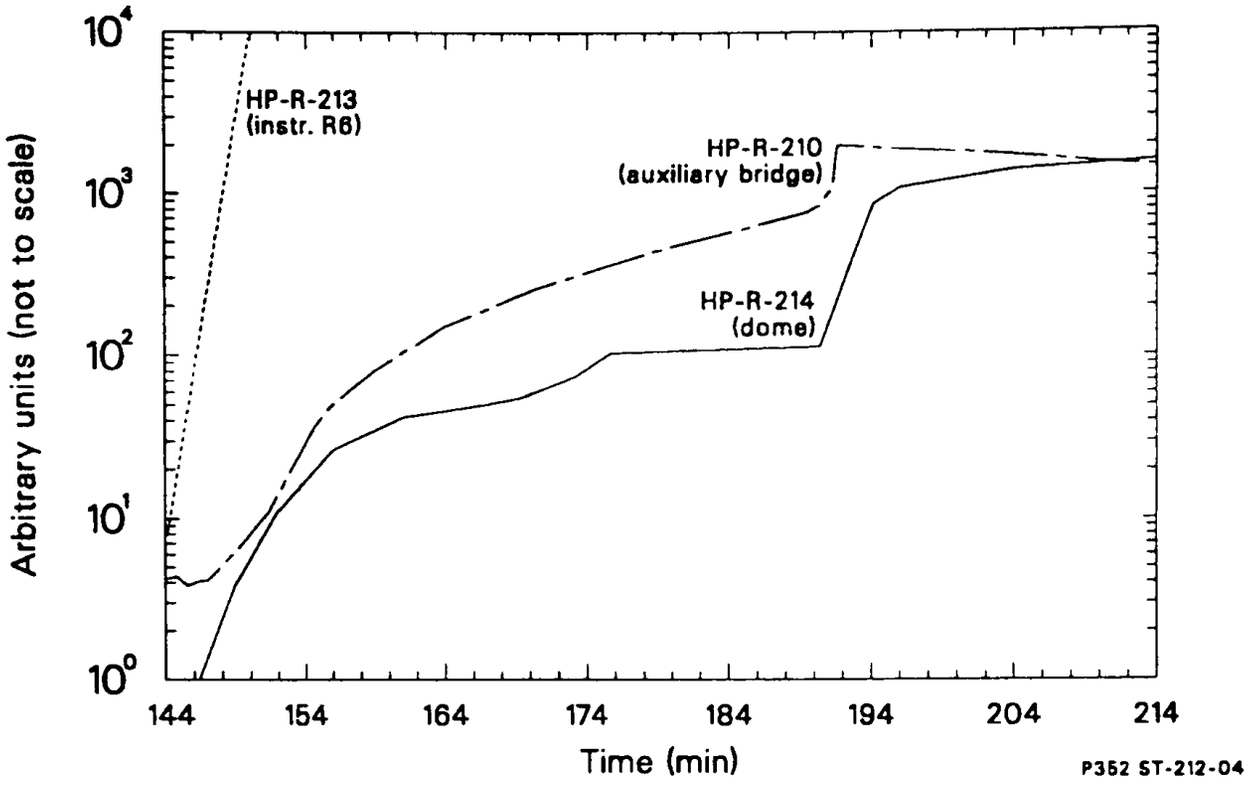

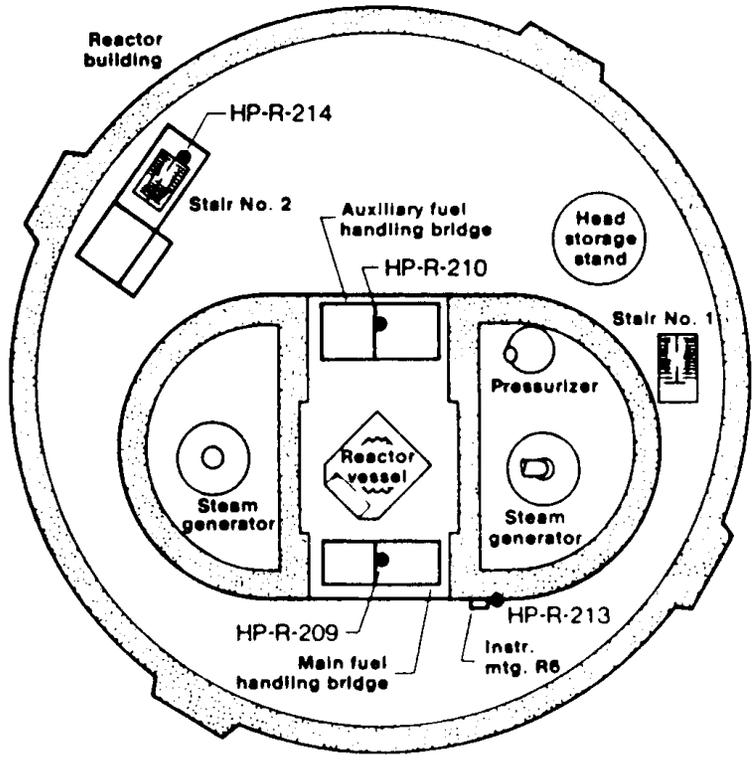

Figure 22. TMI-2 containment radiation measurements indicating the first significant radiation release from the RCS.

associated with rapid oxidation of the surrounding fuel rod cladding. This occurred at cladding temperatures exceeding 1800 K.

From the SPND data recorded on strip charts, it is clear that high positive output currents (indicating instrument temperatures greater than 1350 K) were observed by as early as 150 min at locations near the top of the core (instrument Level 6, 2.9 m from the bottom of the active fuel) and by 165 min at lower core elevations (instrument Level 2, 0.76 m from the bottom of the active fuel).

The SPND alarm data provide additional qualitative information relative to the core damage progression. Many of the SPNDs had alarmed off-scale prior to 168 min. The details of these alarms are not known, because these data were purged by the operators during the accident. However, it appears that none of the SPNDs below 0.24 m (Level 1) went off-scale during this period of the accident, indicating that core temperatures at this elevation remained below 850 K.

The measured RCS pressure provides additional information relative to the timing of initial core damage. The RCS pressure increased significantly from 150 to 173 min. Increasing RCS pressure can be attributed to two mechanisms, both related to core damage. The first is the production of hydrogen from core oxidation. Hydrogen, as a noncondensible gas, reduces RCS natural circulation flows and steam generator heat transfer, thereby resulting in increased RCS pressure due to higher temperatures. The second mechanism is water flashing as a result of relocating molten core materials flowing into the coolant in the lower regions of the core. The relative importance of these mechanisms on the RCS pressurization has yet to be evaluated. Figure 23 summarizes the above major TMI-2 events relevant to core damage progression by overlaying them on the measured RCS pressure response from 100 to 174 min.

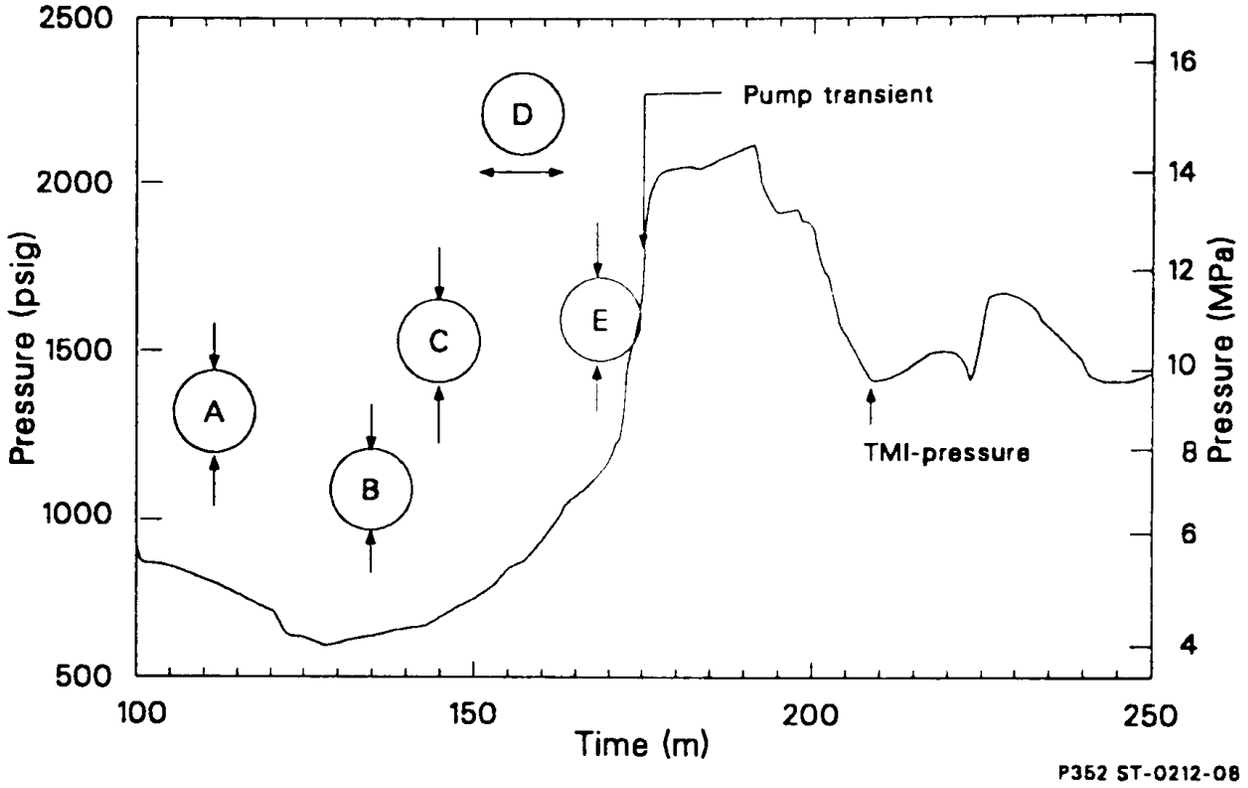

(A) - Initial hot leg superheat (110 to 113 min)

(B) - First negative SPND signal (135 min)

(C) - Significant increase in containment radiation

(D) - Positive SPND signals (150 to 165 min)

(E) - In-core thermocouples and SPNDs (<Level 1) off scale

Figure 23. Overlay of RCS pressure and important TMI-2 observations during the initial core heatup and degradation period prior to 174 min.

3.2.2 Core Heatup

To aid in interpreting the TMI-2 data, core heatup calculations were conducted using the Severe Core Damage Accident Package (SCDAP) computer code.[19] The code was developed for the U.S. Nuclear Regulatory Commission to model the physical processes controlling severe core damage behavior and has been extensively verified against PBF[20] and other severe fuel damage experiments. Appendix G summarizes the major SCDAP model features.

The calculations require core liquid level as a time-dependent boundary condition for estimating core heat transfer. The initial calculations utilized the best-estimate core liquid level from the NSAC core heatup analysis.[21] Using these boundary conditions, cladding rupture was not predicted until approximately 160 min. Core temperatures greater than 1800 K (onset of rapid core oxidation) were predicted by approximately 170 min; and, by 174 min, core temperatures greater than 2400 K were predicted.

Comparison of these predictions to the data summarized in Figure 23 suggests that core temperatures versus time were significantly underpredicted by this initial calculation. A second calculation was conducted assuming a more rapid core boildown. The core liquid level was assumed to decrease at the same rate as used previously; however, the initial liquid level at 100 min was assumed to be at the top of the core. This is equivalent to shifting the NSAC-estimated liquid level earlier in time by approximately 14 min, thus resulting in initial core uncovery at 100 min. The calculated core peak temperature (mid-core axial elevation) for this earlier core uncovery scenario is more consistent with the inferred fuel rod ruptures at 140 min and rapid core oxidation at 150 min. For this case, core temperatures greater than 2400 K are predicted between 150 and 174 min.

A third calculation was conducted to provide an estimated upper bound on core heatup. The core liquid level for this case was calculated

assuming no RCS makeup flow and thus represents the maximum possible core boildown rate; i.e., minimum coolant liquid level. The predicted core temperatures for this case exceed 1800 K by as early as 120 min and 2400 K by 137 min, clearly showing the importance of RCS makeup flow on the core liquid level and core heatup during this period of the accident. The core liquid levels and peak core temperatures for the three SCDAP cases are shown in Figure 24.

Two important conclusions can be made on the basis of the core heatup analysis:

1. Core heatup is very sensitive to the core liquid level. Thus, uncertainty in the initial core liquid level at the time of pump shutdown (100 min) and the RCS makeup flows during this period of the accident strongly impact the calculated core heatup.

2. It appears that the NSAC-estimated core liquid level vs time may represent a slower boildown than that which actually occurred. However, even using these non-conservative boundary conditions, core temperatures are predicted to exceed the onset of rapid core oxidation (1800 K) by 170 min.

3.2.3 Core Configuration Just Prior to the RCS Pump Transient

The anomalous SPND responses, increasing RCS pressure, and supporting SCDAP calculations suggest that by 150 min the core temperatures had increased sufficiently to result in rapid cladding oxidation in the central regions of the core. The oxidation process would rapidly increase fuel rod temperatures sufficient to melt the cladding and eventually the UO_2 fuel pellets. The molten zircaloy would flow downward within the fuel/cladding gap; and, when in contact with the UO_2, the UO_2 would be dissolved. Dissolution of the UO_2 can significantly increase the volume of liquefied or molten core material. Eventually, the molten material will rupture the outer zirconia sheath (formed as the zircaloy cladding oxidized) and will

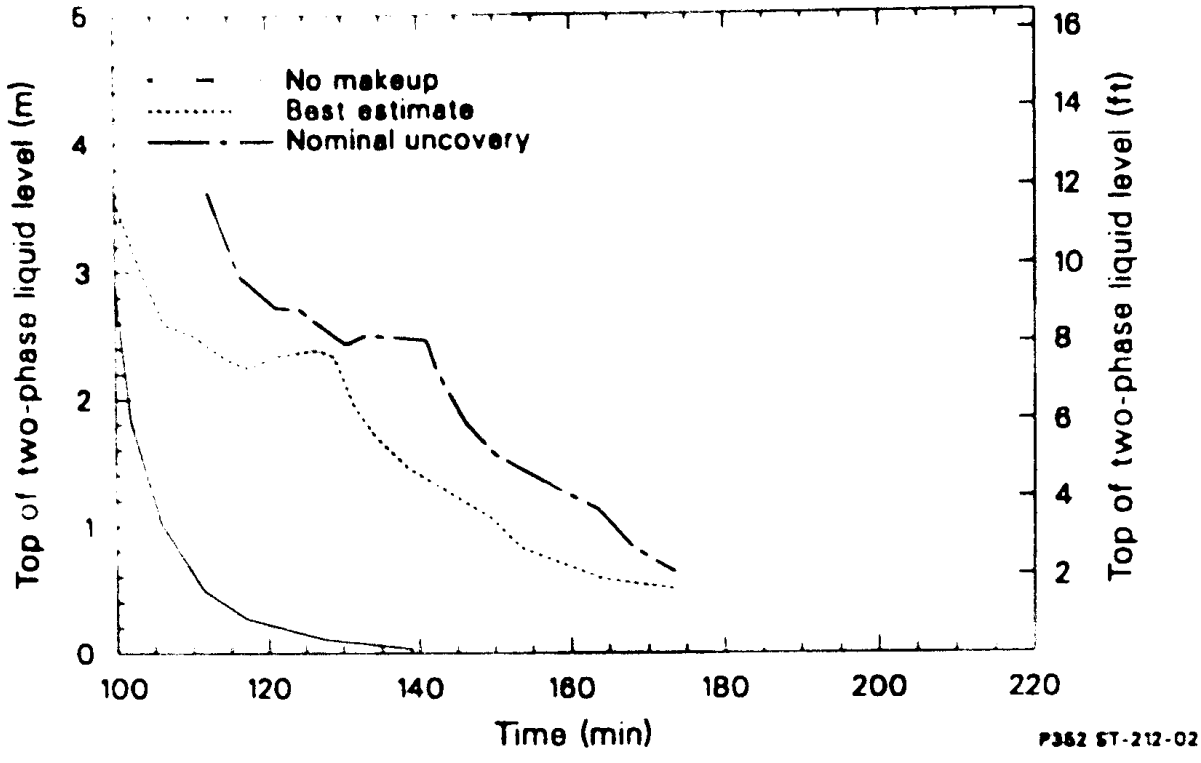

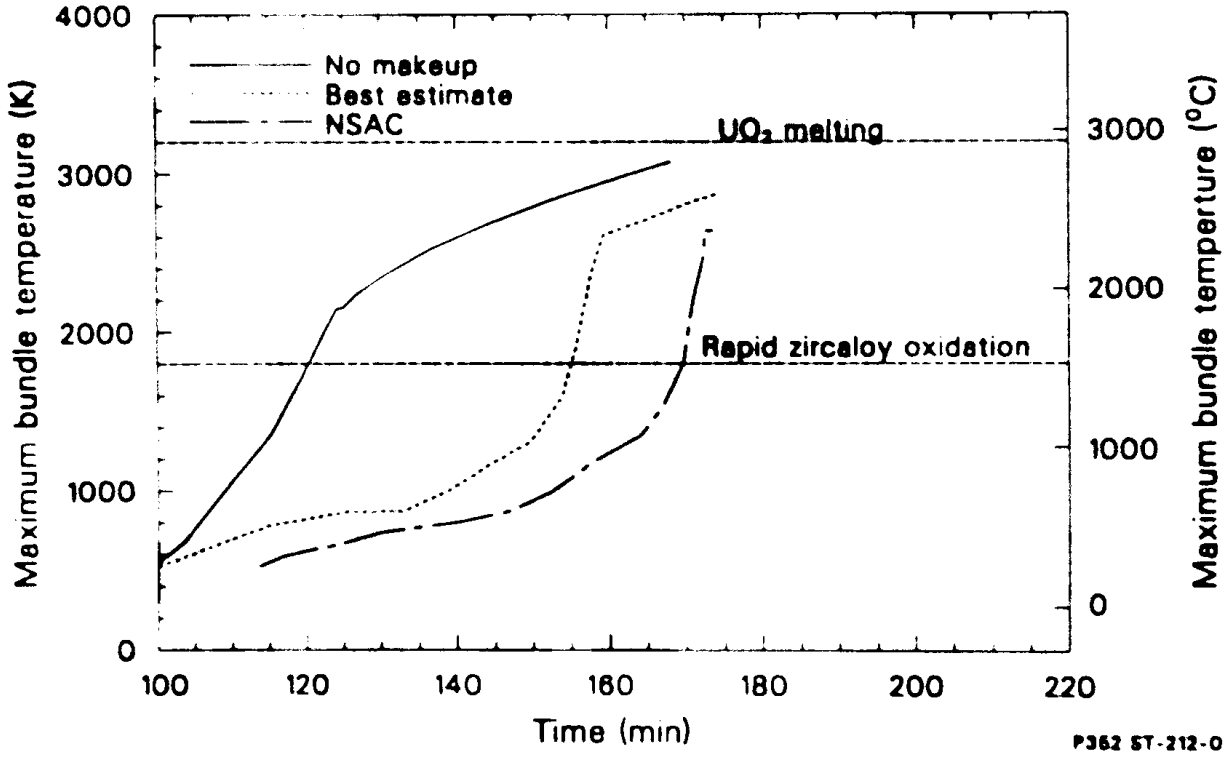

Figure 24. Summary of SCDAP calculations (assumed bounding cases for core liquid level and peak core temperatures).

continue flowing downward on the outer surface of the fuel rod. This process has been observed in separate-effects experiments. The molten material continues its downward flow until the temperatures of surrounding structures are sufficiently low to freeze the material or until it contacts water near the bottom of the core. Visual evidence suggests that the molten material flowed downward to the water near the bottom of the core, at least in the core center.

Separate-effects and in-pile integral-effects fuel behavior experiments provide the necessary data for understanding the zircaloy melting and fuel dissolution process. The end-state configuration of an electrically heated cluster of UO_2 fuel rods which experienced a heatup and melting transient similar to the SCDAP-predicted TMI-2 early uncovery case is shown in Figure 25.[22] Extensive cladding melting and relocation of the molten fuel rod material is evident. The relocated fuel rod materials result in nearly complete coolant flow blockage at the bottom fuel rod spacer grid. Larger-scale nuclear experiments conducted in the Power Burst Facility (PBF)[23,24] under varying core heatup conditions also demonstrate the significance of core material relocation and coolant flow blockage via clad melting and fuel dissolution. Flow blockages in the lower regions of the PBF test bundles were extensive, ranging from 70 to 95%.

The recent visual examination of the lower portion of the TMI-2 core confirms that core material relocation similar to that observed in separate-effects experiments occurred during the TMI-2 accident. Relocation of molten zircaloy and some liquefied fuel from the upper core regions would have resulted in a region of consolidated, previously molten material completely surrounding the fuel rods in the lower core region at or near the coolant interface. The configuration of the TMI-2 end-state lower core crust, as shown in Figure 8, suggests that the initial molten core material flowed downward to within approximately 0.7 m of the bottom of the core. The best-estimate core conditions during the period of initial core oxidation and fuel rod materials relocation between 150 and 160 min is shown in Figure 26. The location of the lower crust suggests

Figure 25. End-state condition of fuel rods from ESBU-1 experiment (reproduced from Reference 24).

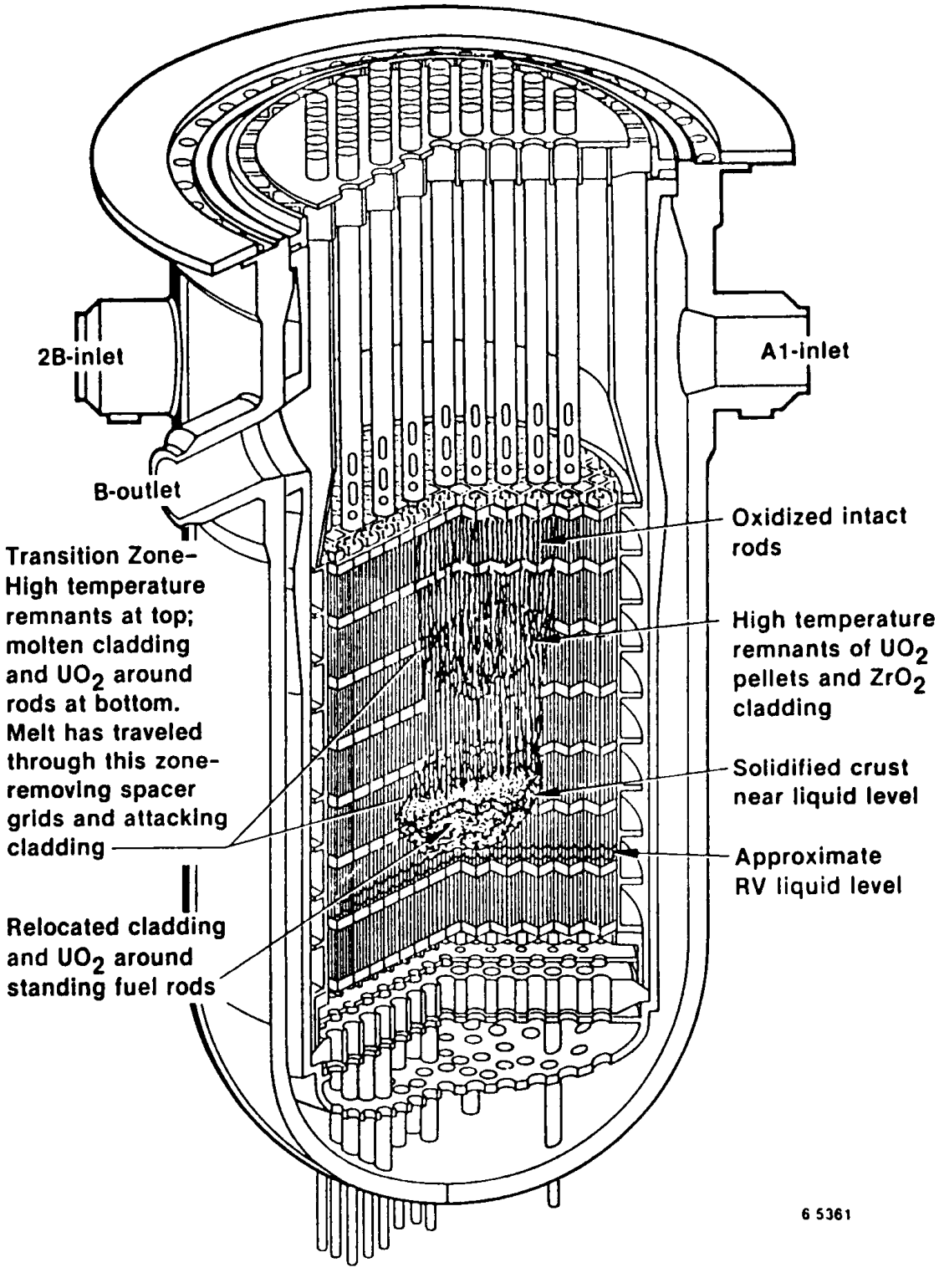

Figure 26. Estimated TMI-2 core damage configuration at 150 min, showing the initial relocation of core materials into the lower core region.

that the core liquid level during this time period was near or slightly below the second fuel assembly spacer grid location (approximately 38 cm from the bottom of the fuel).

Between 160 and 174 min, cladding temperatures near the top of the core and out near the core periphery are believed to have increased such that rapid oxidation of the cladding was initiated. Downward relocation of core materials would be expected, substantially increasing the size of the consolidated region of previously molten and encased fuel rods. As the core flow blockage formed near the core center, the steam flow would be diverted towards the periphery of the core, thus reducing the steam flow through the central core regions and providing enhanced cooling for the peripheral fuel assemblies. The reduced steam flow through the central core regions would limit the oxidation and hydrogen production in this region. The flow diversion, enhanced peripheral core cooling, and reduced hydrogen production above the core blockage region have yet to be reproduced by computer calculations.

By 174 min (just prior to the pump transient), core heatup analysis indicates that core peak temperatures probably exceeded 2400 K and may have reached fuel melting temperatures. The core configuration hypothesized for 174 min, just prior to B-pump transient, is shown in Figure 27. The consolidated region of relocated core material forms a region from 1 to 2 m in height, extending radially outward to near the core perimeter; i.e., 1 to 1.5 m in diameter. The presence of intact rod stubs below the region of previously molten core material confirms that core cooling was maintained below about 0.5 m. The lower crust configuration shown in Figure 27 is based on the end-state core configuration.

Damage to the upper fuel assembly grid plate (see Figure 3) may have been caused by the initial rapid core oxidation and convective transfer of heat to the grid structure. It is also noted, that the grid damage may have occurred later in the accident, as coolant was injected into the reactor vessel and the upper core (debris) was gradually quenched.

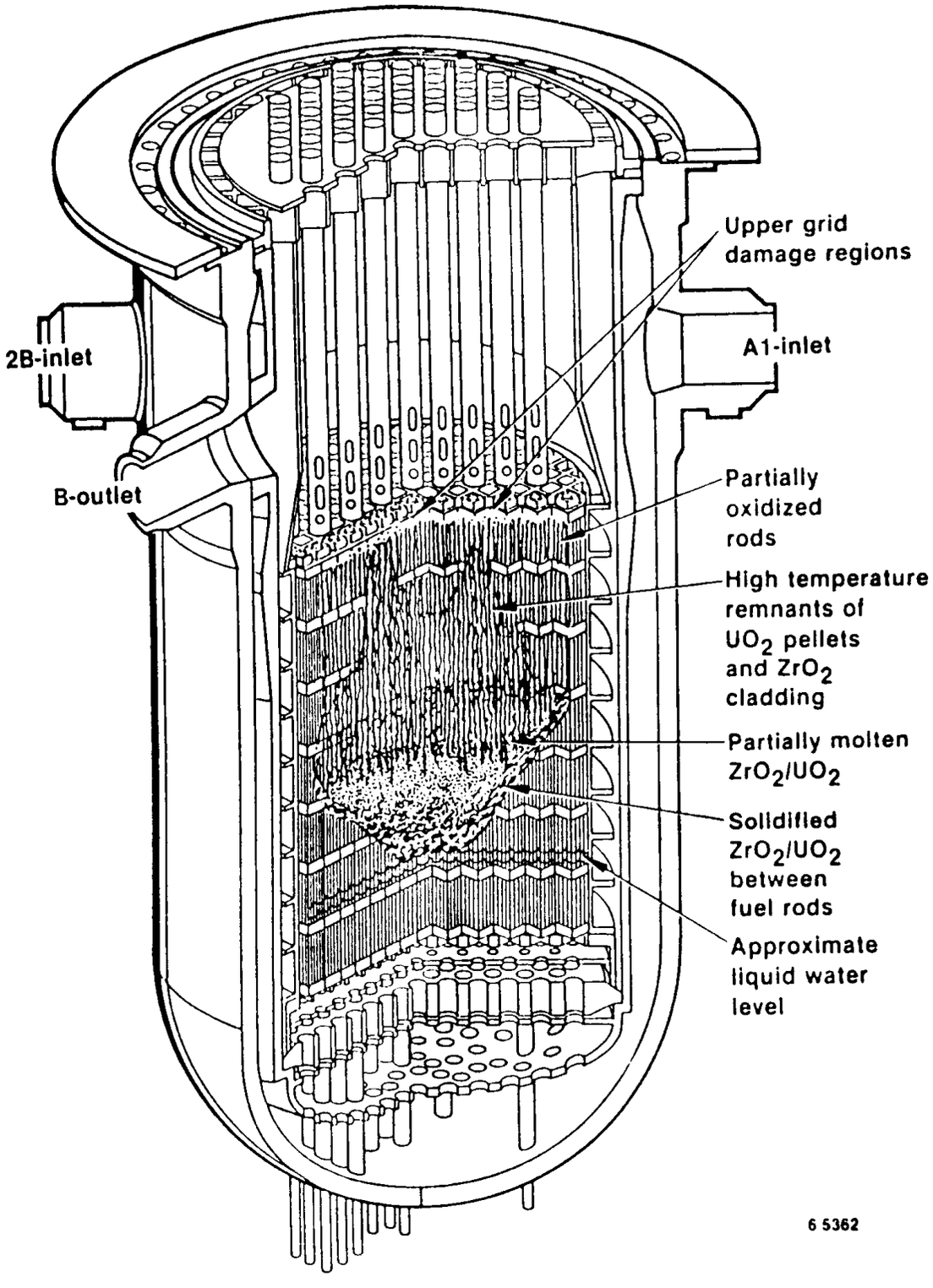

Figure 27. Estimated TMI-2 core damage configuration at 174 min, just prior to the pump transient, showing extensive relocation of core materials into the lower core regions.

Detailed thermal hydraulic analysis of hydrogen production, steam flow, and associated energy transfer to the upper plenum region have yet to be completed to evaluate and assess the validity of either hypothesis.

Thus, the available data and supporting analysis suggest that core damage by 174 min was extensive. The center regions of the core were blocked, and a consolidated region of at least partially molten core material extended upward and outward for 1 to 2 m. As will be shown in the following section, the consolidated core material continued to heat up even though the reactor vessel coolant inventory was replenished.

3.3 Degraded Core Heatup (174 to 224 Min)

During the 50 min following the pump transient, the TMI-2 data and supporting analysis indicate that the severely degraded core continued to heat up in spite of coolant addition to the reactor vessel. Analysis of the thermal response of the degraded core configuration is the key for interpretation of on-line data and estimating the condition of the core just prior to failure of the support crust that permitted relocation of molten core material into the lower plenum at about 224 min.

3.3.1 Impact of the Pump Transient on the Degraded Core

The first significant coolant addition to the reactor vessel occurred at approximately 174 min when the 2B coolant pump was turned on. Even though the pump continued to run for approximately 19 min, significant flow duration in the B-loop hot leg was measured to be less than 15 s, as shown in Figure 28. Original estimates suggest as much as 28 m^3 (1000 ft^3) of water may have been displaced into the reactor vessel.[21] However, due to the extensive core flow blockage, flow through the central regions of the degraded core was probably not appreciable.

The coolant delivery to the reactor vessel rapidly pressurized the reactor system, as noted earlier in Figure 23. The resulting thermal-mechanical forces are believed to have fragmented the highly

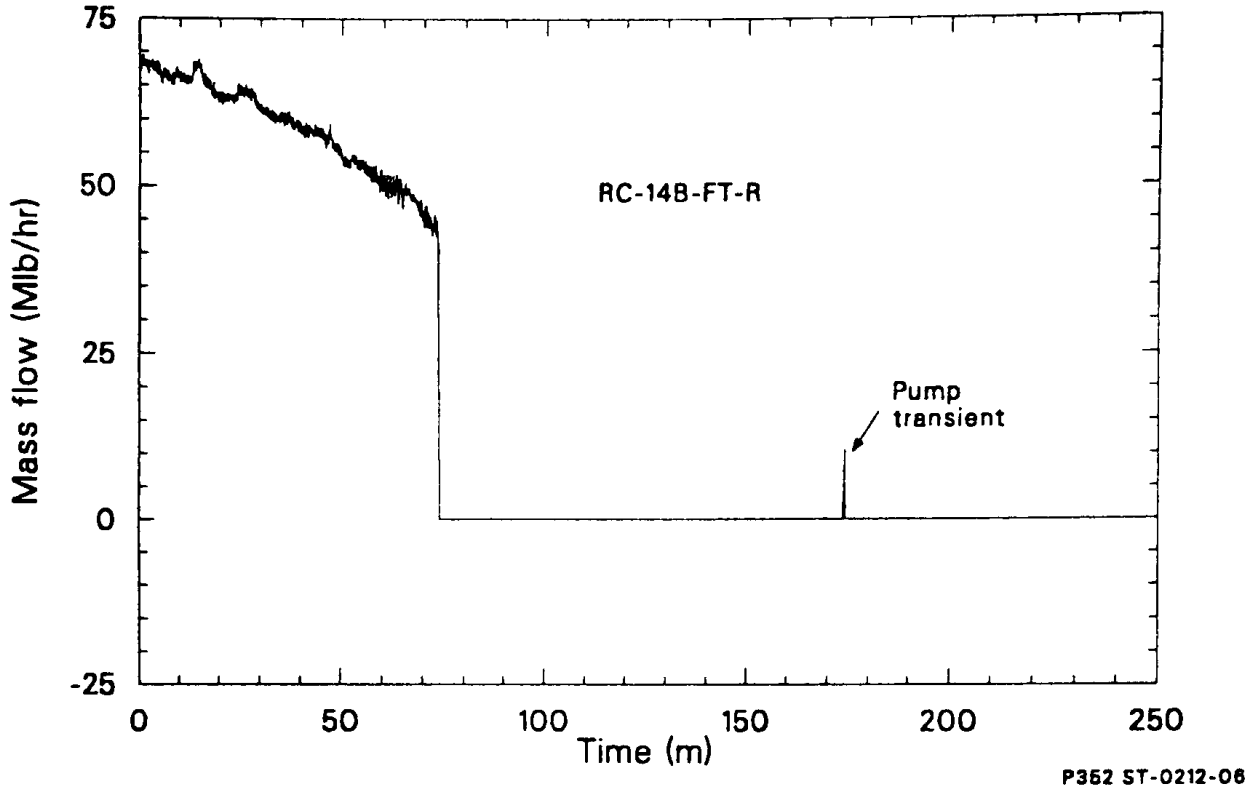

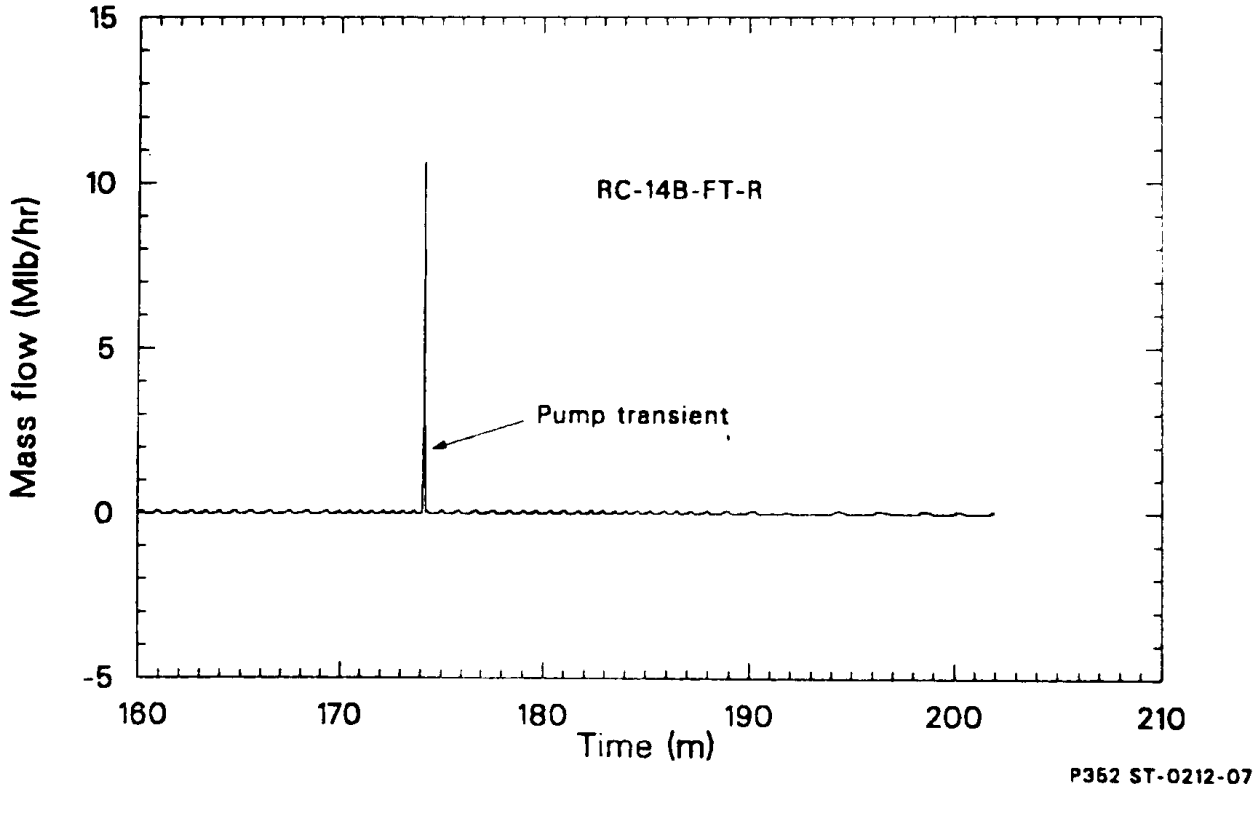

Figure 28. Measured TMI-2 hot leg flow resulting from the B pump transient initiated at 174 min.

oxidized fuel rod remnants in the upper core region, forming a rubble bed on top of the relocated core materials in the center region of the core. Thus, the core configuration just after the pump transient is shown in Figure 29.

Coolant flow into the reactor vessel at the time of the pump transient was substantiated by both the in-core thermocouple alarm data and the source range monitor response. The locations of those core thermocouples that were cooled (alarmed on-scale) as a result of the pump transient are shown in Figure 30. Also shown in Figure 30 are best-estimate contour lines showing the end-state configuration of the lower crust (the same as that shown in Figure 7) as determined via core bore inspection data.[9] Notice that only those thermocouples generally on the periphery of the lower core crust were cooled. Thermocouples towards the center of the core would have been severely damaged, probably melted, and their relocated junctions located within the higher-temperature regions of the consolidated core material. The thermocouple alarm data suggest that coolant flow through the core occurred only at the core periphery which is consistent with the damaged core configuration as shown in Figure 27. Subsequent alarm data between 180 and 200 min show that all the peripheral core thermocouples initially cooled by the pump transient again alarmed off-scale high prior to emergency core coolant injection at 200 min.

The source range monitor response also indicates reactor vessel coolant addition as a result of the pump transient and subsequent boildown (see Appendix E). The rapid decrease in SRM response at 174 min has been duplicated via neutronic analysis by assuming that coolant filled the core and downcomer regions with a degraded core configuration similar to that shown in Figure 27.[25]

Analysis estimating steam production within the RCS[26] from 192 to 197 min indicates that heat transfer from the core is less than nominal decay power, thus suggesting that the core is continuing to heat up during this time period.

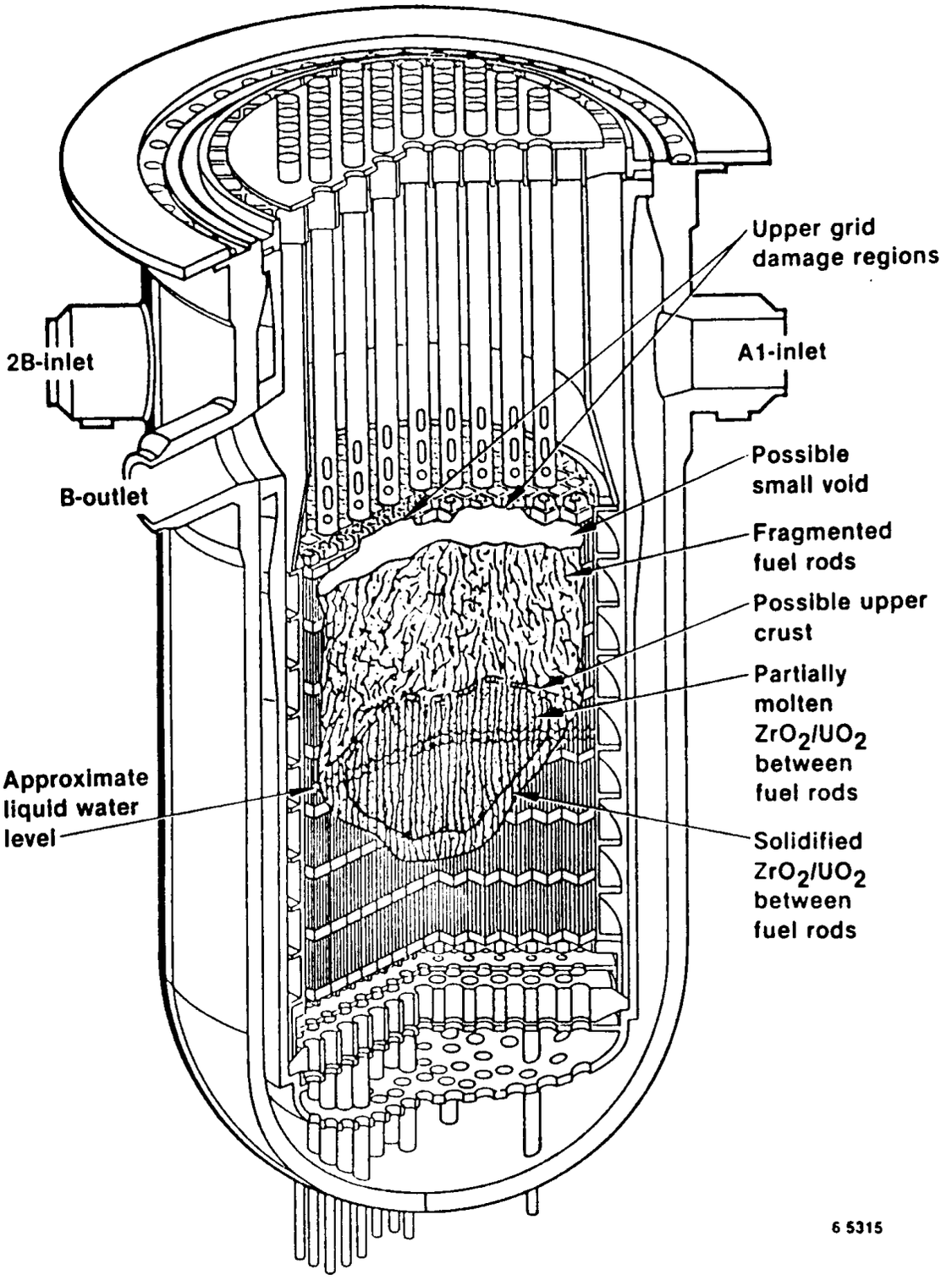

Figure 29. Estimated TMI-2 core configuration at 175 to 180 min, after the pump transient, showing the upper debris bed formation.

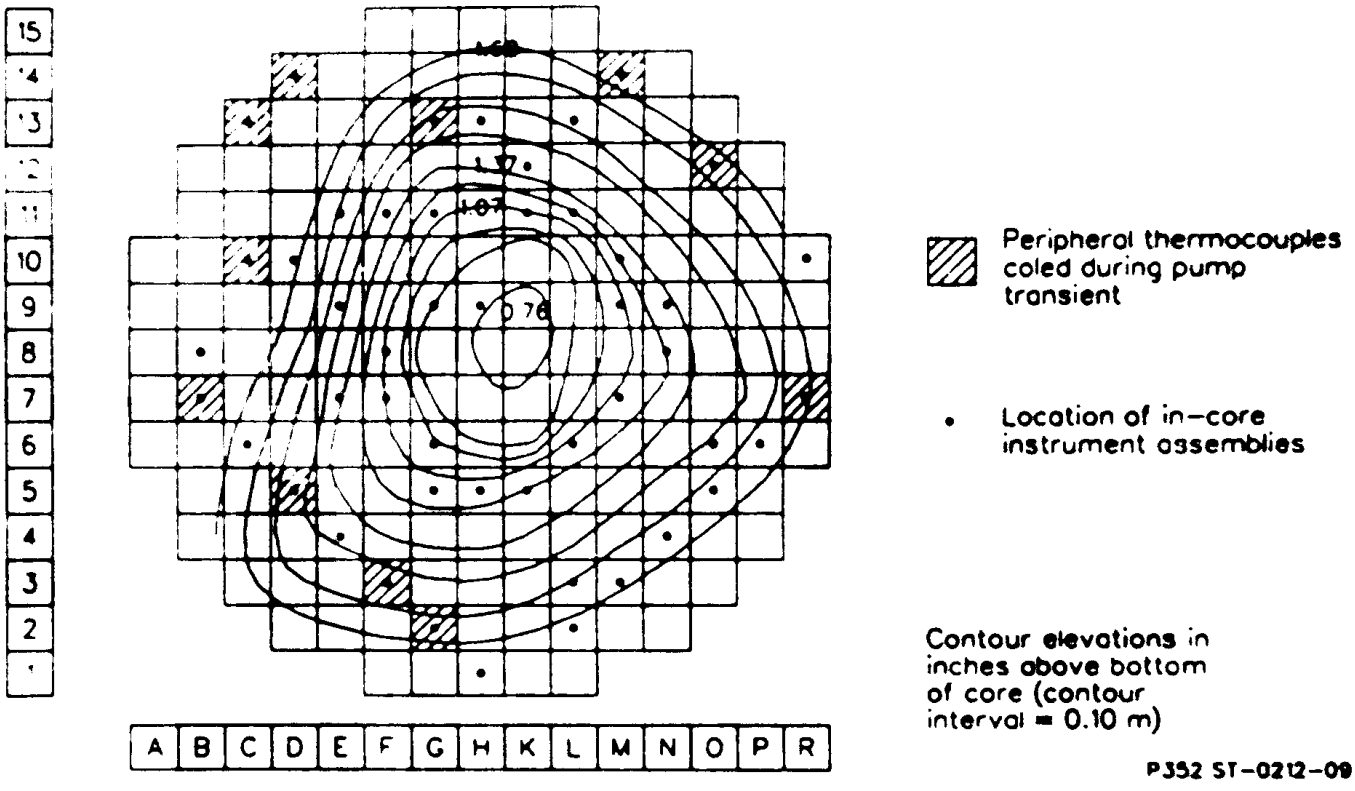

Figure 30. Overlay of TMI-2 in-core thermocouple positions that were cooled by the pump transient and the end-state contour of the lower molten zone crust.

There is evidence from the upper debris bed sample examination that the coolant mixed the upper debris bed and upper consolidated core (see Appendix A).[7] Thermal-hydraulic analysis of the upper debris bed cooling during this period has yet to be done.

3.3.2 High Pressure Injection from 200 to 217 Min

At 200 min, the high-pressure injection system was actuated for approximately 17 min. Reactor system analyses[26] to interpret the RCS thermal-hydraulic data (hot and cold leg temperatures, system pressure, and pressurizer response) indicate that the reactor vessel filled by 207 min. A significant contribution to the reactor vessel coolant inventory is estimated to have come from coolant drainage from the pressurizer as the RCS pressure decreased. The analyses also indicate that the downcomer and cold legs filled with steam and hydrogen as a result of the initial high pressure injection and RCS depressurization.

Estimates[26] of the RCS steaming rate during this period also substantiate that core heat transfer was less than decay heat generation, indicating continued core heatup.

3.3.3 Degraded Core Heatup

The degraded core configuration as shown in Figure 29 is difficult to cool due to (a) little or no flow through the consolidated core material, (b) the high thermal resistance of the U-Zr-O ternary oxide, and (c) the thermal capacitance of such a large consolidated mass. Consequently, the central regions of the consolidated core material could continue to heat up due to decay heat for some time despite the potential for cooling at the periphery.

Thermal analyses of this basic configuration were conducted to provide insight relative to timing of core heatup and potential core failure mechanisms.[27] The core configuration assumed for the one-dimensional,

degraded core thermal analysis consisted of three regions, as shown in Figure 31. The dimensions and composition of the three degraded core regions were based on initial examination results of the TMI-2 upper core debris material and examination results from independent severe fuel damage experiments. As shown in Figure 31, Region A at the bottom of the solid structure represents a consolidated mass of relocated zircaloy surrounding unoxidized fuel rods. Region B represents a ternary U-Zr-O oxide surrounding partially oxidized fuel rods. Region C represents the upper rubble bed comprised primarily of UO_2 and ZrO_2. The initial axial core temperature profile was based on SCDAP-calculated temperatures from Reference 19 at 175 min, just after the 2B pump transient. The upper and lower surfaces of the debris bed were assumed to radiate to heat sinks representative of the steel masses in the upper and lower plenums, initially assumed to be at 1200 and 750 K respectively. No water was assumed to be present in the core.

The calculated temperature profiles for the degraded core versus time are shown in Figure 32. During the 50-min interval between 174 and 224 min, the temperatures of both lower and upper heat sinks approached 1400 K, with surface temperatures about 100 K higher. Most of the lower, zircaloy-rich layer remained below the zircaloy melting point. The ceramic-rich mid-core region, however, was predicted to be mostly molten (temperature greater than 2800 K) by 224 min. The average temperature in the rubble region at 224 min was about 2600 K, below the melting point of either ZrO_2 or UO_2.

The following conclusions are based on the analysis:

1. The central part of the large, consolidated region could be molten by 224 min, and

2. Melt-through of the lower supporting crust is not likely if the bottom crust is rich in metallics (zircaloy or iron).

Clearly, the above thermal analysis is very simplified and does not account for the known configuration of the degraded core or radial heat

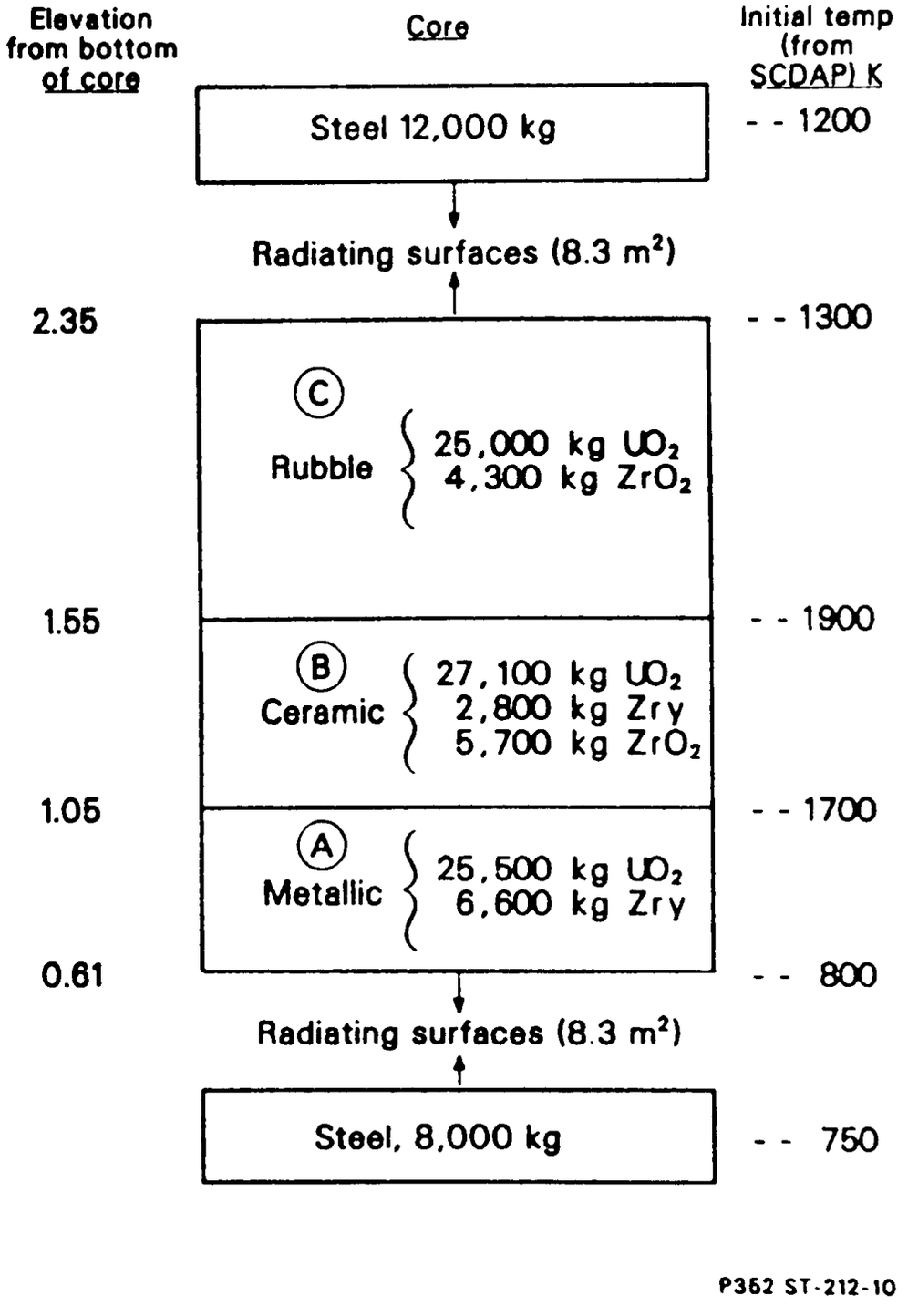

Figure 31. TMI-2 core configuration used for degraded core heatup analysis.

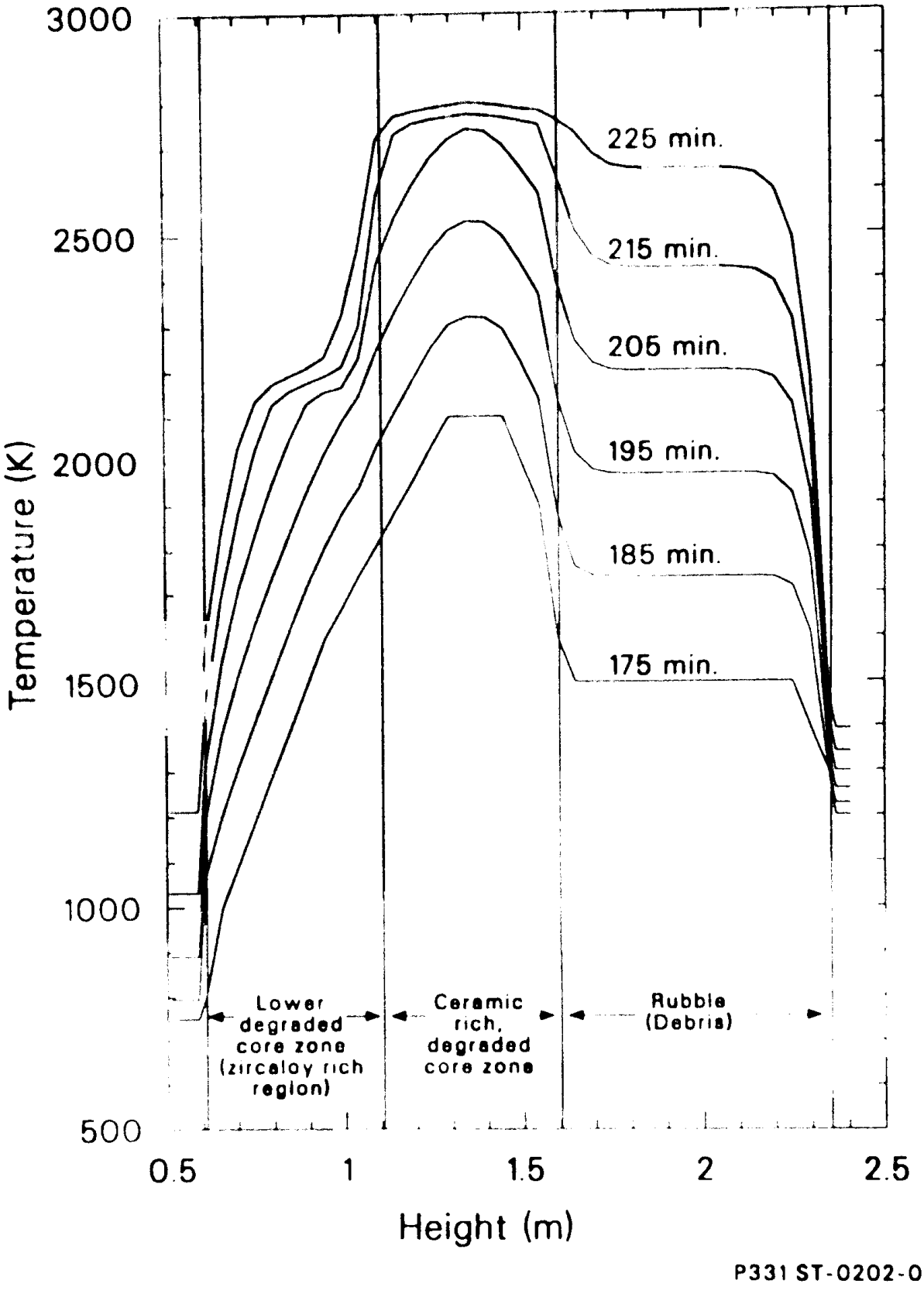

Figure 3?. TMI-2 degraded core thermal response from 175 to 224 min.

transfer at the core periphery. In addition, the analysis did not model the convective heat transfer within the molten core region. Pool boiling experiments using water with internal heat generation show turbulent mixing in the upper pool regions, while the lower region is characterized by a more random motion resulting in much less mixing.[26] Under such boiling conditions, the energy within the pool would be transferred predominantly upward. However, the hydrodynamics within the TMI-2 molten core region are more complex than the water experiments, primarily because the core materials involved have significantly different densities and melting points. Also, the pool configuration is changing with time. Thus, the thermal response of the molten core materials and the formation of the surrounding crusts are not presently well understood. However, it is likely that (a) the estimated temperature gradient near the bottom of the consolidated material from the simplified analysis may be significantly overpredicted and, therefore, the lower core crust thickness may be greater than estimated; and (b) the estimated energy transferred to the upper regions of the consolidated material may be significantly greater than indicated by the above analysis, which could significantly reduce the estimated thickness of the upper crust.

Additional analytical work will be necessary to evaluate (a) uncertainties in the convective heat transfer and physical interaction between the molten core materials within the expanding molten zone, and (b) a more realistic estimate of the heat transfer at the core periphery (sides and upper debris bed) on the thermal response of the molten core region.

3.3.4 Core Configuration Just Prior to Core Relocation

The hypothesized core configuration just prior to failure of the crusts supporting the molten core materials at 224 min is shown in Figure 33 and follows from (a) the configuration of the core prior to 174 min, (b) analysis and interpretation of the plant neutronic and thermal-hydraulic measurements recorded during 174 to 224 min (as discussed above), and (c) the estimated thermal response of the large consolidated

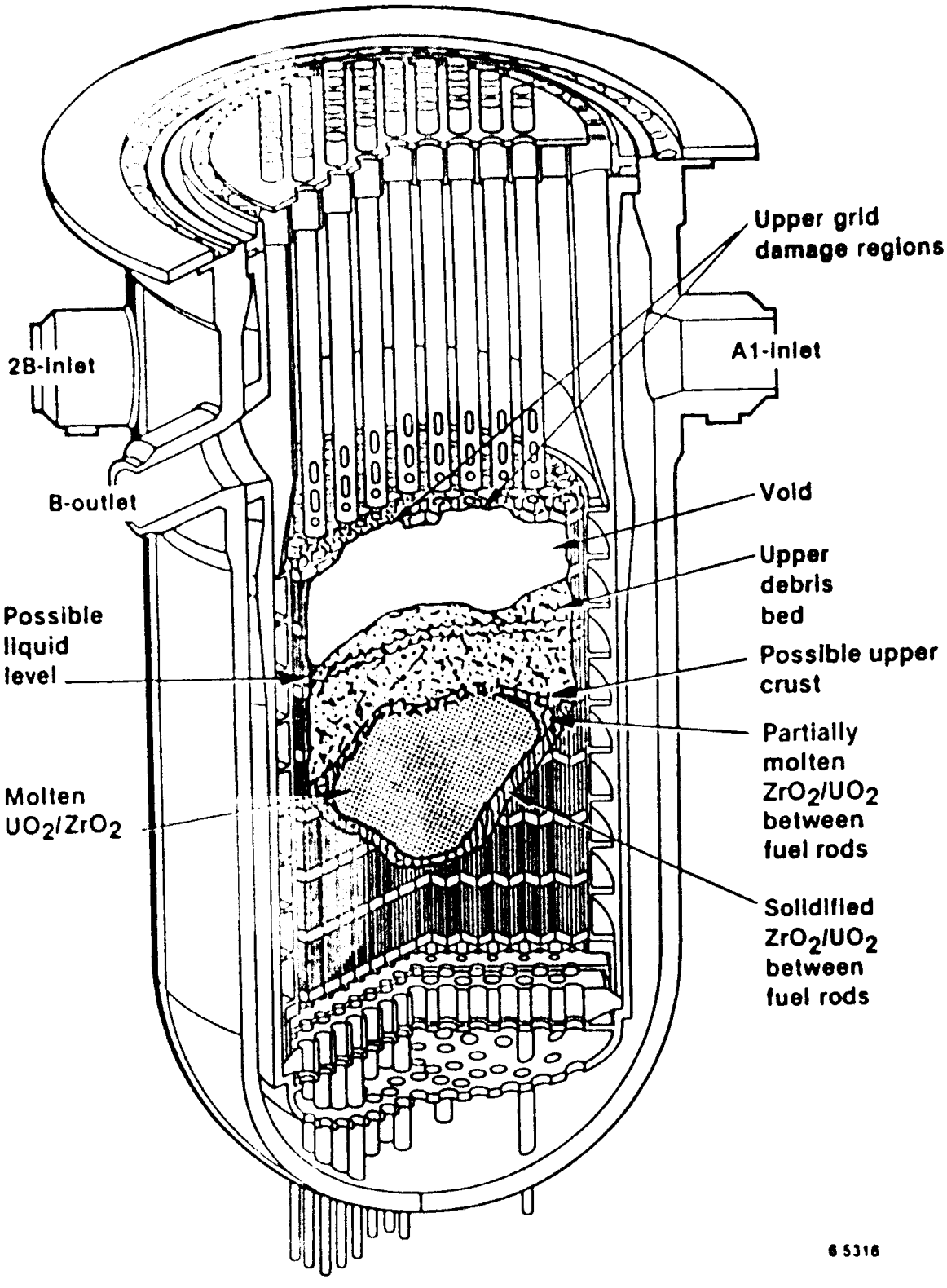

Figure 33. Estimated TMI-2 core configuration just before the crust failure and relocation at 224 min.

region of core material. Most of the consolidated core material is estimated to be molten, and the core liquid level is estimated to be above or near the top of the core. In general, heat transfer from the core occurs only at the periphery of the core (i.e., solid structure) and is less than the decay heat generation. The central region of consolidated core material continues to slowly heat up and, as discussed in the next section, failure of the supporting crust that contained the molten material within the original boundary of the core occurred between 224 and 226 min.

3.4 Core Relocation (224 to 230 Minutes)

Selected data recorded during the accident support the conclusion that a major reconfiguration of the core occurred during this period. Visual inspections of the core, CSA, and lower plenum substantiate that a major relocation of molten core material occurred and provide substantive information regarding the failure location of the supporting/confining crust. Supporting analysis has identified several possible mechanisms controlling crust failure and provides initial estimates of the potential damage to the CSA and lower plenum structures. This information is summarized in the following sections, as it provides the basis for inferring the core configuration when molten core materials relocated into the lower plenum.

3.4.1 Core Relocation Data

3.4.1.1 Reactor System Data. The SRM response, RCS pressure response, and measured cold leg temperatures all indicate that a global change in the core and reactor vessel conditions occurred between 224 and 226 min. Their responses are shown in Figure 34.

The SRM directly measures neutron leakage from the core region and is a direct indicator of changes in the core configuration. The SRM count rate increased approximately 100% in less than 2 min (between 224 and 226 min) and then indicates a normal decay profile. Previous neutronic data and analysis has confirmed the existence of between 5 and 20 metric

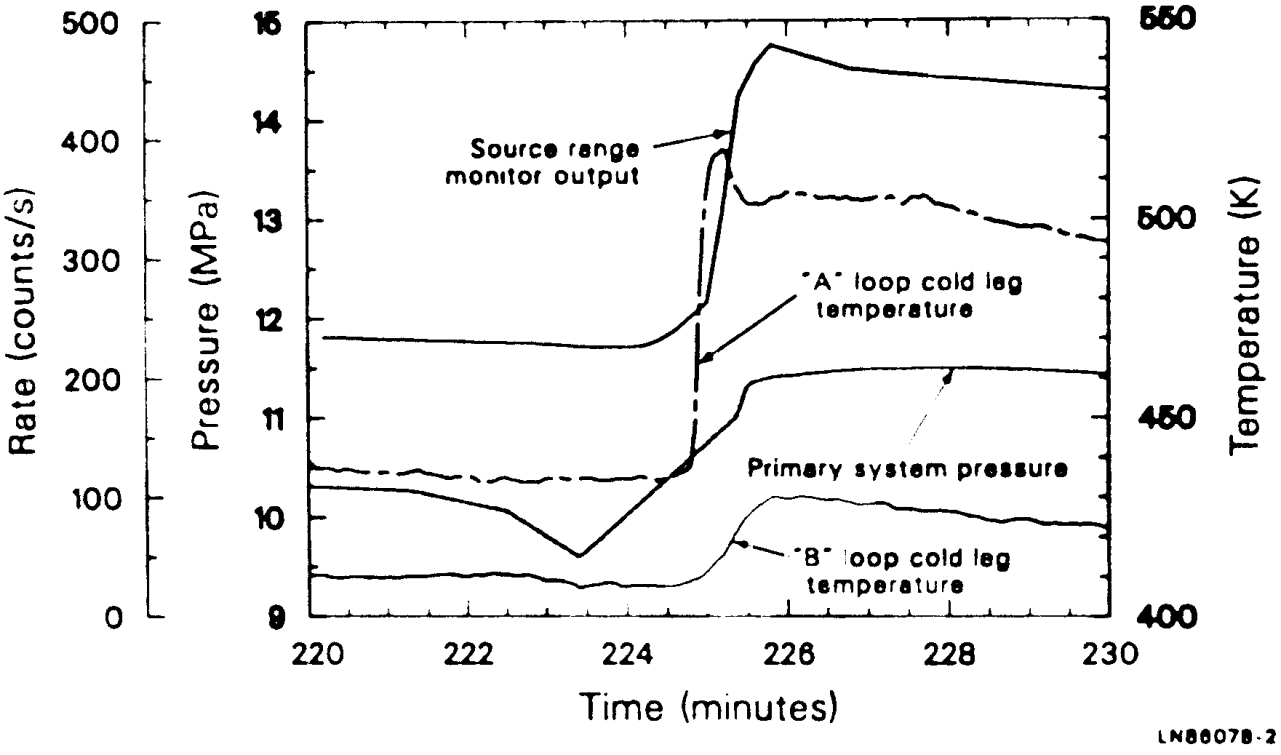

Figure 14. Overlay of TMI-2 SRM output, RCS pressure, and cold leg temperature response showing rapid changes at around 224 min.

tons of fuel in the lower plenum.[11] Recent analysis of the SRM response indicates that several tons (10 to 20) of molten core material relocating into the lower plenum would cause the observed increase in SRM output between 224 and 226 min, since less neutron attenuation exists in selected pathways from the lower plenum to the SRMs compared to the core-to-SRM neutron attenuation.[25]

The measured cold leg temperatures shown in Figure 34 are also seen to increase rapidly, nearly coincident with the abrupt increase in the SRM response. The thermal-hydraulic mechanisms causing the rapid and sustained cold leg temperature response have yet to be evaluated. The A-loop temperature increased to its peak value in less than 20 s, while the B-loop temperature reached its peak value in approximately 1 min.

The RCS pressure is also seen to rapidly increase between 224.5 and 225.5 min. The magnitude and timing of the RCS pressure response indicates that significant fuel/coolant thermal interaction and rapid steam generation occurred over a relatively short time. Subsequent, but significantly reduced, heat transfer from the relocated core material and resultant steam generation maintained the RCS pressure for several minutes even though the PORV was open (see Figure 23). There is no evidence of an energetic molten fuel/coolant interaction such as that characteristic of a steam explosion.

During the 224- to 226-min period, many of the lower level in-core SPNDs alarmed off-scale high for the first time during the accident. In addition, for many of the SPND locations (particularly those located near the center of the core), alarms were recorded at all instrument levels. The SPND alarm activity within the 224- to 226-min interval is summarized in Figure 35 and suggests that the SPNDs were being subjected to high temperatures at this time.

The relative timing of the SPND alarms provides supportive information relative to the core region where the molten material flowed from the core into the lower plenum. The first alarm signals for the SPNDs and the

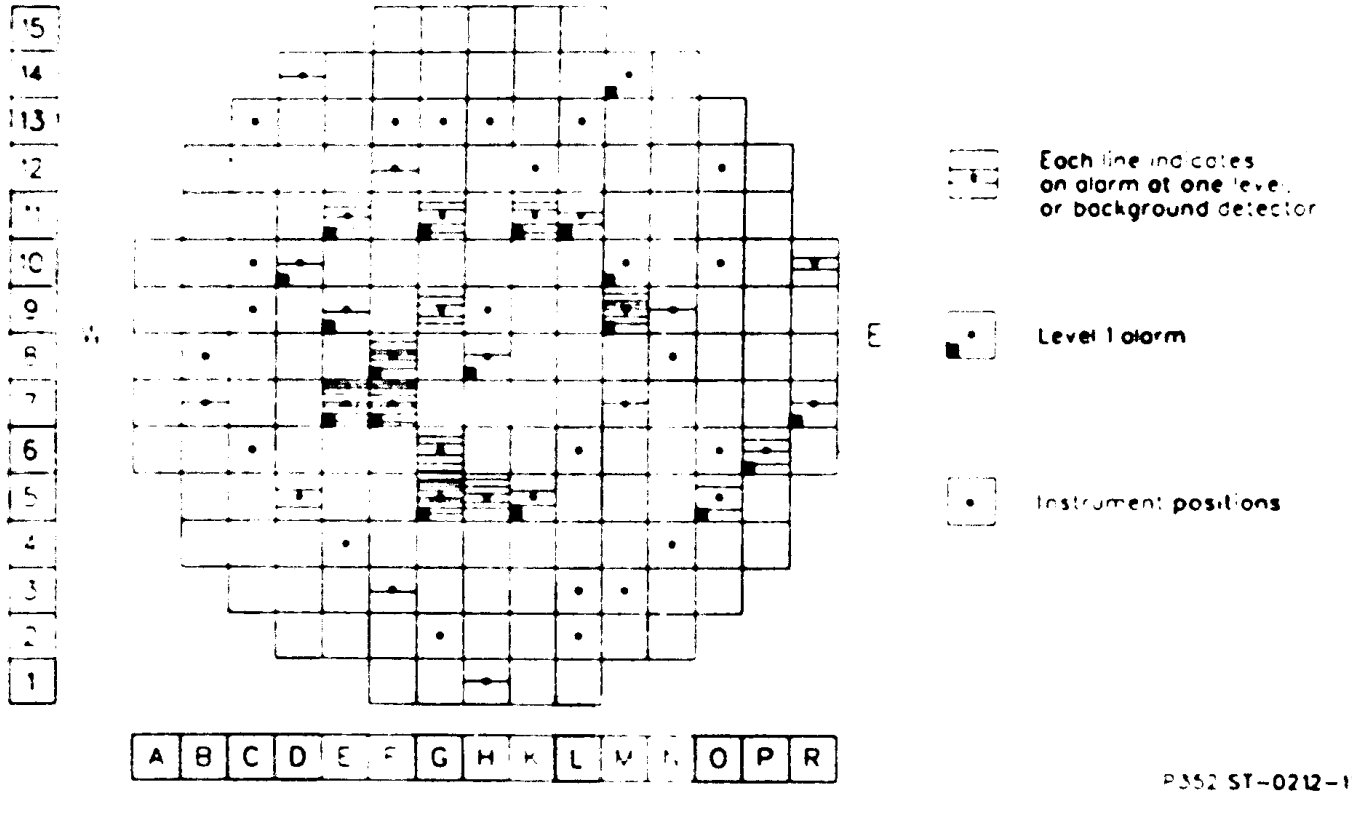

Figure 35. Summary of data from IMI-2 SPND that alarmed during the 224- to 226-min core relocation period.

thermocouples occurred in the R7 and P6 fuel assemblies located in the southeast quadrant of the reactor vessel, as shown in Figure 36. Subsequent SPND alarms progressed towards the core center but showed a core-wide bias towards the east quadrant of the vessel.

3.4.1.2 End-State Core and Lower Plenum Configuration. Additional information regarding the crust failure location and region within the core where the molten material relocated into the lower plenum is present in the end-state configuration of the top crust of the solid structure of previously molten core material and in the locations within the CSA where previously molten material has frozen in place. These data are discussed below.

A core cross section showing the end-state core configuration through the Row 6 fuel assemblies is shown in Figure 37. Note that at the core periphery, in fuel assemblies O, P and R, the upper surface of the molten core zone (determined from core probe data) is significantly depressed and, in fact, is lower than the estimated lower core crust as projected from the coutour surface shown in Figure 7. This localized depression of the crust in the east quadrant suggests crust failure in this location. A similar localized depression in the upper crusts at fuel assembly locations P7 and P6 was also observed in the core cross section map through the Column P fuel assemblies.

The lowest point of the upper debris bed was also located in the area just above the P5 and P6 fuel assemblies (see Figure 5). Failure of the supporting crust below this location would allow localized slumping of the upper debris material.

The visual inspection of the CSA during the core boring operations also provided supporting information that the crust failed in the east/southeast quadrant of the reactor vessel. As noted previously, significant amounts of previously molten material in the CSA regions were observed only in the east quadrant of the reactor vessel (Figure 10).

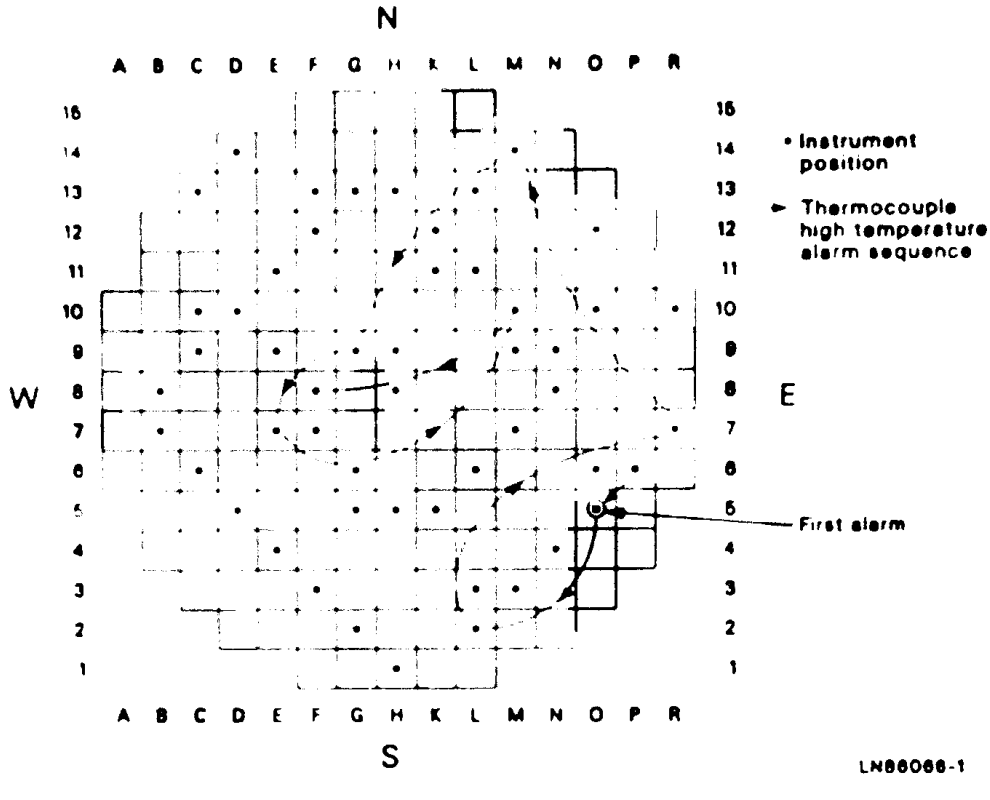

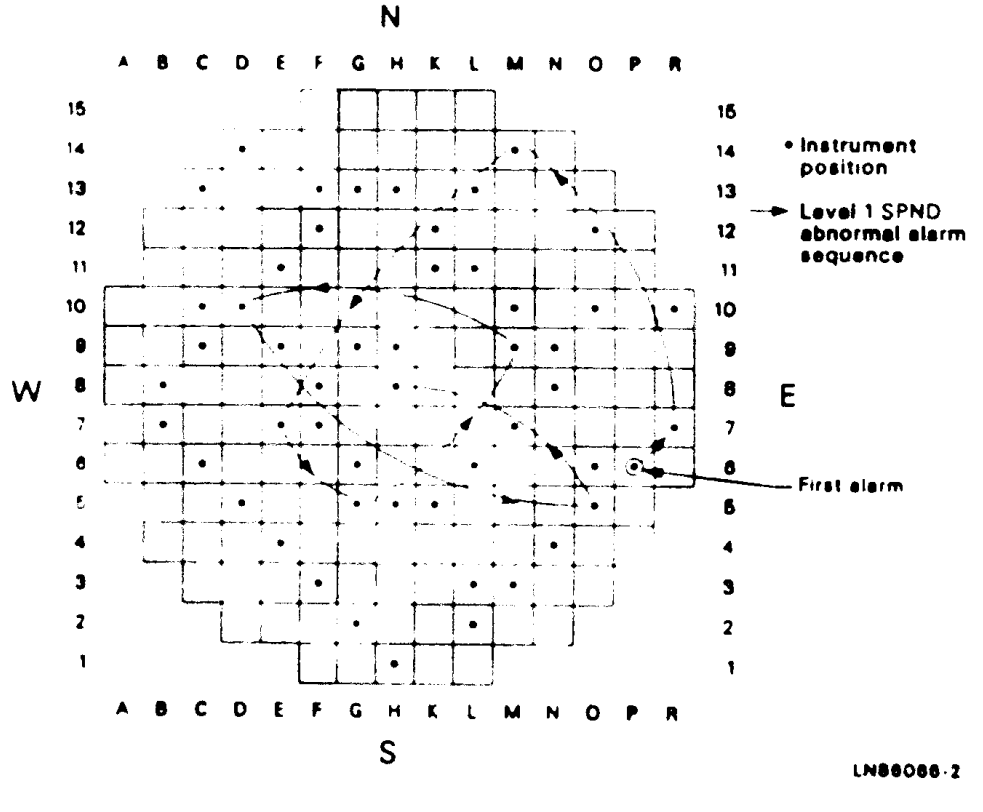

Figure 36. Relative timing of the TMI-2 in-core instrument alarms between 224 and 226 min.

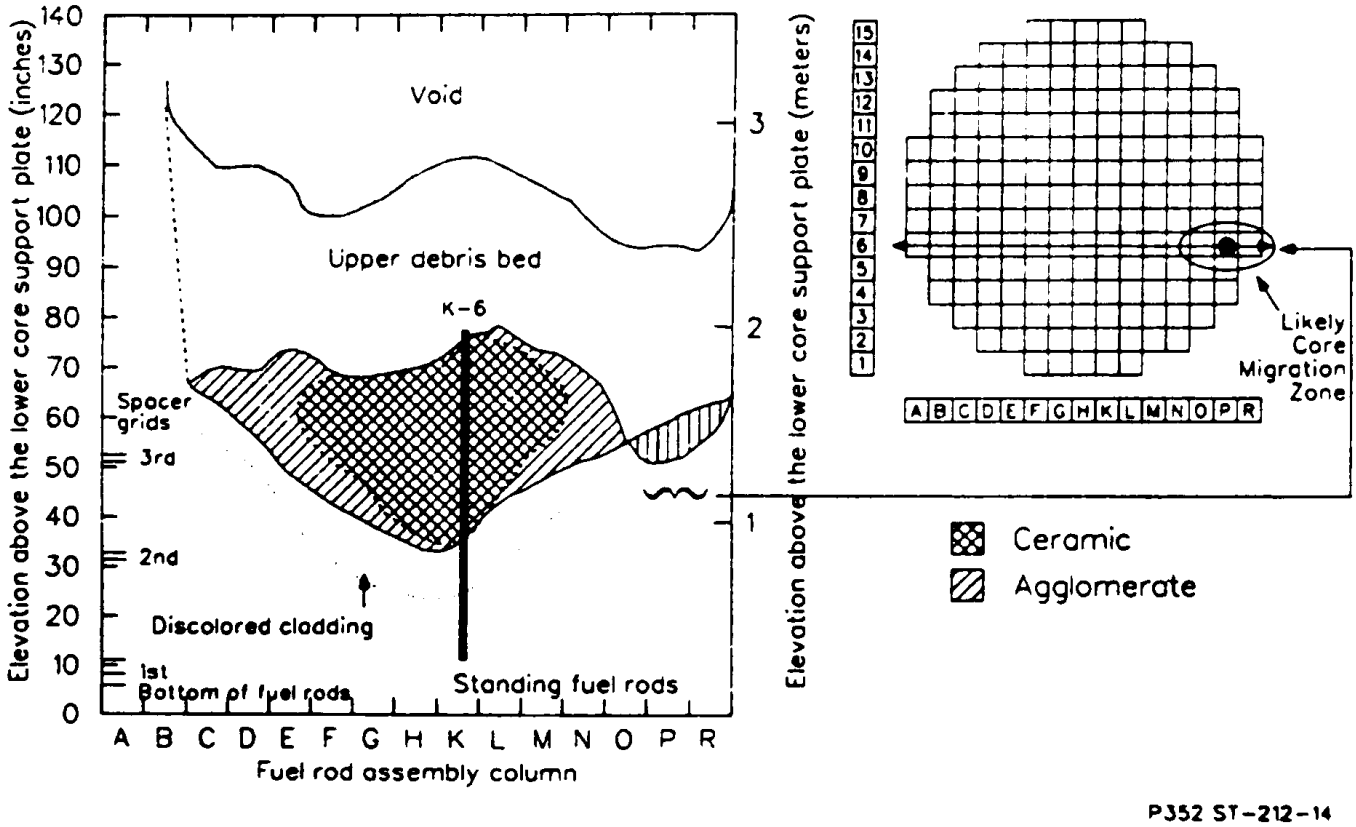

Figure 37. Vertical cross section of TMI-2 end-state core configuration through the Row 6 fuel assemblies.

Furthermore, what appears to be the most severe interaction of molten core material with the lower core support structures is observed beneath the 07 fuel assembly.

In summary, the best-estimate end-state configuration of the degraded core, the relative timing of the in-core instrument alarms, and the inspection of the CSA region all indicate core failure in the southeast quadrant of the reactor vessel in a general area, as shown in Figure 37.

3.4.2 Crust Failure Mechanisms

Several core failure mechanisms have been hypothesized and evaluated in recent analytical studies.[26-28] The most likely failure mechanisms are (a) thermal-induced failure of the upper crust as the consolidated core material continued to heat up, thus increasing the size of the central molten region; (b) mechanical stress on the crust due to pressure differences between the molten interior and exterior of the supporting crust induced by rapidly changing RCS pressures; and (c) possible interactions between the supporting crust of degraded core materials and the core former wall at the core periphery.

It is not possible at this time to select a best-estimate crust (or core) failure mechanism from among those cited above. The various mechanisms will be evaluated and considered against the available data from the sample examination and defueling operation. These data should help clarify (a) whether or not the top crust was, in fact, the melt front or interface between the upper debris and the molten material that may have existed during the degraded core heatup from 175 to 224 min; (b) the extent of the core directly affected by relocating molten materials; and (c) possible damage to the CSA and lower plenum structures.

3.4.3 Damage to the CSA, Lower Reactor Vessel, and Instrument Penetrations

Visual inspection of the CSA indicated that the structure did not suffer significant global damage. Some discoloration of the structures was

noticeable, and some minor damage to the support posts between the grid forging and flow distributor plate was discernible below the 07 fuel assembly. Thermal analysis to estimate the heatup of the CSA structures resulting from the flowing core material [28] indicates that the CSA structure temperatures probably did not exceed 1000 K.

The potential chemical interactions between the core materials and the stainless steel CSA structures have been investigated.[29] This investigation indicates that the stainless steel CSA structures would have been significantly damaged if they had come in contact with molten zircaloy for a significant time. However, because the core material relocated rapidly and little metallic zircaloy has been found in the lower plenum material, no significant chemical attack of the CSA structures would be expected, consistent with the visual examination.

Thermal analyses have also been completed to estimate possible damage to the reactor vessel lower head and the in-core instrument assemblies in the lower plenum regions.[30] The instrument penetration tubes were modeled as shown in Figure 38 to evaluate the tube thermal response versus size, physical composition, and temperature (ceramic versus metallic) of adjacent debris particles. The vessel analysis assumed energy equilibration between the relocated core material and the vessel wall below the debris. Major findings from the analysis include:

- Melt failure of the Inconel instrument penetration tubes is possible due to attack by either solid heat-generating ceramic or molten metallic debris followed by stable plugging of the failed instrumentation tubes by freezing of the molten material.

- The stainless steel reactor vessel liner may have experienced eutectic melting by zirconium-bearing melt debris. However, melt failure of the lower reactor vessel head is not predicted.

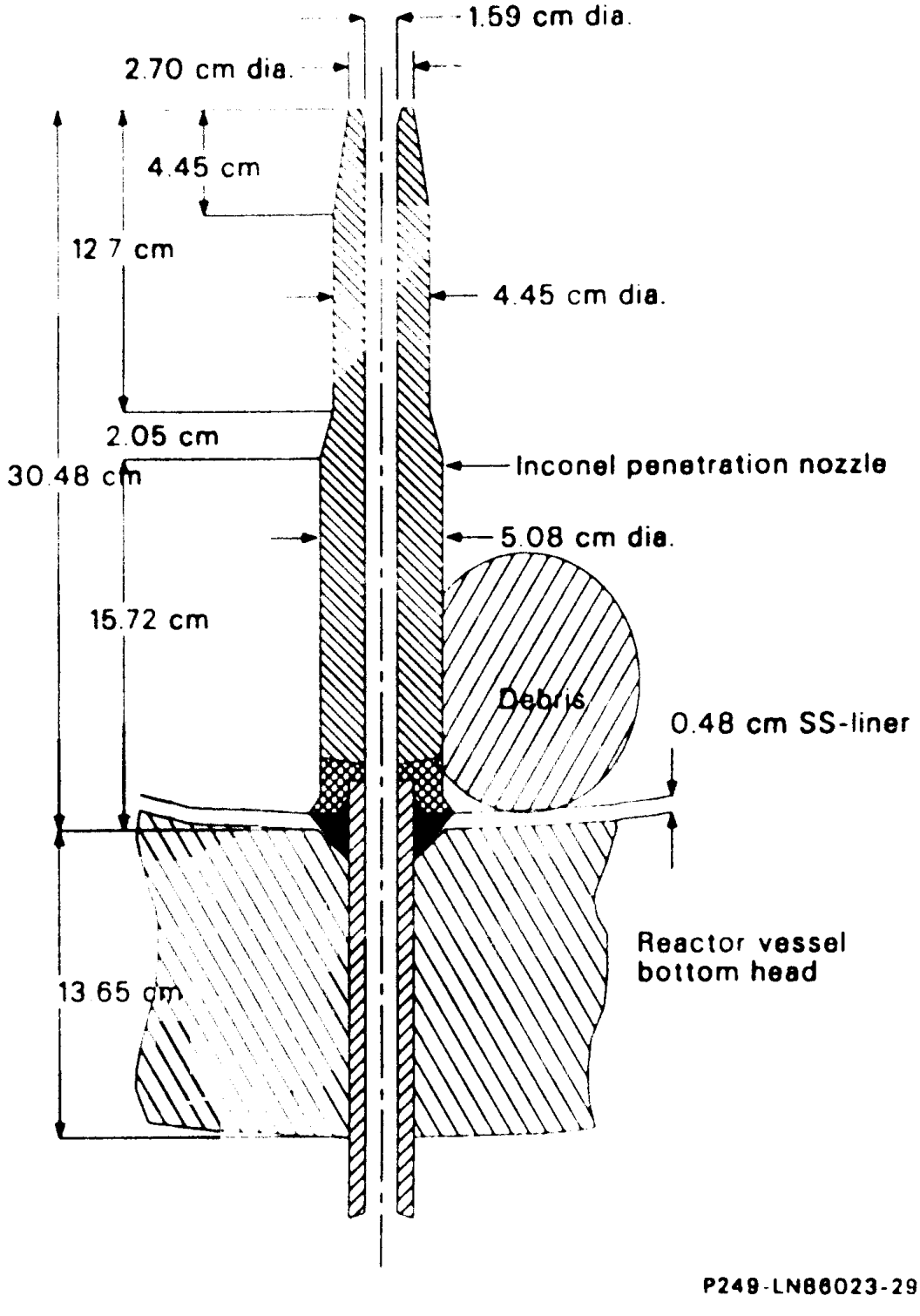

Figure 38. Configuration of TMI-2 instrument assembly at vessel wall penetration used for thermal analysis.

3.4.4 Estimated Core Configuration During the Core Relocation Period

The above data and supporting analyses have been used to develop the best-estimate core configuration during the core relocation event, as shown in Figure 39. The core failure location is hypothesized to be near the top of the supporting crust near the core periphery. The reactor vessel liquid level at the time of crust failure and relocation was near or above the top of the upper debris bed. Migration of the core materials to the lower plenum was rapid (as discussed in Section 3.4.1), with most of the material relocating in less than 1 min. Damage to the CSA structures and the lower plenum head appear to be minimal; however, melting and refreezing (plugging) in the instrument penetration nozzles is predicted.

The core damage progression scenario presented in this section provides a best-estimate interpretation of the TMI-2 data to date. As noted in the Introduction, the scenario is not complete, particularly regarding the details of the degraded core heatup after 174 min, failure of the crusts supporting the consolidated, molten core material, thermal-hydraulic interaction between the molten core material and the vessel coolant, and the damage to the reactor vessel lower head. Uncertainty in each of these areas must be resolved for optimum use of the TMI-2 data towards resolving important safety issues relative to core damage progression and vessel failure. However, interpretation of the accident up to 174 min is fairly complete and provides a baseline interpretation for participants of the TMI-2 Standard Problem and for assessing the fission product data summarized in the next section.

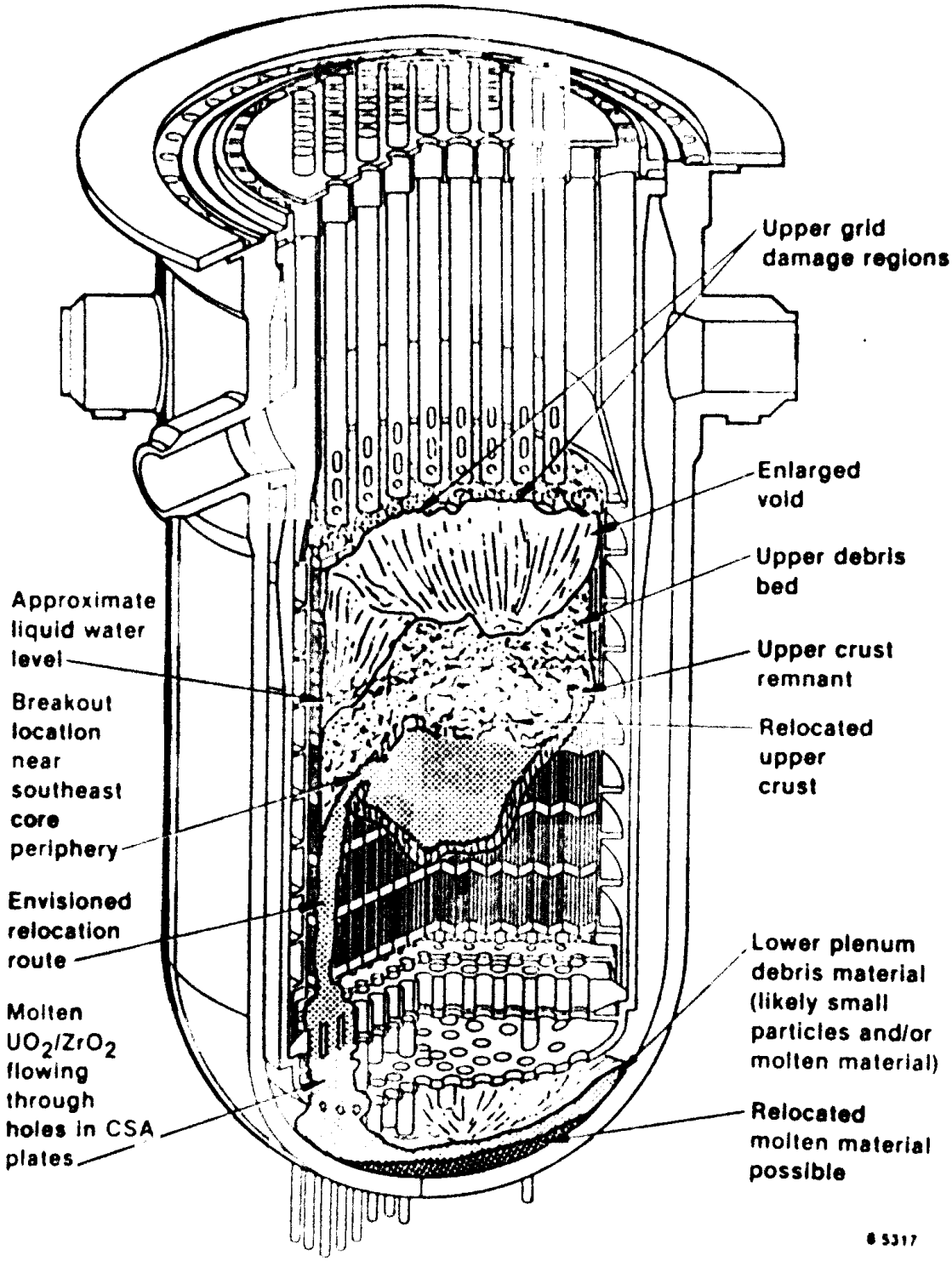

Figure 39. Estimated TMI-2 core configuration during the 224- to 226-min core failure and relocation period.

4. FISSION PRODUCT BEHAVIOR

4.1 End-State Fission Product Distribution

An objective of the TMI-2 Accident Evaluation Program is to determine the end-state fission product inventory and distribution. This effort includes the establishment of a fission product data base that permits the calculation of the inventory and distribution for key fission products. This section summarizes the results of this effort through FY-1986 and includes examination results for the first samples extracted from the reactor vessel lower plenum.

Table 2 is a listing of the currently known fission product repositories and the fractions of the total fission product inventory that are located in these repositories. Figure 40 is a schematic of TMI-2, showing the location of the various components that contain fission products released from the core. The gaseous and liquid flow paths between the various buildings and components which formed the transportation paths for fission products during and after the accident are also shown in Figure 40. The principal fission product repositories are the reactor building components that contain approximately 98% of the total inventory of non-gaseous fission products. About 1% of the radioactive cesium and 2% of the radioactive iodine were transported from the reactor building to the auxiliary building, mainly by continued operation of the letdown system. Of this, only very small amounts of radioactive iodine and cesium were released to the environment during the accident (approximately 15 Ci of ^{131}I and <1 Ci of cesium, or 10^{-4} and 10^{-10}% of the total core inventory, respectively). Approximately 1% of the radioactive fission gases was released to the environment during the accident. The krypton content of the reactor building, 45% of the total core inventory, was vented to the atmosphere in 1980 as a controlled release.

Those components outside of the reactor building that have been sampled for fission products are the makeup-purification (MUP) demineralizers in the auxiliary building and the submerged demineralizer system (SDS) components

TABLE 2. FRACTIONS OF CORE INVENTORY IN ASSAYED PLANT COMPARTMENTS

	Phase	I	^{85}Kr	^{133}Xe	^{90}Sr	^{129}Te	^{129}I	^{131}I	^{134}Cs	^{137}Cs	^{144}Ce	Pu/Th	Reference
1 Reactor building													
1.1 Basement liquid[a]		5.7 ± 0.2E-01	--	--	1.6 ± 0.07E-02	2.1 ± 0.6E-03	1.4 ± 0.04E-01	1.9 ± 0.09E-01	6.2 ± 0.18E-01	6.1 ± 0.12E-01	1 ± 0.6E-05 --	6 ± 3E-07 Pu 3 ± E-06	8 8
1.2 Basement sediment		--	--	--	6.1 ± 7.2E-04	1.2 ± 1.4E-03	7.6 ± 6.7E-02	1.6 ± 0.6E-02	4.6 ± 5.7E-04	4.2 ± 4.9E-04	9.1 ± 5.7E-06 --	8 ± 6E-08 Pu 6 ± 5E-07 Pu	8 8
1.3 Basement sump[a]	Solid Liquid	-- --	--	--	8.3 ± 0.9E-07 9 ± E-05	1.4 ± 0.2E-07 --	<5E-07 --	-- --	2.9 ± 0.3E-07 1.4 ± 0.1E-03	2.6 ± 0.3E-07 1.3E-03	1.8 ± 0.3E-07 --	-- --	8 8
1.4 Reactor coolant drain tanks[a]	Solid Liquid	-- 2.9 ± 0.8E-04	--	--	5 ± 5E-04 1.8 ± 0.2E-04	2.6 ± 1E-05 1 ± 1E-05	6.9 ± 6E-09 5.5 ± 1.0E-05	-- --	3.8 ± 6E-06 4.8 ± 1E-05	3.4 ± 3E-06 4.4 ± 0.9E-05	9.5 ± 1E-06 1.2 ± 1E-06	-- 4E-06 Pu	9 8
1.5 Reactor building air		--	4.7E-01	2.0E-01	--	--	--	1E-04	--	--	--	--	7
1.6 Reactor building surfaces[a]		--	--	--	3 ± 3E-06	--	3 ± 1E-03	--	5 ± 7E-04	7 ± 1E-04	--	--	6
2 Reactor coolant system													
2.1 Reactor coolant[a]		2.7E-02	--	--	9.6E-03	--	1.2E-02	1.1E-01	7.7E-03	8.1E-03	--	--	6
2.2 Reactor coolant system surfaces[c]		--	--	--	5.6 ± 0.6E-04	1.4 ± 0.2E-03	1.3E-03	--	1.0 ± 0.1E-03	1.1 ± 0.1E-03	3.6 ± 0.4E-04	--	--[b]
3 Reactor pressure vessel													
3.1 Reactor vessel plenum		--	--	--	9 ± 7E-05	8 ± 5E-04	8 ± 4E-05	--	9 ± 7E-04	8 ± 6E-04	7 ± 4E-05	--	--[b]
3.2 Reactor vessel internal surfaces		--	--	--[d]	--[d]	--[d]							
3.3 Partially intact core rods		--	--	--[d]	--[d]	--[d]							
3.4 Reactor core debris bed		--	--	--	1.2 ± 0.4E-01	8 ± 1E-02	5 ± 1E-02	--	5 ± 2E-02	6 ± 2E-02	2.6 ± 0.4E-0	--	--[b]
3.4a Debris bed extrapolated to entire core		--	--	--	6.0E-01	3.0E-01	2.4E-01	--	2.5E-01	3.0E-01	--	--	--
3.5 Reactor core solid mass		--	--	--[d]	--[d]	--[d]							
3.6 Core material in lower plenum		--	--	--[d]	9.5E-02	5.0E-03							
4 Auxiliary building													
4.1 Makeup and purification demineralizers[c]		--	--	--	6 ± 3E-04	7 ± 3E-05	2 ± 1E-04	--	1.0 ± 0.5E-02	8 ± 4E-03	7 ± 0E-06	--	--[b]
4.2 Reactor coolant bleed tanks		3.0E-02	--	1E-02	1E-04	--	10^{-4} to 10^{-2}	--	--	2E-02	--	6E-07/ 1E-07	7
4.3 Auxiliary building sump		--	--	--	--	--	--	--	--	--	--	--	--
4.4 Other sites		1E-02	--	4E-04	1E-03	--	--	1E-02	2E-02	1.0E-02	--	--	7

TABLE 2. (continued)

	Phase	T	^{85}Kr	^{133}Xe	^{90}Sr	^{125}Sb	^{129}I	^{131}I	^{134}Cs	^{137}Cs	^{144}Ce	U/Pu	Reference
5. Fuel handling building													
5.1 Submerged demineralizers[a,c]		6.2 E-01	--	2.3E-20	--	--	--	--	4.6E-01	4.5E-01	--	--	7
6. EPICOR-II building													
6.1 EPICOR-II resins[a,c]		4.2E-02	--	--	1 E-03	--	--	--	3.7E-02	2.7E-02	--	--	7
7. TMI-1 buildings		--	--	--	--	--	--	--	--	--	--	--	--
8. Releases													
8.1 Gaseous releases		4.0E-04	4.7E-01	7.1E-02	8E-10	--	--	--	--	7 E-12	--	--	7
8.2 Liquid releases[a]		--	--	--	--	--	--	1E-06	--	--	--	--	7

a. Measurement errors are not given in reference.

b. This study.

c. Fission products on the resin beds were transferred from other components by processing of the RCS and leakage coolant. These terms are, therefore, not additive toward the inventory total. They represent activity physically transported offsite on the resins.

d. Not yet measured.

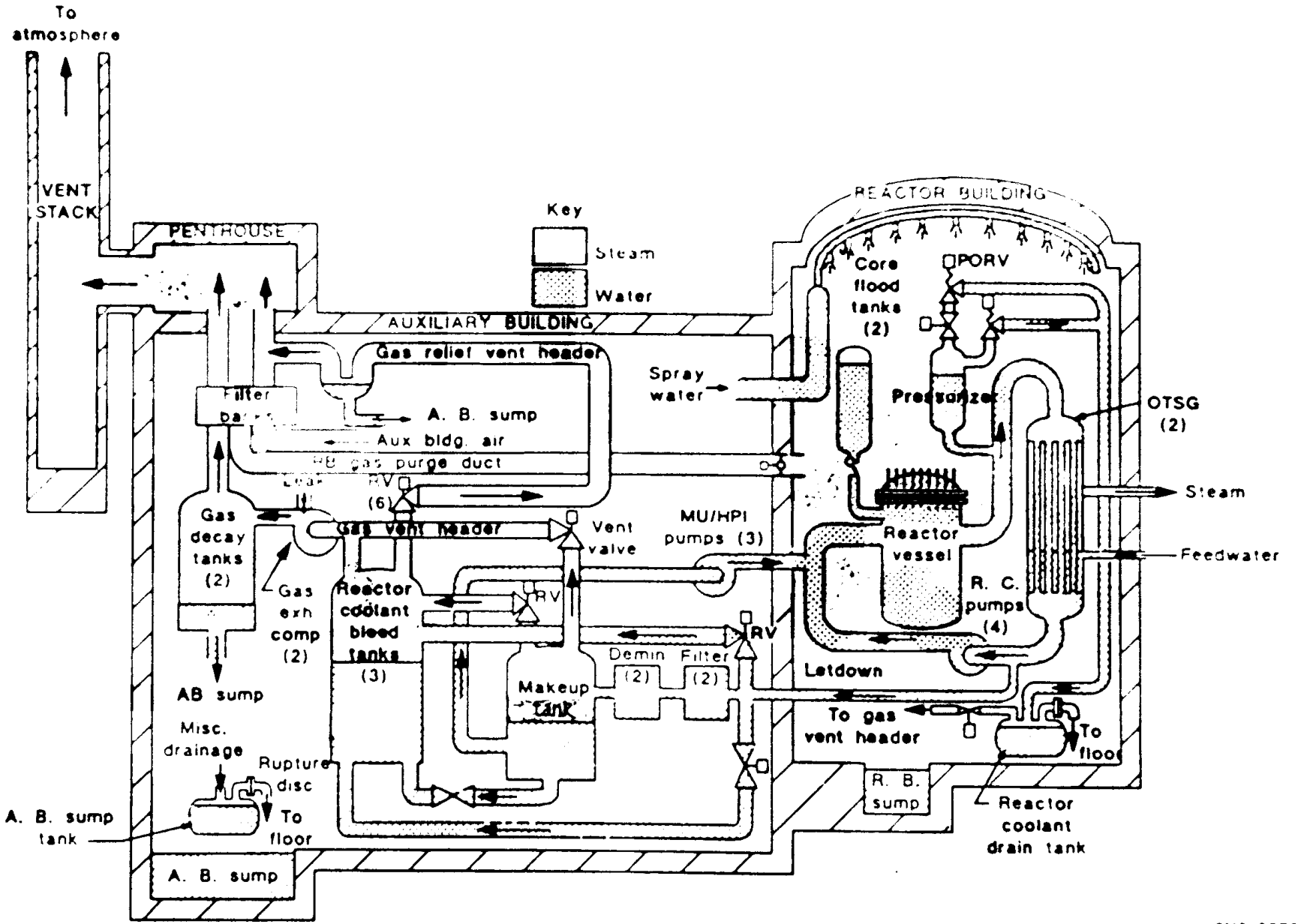

Figure 40. Schematic of TMI-2 accident fission product escape path

in the fuel handling building. The MUP system was operated for a time during the accident until the demineralizer became clogged. After this time, the MUP system was operated with the demineralizer bypassed. The total amounts of fission products that were deposited in the MUP demineralizer were very small, typically less than or of the order of 1% of the total inventory of specific isotopes. The SDS was used to remove fission products from the reactor coolant. Therefore, the radioactivity that was deposited in this system was transported to the fuel handling building in a controlled manner and does not represent accident release from the reactor building.

Three reactor building components were examined that were outside of the RCS. These were the reactor building air coolers, the reactor coolant drain tank, and the reactor building sump. The air coolers were expected to contain significant amounts of fission products, since they contain large surface areas and a large volume of contaminated air flowed through them during and following the accident. However, based on the fission product measurements, it was determined that less than 1% of any isotope was deposited on their surfaces. Similarly, the reactor coolant drain tank was expected to contain significant amounts of fission products, since over half of all the reactor coolant which flowed out of the RCS flowed through this tank. Again, less than 1% of any isotope was found in the samples extracted from this tank. The reactor building sump was not sampled until after cleanup operations of its contents (water and sludge) using the SDS were completed. Thus, the amount of radioactivity which reached the sump during the accident has not been determined. At this time, the sump is considered to be only a minor repository of fission products. Again, it should be noted that the current best-estimate of the fission product transport from the reactor building is via the letdown system, which was operated during and after the principal fission product release from the fuel.

The only RCS surface sample obtained and analyzed to date is a resistance temperature detector (RTD) that was removed from the hot leg of the A steam generator. Since the surface area of this RTD is only

approximately 10^{-5}% of the total surface area of the RCS, it is inadequate to extrapolate the results from this small sample to the entire RCS. However, based on this sample, it is expected that the RCS surfaces do not now represent a significant repository for fission products. If fission products had been deposited on the RCS surfaces (a phenomenon expected on the basis of fission product transport experiments), they were subsequently leached into the coolant. Other RCS surface samples will be obtained and examined which will provide additional confirmatory data.

Three control rod drive leadscrews were removed from the reactor vessel in 1982. Two of these leadscrews have been examined for surface deposits of radionuclides. Again, if fission products had been deposited on these surfaces during the accident, they were largely removed since the accident and the surfaces of the reactor vessel probably represent only a minor fission product repository.

The reactor core is believed to be a principal repository for fission products. For example, based on the measured release of the gaseous fission products, it is believed that approximately one-half of the original inventories of the krypton and xenon isotopes may have been retained in the fuel. This is conjecture at this time, since confirmatory sample examinations have not yet been performed. As discussed in Section 2.2, there are four basic core forms represented in the reactor vessel: the upper debris bed, which represents an estimated 25% of the original core; the resolidified core, a previously molten solid mass which is located below the upper debris bed and represents approximately 20% of the original core; the debris bed located in the lower plenum, a pile of previously molten corium which is gravel-like and which represents approximately 10% of the original core; and those fuel rods that are still in a rod-like geometry, an estimated 45% of the original core, located under the consolidated mass and on the core periphery. Samples have been taken of all four of these core forms, but only small samples of the upper debris bed and lower plenum debris have as yet been analyzed.

Two sets of samples have been extracted from the upper debris bed. The first samples were taken using specially designed sample acquisition equipment which extracted small samples from several different depths (ranging from the surface to 94 cm below the debris bed surface) and at two different locations. The location of these and other core samples are described in Appendix A. A total of 150 g of core debris were extracted for these 11 samples. During the 1986 defueling operations, several samples, ranging in size from 3 to 415 g, were extracted and will be analyzed for fission product content. The results from the analysis of the first samples are shown in Table 3. These results were extrapolated to the entire upper debris bed, and the resultant retention fractions are listed in Table 2. The principal surprises in the results are that the high-volatile fission products like iodine and cesium were retained to a much higher degree and the medium-volatile fission products like ruthenium and antimony were retained to a lower degree than expected based on the temperatures which were reached by the core during the accident and the volatilities of these fission products. Low-volatile fission products, such as europium and cerium, were essentially completely retained, as expected, within the accuracy of the measurements.

Three visual examinations were made of the lower plenum during 1985. The results of these visual examinations are summarized in Reference 10. During one of these examinations, conducted in July 1985, a remote sampling device was inserted into the lower plenum, via an inspection hole in the downcomer, and a number of pieces of the lower plenum debris bed were extracted. Six of these were analyzed for fission product and uranium content. The detailed results from these examinations are shown in Table 4 and in Reference 12. Again, cesium was retained to a much higher degree than expected, though the high iodine release was more in line with expectations. Also, ruthenium and antimony retention was low. There are some indications that the ruthenium and antimony may have been scavenged, in metallic form, by metallics such as zircaloy or stainless steel. Tellurium may also be bound by these structural metals. Similar to the upper debris bed, the low-volatile fission products, europium and cerium, were retained essentially completely in the lower plenum debris. These

TABLE 3. SUMMARY OF RETAINED FISSION PRODUCTS FROM UPPER PLENUM GRAB SAMPLES

	Percent of Inventory Retained	
Radionuclide	Average	Range
^{129}I	22	10-28
^{137}Cs	21	6-32
^{125}Sb	28	18-38
^{106}Ru	55	35-86
^{144}Ce	114	90-130
^{154}Eu	90	60-108

TABLE 4. SUMMARY OF RETAINED FISSION PRODUCTS FROM LOWER PLENUM DEBRIS EXAMINATION

	Percent of Inventory Retained	
Radionuclide	Average	Range
^{129}I	2	0-10
^{137}Cs	16	9-22
^{125}Sb	5	3-10
^{106}Ru	7	4-9
^{144}Ce	114	106-124
^{154}Eu	85	75-94

results were extrapolated to the entire lower plenum debris bed, and the resultant calculated retention fractions are shown in Table 2.

While much progress has been made in identifying and quantifying the principal repositories for fission products, a major portion of the core has not yet been analyzed; and it is expected that a significant fraction of the total fission product inventory is in that portion. Efforts during the next fiscal year will be devoted to analyzing samples of these core forms. When these results are available, a much clearer picture of the end-state fission product distribution will be available. Included in these samples are 10 core bores which were drilled in the solid, previously molten core under the upper debris bed and in the standing fuel elements under this solid mass. On the basis of the drilling operations and subsequent visual inspections, it has been determined that a much larger fraction of the original core remains in rod-like form (~45% versus ~15%) than previously thought.[10] The results from the examination of these samples will be included in the final version of this report.

4.2 Transient Release

The TMI-2 accident provides a unique opportunity to study the response of a full-scale PWR to a severe core damage accident. This is especially true in the area of fission product release and transport. While many experimental studies have been and are currently being conducted to study fission product behavior during core disruption, full-scale data are invaluable to the extrapolation of these experimental results to a commercial PWR. The TMI-2 analysis, in support of this need, has two main objectives: (a) support of the examination and eventual removal of the core by characterizing damage features, fission product retention, hydrogen production, and maximum temperatures during the accident; and (b) identifying the relative importance of core examination data in validating severe core damage models.

Several computer calculations have been made of the TMI-2 accident in an effort to understand the accident scenario. It should be recognized that

the majority of the information about TMI-2 core damage progression lies in the areas of thermal-hydraulics and core degradation. This is because most of the information obtained to date is in these two areas. Only a very limited amount of data has been obtained on the fission product release and location; and this information deals specifically with end-state fission product distribution and inventory, not with the transient release and transport during the accident. Section 3.2.2 describes the calculations made using the SCDAP computer code. In addition to the calculation of the thermal-hydraulic response of the plant, SCDAP also calculated an estimate of the transient release of the gaseous and high-volatile fission products from the fuel into the reactor coolant. The amount of fission product release (percent of initial core inventory) is presented in Table 5 for the calculations based on an assumed core uncovery initiation time of 100 min (early core uncovery) and 113 min (late core uncovery), respectively.

The total fission product releases calculated were known to be much too low, based on measured releases from the RCS. Therefore, an additional calculation was performed, using the same thermal-hydraulic boundary conditions assumed in the "early" core uncovery case, but using an improved UO_2-Zr interaction model. This improved model resulted in a much longer calculated period of time during which rapid fission product release occurred, since the fuel remained liquid longer. The fission product release results are also shown in Table 5. As indicated, the improved UO_2-Zr interaction model resulted in a much larger calculated release of

TABLE 5. REPRESENTATIVE FISSION PRODUCT RELEASE RESULTS AT 174 MIN (%)

Fission Product	SCDAP-Early	SCDAP-Late	SCDAP-New
Xe, Kr	3	0.7	36
Cs, I	0.1	0.0	36

fission products. This study points out the need for accurate fission product release modeling in order to improve our understanding of fission product behavior during the TMI-2 accident.

An additional calculation was performed by Fauske and Associates,[31] using the MAAP computer code.[32] As was the case for the SCDAP calculations, the MAAP calculation was principally done to better understand the thermal and hydraulic response of the plant with a secondary goal of studying the fission product behavior. The calculated fission product releases were very close to those of the last SCDAP calculation (34% for MAAP versus 36% for SCDAP), although the agreement may be fortuitous since the improved UO_2-Zr interaction model was not used in the MAAP calculation.

4.3 Fission Product Chemistry

An understanding of the fission product chemical form is important to a full understanding of fission product transport during the accident. The chemical form affects such things as fission product volatility and reactivity, and thus the potential for release from the fuel as well as the potential for retention within the RCS or, after transport from the RCS, retention within the coolant in the reactor building. However, the current knowledge of chemical form is severely limited due to the small concentrations of fission products in the samples extracted from the various fission product repositories. Thus, much of what we know about fission product chemistry is based on separate-effects data extrapolated to the conditions believed to have existed during the accident. This section is organized by fission product chemical element.

4.3.1 Iodine Chemistry

Since iodine is active both radiologically and biologically, it has been considered in the past as the limiting radionuclide in terms of potential adverse public health effects. Analyses of severe reactor core damage accidents have usually assumed that a large fraction of the fission product iodine inventory in the fuel would be released to the

environment.[33] One aspect of the accident which was surprising was the very low iodine release to the environment. Based on radiation measurements taken during and shortly after the accident, it was concluded that only approximately 15 Ci of ^{131}I were released to the environment[34], compared with a total shutdown inventory of 6.7×10^7 Ci of ^{131}I.[35] In order to gain some understanding of why only a negligible amount of iodine was released to the environment, it is necessary to examine the most likely chemical forms of iodine in the fuel, the RCS, and the containment building.

Iodine isotopes in the fuel are formed mostly by the beta decay of tellurium isotopes, with the exception of ^{135}I which is a direct fission product.[36] Iodine is believed to migrate as an atom to microbubbles where it can either form I_2 or CsI, depending on the environment. Since there were approximately 11 cesium atoms for every iodine atom in the fuel,[35] and since CsI is the most stable iodine species in the Cs-U-Zr-H-I-O chemical system, it is judged that the iodine combined with cesium to form CsI when the fission products migrated from the fuel. Thus, when the fuel elements initially failed due to overheating, the gap inventory of iodine was probably released as CsI. Later, when the fuel elements melted, the iodine was released to the reactor vessel, this time probably as atoms due to the high temperatures. However, as the high-temperature gas reached cooler parts of the reactor vessel, the iodine probably combined with the cesium to form CsI, either as a vapor or an aerosol. The combination of cesium and iodine to form CsI in the fuel has, in the past, been accepted as the most probable scenario. However, recent experiments by Alexander[37] have been made using a very sensitive mass spectrometer. In these experiments, Alexander has measured the individual activation energies for release from the fuel of the cesium and iodine atoms and has determined that these energies differ, indicating that the two elements move through fuel separately as cesium and iodine atoms, rather than CsI. This, however, does not affect the subsequent transport and deposition of iodine, since, based on thermal equilibrium calculations and estimated core exit (upper plenum) temperatures, the formation of CsI should occur during transport if it did not occur prior to release from the fuel elements.

The equilibrium speciation of iodine in the high-temperature RCS has been calculated using the principles of chemical thermodynamics. These calculations indicate that CsI is the dominant stable species at lower temperatures, while HI or iodine become more dominant at higher temperatures. It has been estimated[21] that the upper plenum temperatures remained below 1175 K during most of the accident and never exceeded 1575 K. Under these conditions, CsI is the most thermodynamically stable iodine species. As the iodine was swept from the upper plenum into the cooler regions of the RCS, CsI formation would have been increasingly favoured. A kinetic analysis of the Cs-O-H-I system was performed to determine whether CsI formation could occur rapidly enough (particularly since cesium release could easily have been as CsOH due to the steam environment). The results of this analysis indicated that the time constant was 0.01 s for formation of CsI, starting with CsOH and iodine, which supports the conclusion that iodine probably existed as CsI in the RCS. A separate analysis was made[38] using the SOLGASMIX computer code.[39] This analysis indicates that more than 95% of the iodine would exist as CsI, under a wide range of hydrogen/steam ratios and temperatures. Of course, as CsI is dissolved in water, it would disassociate to form ionic I^- and Cs^+.

After the I^--laden coolant was released from the RCS to the containment and auxiliary buildings, iodine would have eventually partitioned between the aqueous and gaseous phases. It is the partitioning of iodine in the coolant that reached the auxiliary building that ultimately dominated the release of iodine to the environment, since the iodine which remained in the water phase was more efficiently retained inside the buildings whereas some of the gaseous iodine did leak to the environment (~15 Ci). The partitioning of iodine between the two phases can be calculated using the principles of chemical thermodynamics, but it is very complex since iodine can exist in various oxidation states and is subject to hydrolysis and disproportionation in water. This partitioning depends strongly on pH, electrochemical potential, and temperature. For example, if the pH is greater than about 3, the predominate species are iodide and iodate under reducing and oxidizing conditions, respectively. The same

holds true for the higher, basic, pH of 8. Even at neutral pH, and with the low iodine concentrations which existed in the water in the containment and auxiliary buildings, the equilibrium concentration of elemental iodine is always at least four orders of magnitude less than that of HOI, which is, in turn, always lower by at least two orders of magnitude than the concentration of either I^- or IO_3^-. Since the latter two species have much lower volatilities than the first two, this indicates that very little iodine would have been partitioned to the gas phase and thus be available for release to the environment. An analysis of the expected conditions at TMI-2 was made with the result that thermodynamic equilibrium would favor low-volatile species of iodine in the water. One assumption used in this analysis was that CsI is a stable compound, which in most cases is a valid assumption. However, experiments conducted at Sandia National Laboratories indicate that under some conditions CsI will react with stainless steel surface oxide to form $CsSiO_3$ and HI. It is not expected that this additional complexity would alter the ultimate conclusion (low volatility of iodine at TMI), since the form of iodine is still iodide in water. Additionally, since HI is more reactive with stainless steel than CsI, some of the iodine may be expected to be "fixed" to the steel surfaces, further reducing the amount of iodine available for volatilization.

4.3.2 Cesium Chemistry

Only about 10% of the cesium could have been released from the fuel as CsI, because the Cs/I atom ratio was approximately 11 at TMI-2 shutdown conditions. Studies conducted at AECL,[40] INEL,[23] and EPRI[41] indicate that the remaining cesium would be released into the steam rich environment of the RCS as CsOH. Whereas CsI is relatively unreactive, CsOH would react readily with the metal surfaces in the RCS. Also, CsOH is very soluble in water; and it would be expected to be transported from the RCS to the containment and auxiliary buildings in the coolant and remain there.

4.3.3 Other Fission Products

Based on the conclusion that the hydrogen/steam ratio in the reactor vessel was less than 1 over long periods of time, a thermodynamic

equilibrium analysis of various fission products was made and reported in Reference 38. This analysis indicated that the fission products zirconium, lanthanum, cerium, barium, and strontium were stable as the oxides ZrO_2, La_2O_3, Ce_2O_3, BaO, and SrO, respectively. Pure steam under high pressure in the upper plenum would have oxidized fission product tellurium but not ruthenium, which would remain a metal. However, even 1% of hydrogen (produced by the zirconium-steam interaction) would inhibit the oxidation of tellurium. Both antimony and ruthenium may have been retained in metallic melts in the lower core and lower plenum. In addition, antimony may have reacted with tellurium to form antimony telluride which would be expected to remain in the core.

Much work remains to be done in the area of fission product chemistry. This work will be hampered by the low concentrations of fission products in the core materials and by the length of time during which the core has been underwater.

5. CONCLUSIONS AND FUTURE WORK

The IMI-2 data provide an important, large-scale benchmark for (a) studying severe accident phenomenology, (b) assessing the capability of severe accident analytical models, and (c) evaluating the typicality and applicability of smaller-scale experiments to simulate severe accidents.

Important conclusions relative to our understanding of severe accident phenomenology based on the IMI-2 research findings are:

1. The initiation of HPIS at 200 min restored core cooling but did not terminate accident progression.

2. The formation of large regions of consolidated core materials is possible. These regions may continue to heat up independent of the surrounding coolant conditions if the heat transfer is less than the decay heat input and could eventually fail their mechanical constraints until a more coolable geometry is achieved.

3. There is no supporting evidence that a steam explosion occurred when the molten core material broke through the constraining crust into the water-filled vessel and relocated into the lower plenum.

4. Water in the lower plenum terminated the accident progression and prevented failure of the vessel lower head.

5. The reactor vessel coolant inventory is crucial in limiting not only the extent of the initial core relocation (due to molten zircaloy and liquefied fuel) but also the consequences of later stages of global core relocation involving large masses of molten core material.

6. Fission product release from the fuel and the RCS was very sensitive to the volatility of the individual elements. Release of the high-volatile fission products (iodine and cesium) was less than expected, especially cesium, up to 20% of which was retained in the previously molten corium that relocated to the lower plenum. Retention of the medium- and low-volatile fission products in the RCS was nearly complete, although significant amounts of antimony and rubidium were released from the fuel and are believed to be bound to metallic deposits in the reactor vessel.

Some details of the accident scenario remain to be more completely understood and quantified. This will require both additional characterization work and supporting analysis. Specific tasks relative to each of these areas include the following:

Inspection and Examination Work

1. Detailed visual inspections during core defueling of the core, CSA, and lower vessel head are desired to complete characterization of the upper core crusts in the east quadrant of the reactor vessel, the extent of damage to the core and CSA in the direct flow path of the relocating molten material, and the damage to the reactor vessel lower head and instrument penetration tubes.

2. Additional core material samples will be required to complete understanding of the physical state of the core and to confirm important material interactions relative to the progression of core damage. Specific samples from the following regions are desired:

   - large volume samples of consolidated core material and lower plenum debris

upper crust remnants near the core periphery
partially damaged fuel assemblies near the core periphery
material samples from flow paths in the core and CSA

3. Samples of damaged instrument guide tubes and penetration nozzles will be required to confirm the extent and type of damage.

4. Samples of the reactor vessel lower head are required if the inside surface has suffered significant damage.

Analytical Work

1. Analytical work is necessary to improve our understanding of the dynamics of the initial core degradation and formation of the consolidated, solid structure of core material and the subsequent impact on fission product behavior and hydrogen production. Much of this work will be an integral part of the TMI-2 Standard Problem effort.

2. Analysis is necessary to evaluate the cooling influence of the pump transient and emergency core cooling system injection on the upper core debris. The thermal response of the upper debris bed is an important boundary condition for estimating the possible expansion of the molten core region.

3. Analysis is required to determine the mechanisms controlling natural convection in the molten region, the growth of the molten core region, and the mechanical behavior of the upper crust.

4. Analysis is needed to study the interaction between the fuel and coolant during the primary relocation of molten core materials and the dynamics controlling debris formation from the molten material.

5. Thermal analyses are necessary to estimate the long-term thermal-mechanical response of the reactor vessel and the long-term cooling of the consolidated core region and lower plenum debris,

6. Analyses are needed to complete our understanding of the TMI-2 fission product data relative to the accident scenario determined from the separate- and integral-effects fission product release and transport experiments.

Most recent TMI-2 characterization work, together with supporting analysis to improve our understanding of the TMI-2 measurements and the thermal response of the degraded core, has led to an accident scenario that is consistent with the data recorded during the accident, the end-state condition of the reactor system, and independent severe fuel damage experiments. The initial TMI-2 core damage progression is generally consistent with independent severe fuel damage experiments and qualitatively confirms our understanding of zircaloy oxidation, fuel liquifaction, and core material relocation. As core material examination results become available, a more quantitative confirmation of these mechanisms is expected.

6. REFERENCES

1. D. W. Croucher, Three Mile Island Unit-2 Core Status Summary: A Basis for Tool Development for Reactor Disassembly and Defueling, GEND-007, May 1981.

2. E. Tolman et al., TMI-2 Accident Evaluation Program, EGG-TMI-7048, February 1986.

3. J. Broughton, "Core Condition and Accident Scenario," Proceedings of the First International Information Meeting on the TMI-2 Accident, Conf-8510166, October 1985.

4. K. Vinjamuri et al., Examination of H8 and B8 Leadscrews from Three Mile Island Unit 2 (TMI-2), GEND-INF-052, September 1985.

5. G. Bain, G. Hayner, Initial Examination of the Surface Layer of a 9-Inch Leadscrew Section Removed from Three Mile Island-2, EPRI-NP-3407, January 1984.

6. L. Beller, H. Brown, Design and Operation of the Core Topography Data Acquisition System for TMI-2, GEND-INF-012, May 1984.

7. D. Akers et al., TMI-2-Core Debris Grab Samples -Examination and Analysis (Part 1), GEND-INF-075, September 1986.

8. GPU Memorandum No. 4730-86-0037, from D. M. Lake to R. H. Fillnou, "Debris Bed Topography", March 31, 1986.

9. E. Tolman et al., TMI-2 Core Bore Acquisition Summary Report, EGG-TMI-7385, September 1986.

10. J. Adams, R. Smith, Lower Plenum Video Data Summary, EGG-TMI-7429 (to be published).

11. A. Baratta, B. Bandini, Determination of Fuel Distribution in The TMI-2 Based on Axial Neutron Flux Profile, GPU Report TPO/TMI-165, April 1985.

12. D. Akers et al., "TMI-2 Lower Vessel Debris Examinations," Proceedings of the 14th Water Reactor Safety Information Meeting, Gaithersburg, MD, (to be published).

13. J. Anderson, Analysis of TMI-2 Pressurizer Level Indications, EGG-TMI-7100, January 1986.

14. NSAC/28, Interpretation of TMI-2 Instrument Data, Nuclear Safety Analysis Center (NSAC), Electric Power Research Institute (EPRI), Palo Alto, CA, March 1980.

15. R. Wooton et al., Analysis of the Three Mile Island Accident and Alternate Sequences, NUREG/CR-1219, January 1980.

16. NSAC-80-1 (NSAC-1 Revised), Analysis of Three Mile Island-Unit 2 Accident, Nuclear Safety Analysis Center (NSAC), Electric Power Research Institute (EPRI), Palo Alto, CA, March 1980.

17. D. J. N. Taylor, "TMI SPND Interpretation," Proceedings of the First International Information Meeting on the TMI-2 Accident, CONF-8510166, Germantown, Md, October 1985.

18. J. Adams, et al., Quick Look Report on OECD LOFT Experiment LP-FP-02, OECD-LOFT-T-3804, September 1985.

19. C. Allison et. al, SCDAP/MOD1 Analysis of the Progression of Core Damage During the TMI-2 Accident, SE-CMD-84-006, July 1984.

20. L. Siefken et al., Assessment of SCDAP/RELAP5 Using the PBF SFD Tests, (EG&G Idaho, Inc. Internal Report, Draft), January 1986.

21. K. Adron, D. Cain, TMI Accident Core Heatup Analysis, NSAC-24, Nuclear Safety Analysis Center (NSAC), Electric Power Research Institute (EPRI), Palo Alto, CA, January 1981.

22. S. Hagen et al, Temperature Escalation in PWR Fuel Rod Simulator Bundles due to Zircaloy/Steam Reaction--Test ESBU-1 Test Results Report, Kernforschungszentrum Karlsruhe Report KfK-3508, December 1983.

23. A. D. Knipe, S. A. Ploger, and D. J. Osetek, PBF Severe Fuel Damage Scoping Test--Test Results Report, NUREG/CR-4683, EGG-2413, August 1986.

24. Z. R. Martinson, D. A. Petty, and B. A. Cook, PBF Severe Fuel Damage Test 1-1, Test Results Report, NUREG/CR-4684, EGG-2463, October 1986.

25. A. Baratta, personal communication, Results based on neutronic studies to evaluate the TMI-2 source range monitor response (currently being documented), November 1986.

26. R. Henry et al., "Core Relocation Phenomenology, Proceedings of the First International Information Meeting on the TMI-2 Accident, CONF-8510166, Germantown, Md, October 1985.

27. P. Kuan, TMI-2 Core Debris Bed Coolability, EGG-TMI-7150, March 1986.

28. P. Kuan, Core Relocation in the TMI-2 Accident, EGG-TMI-7402, December 1986.

29. E. Carlson, B. Cook, "Chemical Interaction Between Core and Structural Materials," Proceedings of the First International Information Meeting on the TMI-2 Accident, CONF-8510166, Germantown, Md, October 1985.

30. A. Cronenberg et al., Assessment of Damage Potential to the TMI-2 Lower Head Due to Thermal Attack by Core Debris, EGG-TMI-7222, June 1986.

31. M. A. Kenton et al., Simulation of the IMI-2 Accident Using the Modular Accident Analysis Program Version 2.0, EPRI NP 4292, April 1985.

32. MAAP User's Manual, Vols. 1 and 2, IDCOR Technical Report 16.1, Fauske & Associates, Inc., 1983.

33. N. C. Rasmussen, Reactor Safety Study, WASH-1400, 1975.

34. "Three Mile Island. A Report to the Commission and to the Public," (Rogovin report), Vol. II, Part 2, Washington, D.C., February 1980.

35. B. G. Schnitzler and J. B. Briggs, IMI-2 Isotopic Inventory Calculation, EGG-PBS-7698, August 1985.

36. J. Paquette, D. J. Wren, and B. L. Ford, "Iodine Chemistry," ACS Symposium Series, 189th Meeting of the American Chemical Society, Miami Beach, FL, April 28-May 3, 1985.

37. C. A. Alexander and J. S. Ogden, "Real Time Mass Spectrometric Evaluation of Fission Product Transport at Temperature and Pressure," Proceedings of the American Chemical Society Symposium on Chemical Phenomena Associated with Radioactivity Release during Seven Nuclear Plant Accidents, NUREG/CR-0078, 1986.

38. R. R. Hobbins et al., "Insights on Severe Accident Chemistry from IMI-2," Symposium on Chemical Phenomena Associated with Radioactive Releases During Source Nuclear Accidents, Anaheim, California, September 1986.

39. T. M. Besmann, SOLGASMIX-PI, A Computer Program to Calculate Equilibrium Relationships in Complex Chemical Systems, ORNL/TM-5775, 1977.

40. D. J. Wren, Kinetics of Iodine and Cesium Reactions in the CANDU Reactor Primary Heat Transport System, AECL-7787, 1983.

41. P. Cubiciotti and B. R. Sehgal, "Vapor Transport of Fission Products in Postulated Severe Light Water Reactor Accidents," Nuclear Technology 65, 266, 1984.

APPENDIX A

SUMMARY OF LABORATORY EXAMINATION OF TMI-2 CORE DEBRIS PARTICLES

APPENDIX A

SUMMARY OF LABORATORY EXAMINATION OF TMI-2 CORE DEBRIS PARTICLES

Eleven core debris grab samples (totaling 0.001% of core weight) were obtained from the two fuel assembly locations, H8 (center) and E9 (midradius) shown in Figure A-1. One sample was examined at the Babcock and Wilcox (B&W) Lynchburg Research Center, and ten samples were examined at the Idaho National Engineering Laboratory (INEL). Of the ten samples examined at INEL, fragmented chips from seven particles were examined by Rockwell Hanford Operations using differential thermal analysis. Twenty-two particles were shipped to Argonne National Laboratory (West and East) for metallurgical and chemical analyses.

The primary objectives of examining the core debris grab samples include the following:

- Supporting the plant recovery effort being performed by GPU Nuclear
- Determining the physical, chemical, and radiochemical condition of the core debris bed
- Providing data to support the assessment of severe fuel damage codes, primarily with regard to core damage progression and fission product behavior.

This Appendix presents the results of and conclusions from analysis of the core debris grab samples.

Sample Acquisition, Examination Plan, and Analytical Methods

The core debris grab samples were removed from the debris bed at depths ranging from the surface to 77 cm at the H8 location and from the surface to 94 cm at the E9 location. A hard stop was encountered at 77 cm at the H8

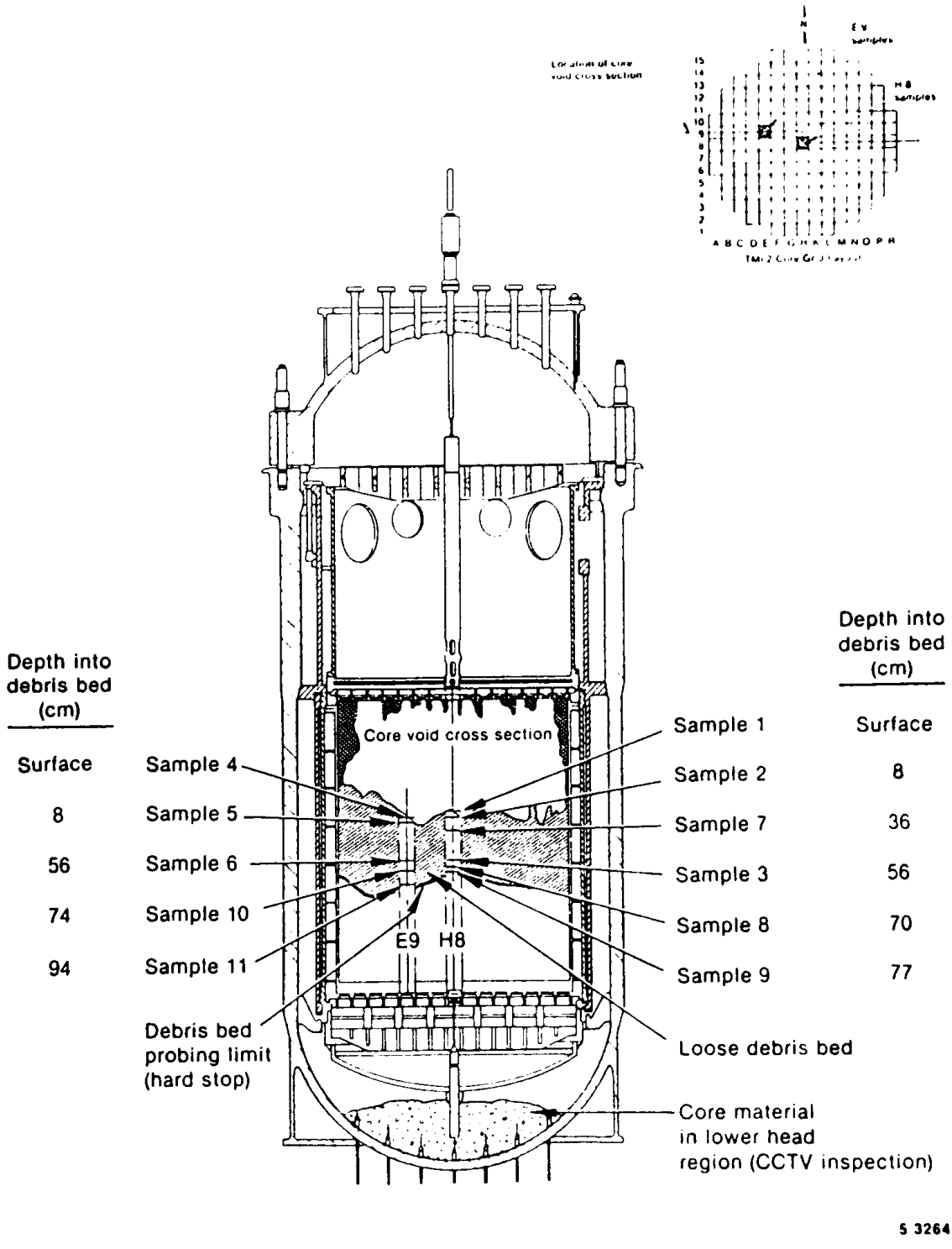

Figure A-1. Schematic showing the current known condition of the TMI-2 core and the locations of the core debris grab samples.

location, and friction prevented penetration of the debris bed beyond 94 cm at 19. Sample weights obtained ranged from 17 g (Sample 4) to 174 g (Sample 10).

Figure A-2 is a flow diagram showing the examinations performed on the core debris grab samples. There were four general types of samples examined: (a) bulk samples, as received from TMI-2; (b) particle size fractions--subgroupings of the bulk samples by size, obtained by sieving the bulk samples; (c) recombined bulk samples--approximately one-third of each particle size fraction, recombined to approximate the original bulk sample; and (d) particles and aliquots -individual particles from the larger (>1000 μm) particle size fractions and aliquots [representative portions from the smaller (<1000 μm) particle size fractions]. Analytical methods used for the examinations are standard examination techniques, with some modifications necessitated by the high radiation fields and insoluble nature of the core debris.

Physical Examinations

The physical examinations included visual and photographic examinations, weighing, bulk tap density measurements, particle size distribution analysis, and ferromagnetic and pyrophoricity tests. In general, the core debris was composed of particulate material that was not identifiable as core components. Five categories of particles were identified, based on visual appearance: (a) apparent fuel pieces; (b) cladding chunks; (c) foamy/porous, previously molten material; (d) particles that are a composite of fuel and previously molten material; and (e) metallic appearing, previously molten particles.

Bulk tap density measurements indicate that there are two density ranges for the samples. Samples 1, 3, and 6 have densities ranging from 3.5 to 3.8 g/cm^3, whereas Samples 9, 10, and 11 have densities ranging from 5.0 to 5.5 g/cm^3. The particle size distribution analysis indicated that Samples 1 and 3 have the largest fraction of material in the 1680 to 4000-μm particle size range, whereas Samples 9, 10, and 11 show a bimodal

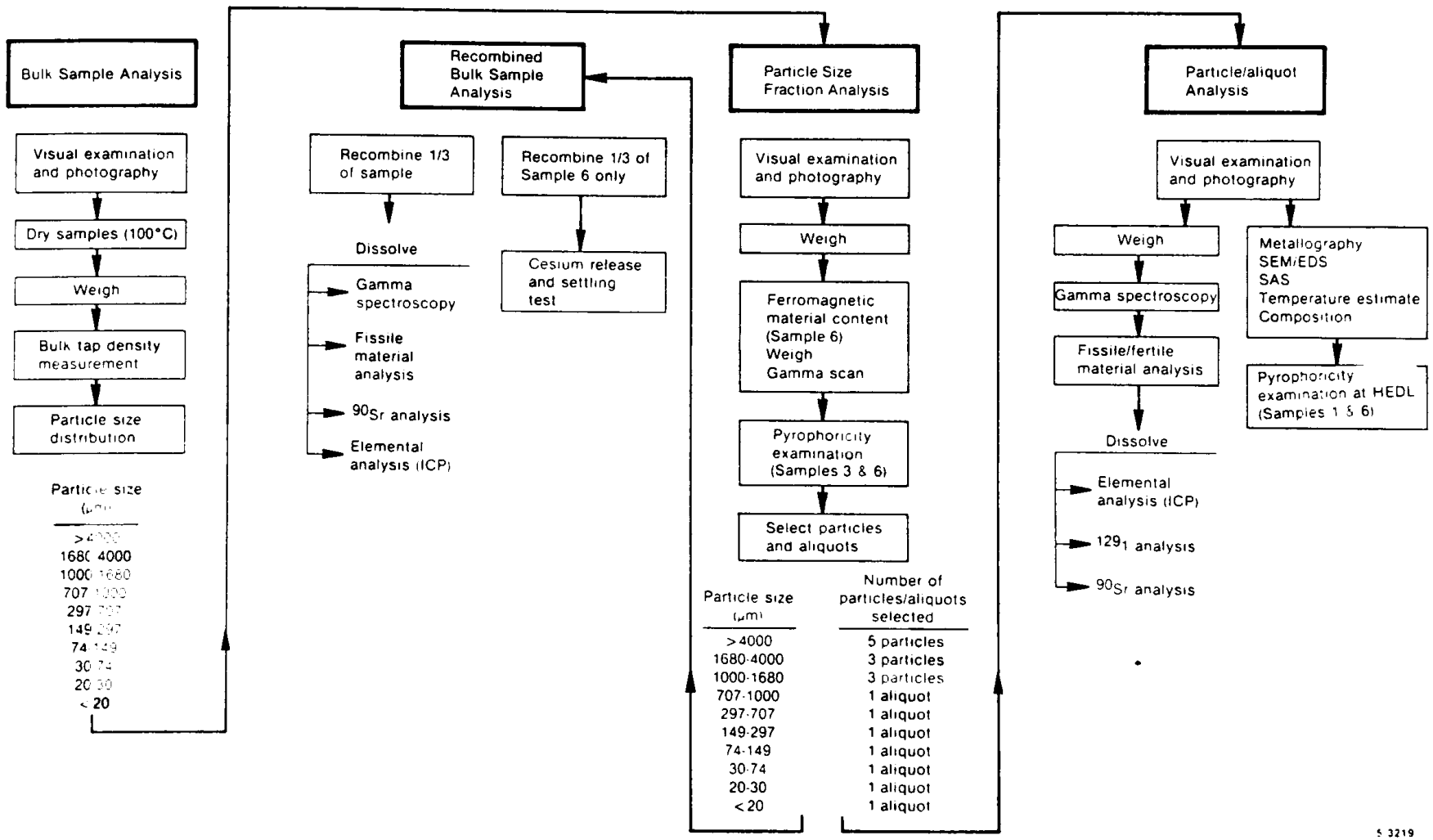

Figure A-2. Flow diagram showing the examinations performed on the TMI-2 core debris grab samples (typical for each sample).

distribution, with peaks at the 1680 to 4000-μm and 297- to 707-μm sizes. The bimodal distribution probably resulted in more efficient packing of the debris material and may explain the higher densities of Samples 9, 10, and 11. The particle size distribution analysis indicates the presence of mostly (>80%) larger particles (>1000 μm). Stratification of the debris bed into two layers also is indicated by the particle size distribution: a surface layer, and another beginning between 36 cm and 56 cm below the debris bed surface. The lower layer contains larger quantities of smaller-sized particles. The measurable ferromagnetic material content of Sample 6, the only sample analyzed for ferromagnetic content, was 0.9% of the total sample weight.

Metallurgical Examinations

Twenty-nine particles were selected from the ten core debris grab samples for detailed metallurgical analysis, which included optical and scanning electron microscopy for microstructural information and energy dispersive X-ray spectroscopy and scanning Auger spectroscopy for information on elemental composition.

Most of the particles examined contained regions of previously molten U-Zr-O, indicating peak temperatures of greater than 2200 K. Of these, many are previously molten $(U,Zr)O_2$, indicating peak temperatures greater than 2800 K. There are a few examples of previously molten material that are almost pure UO_2, indicating temperatures up to 3100 K. (The effect of small amounts of impurities on the melting point of UO_2 is not well known.) However, much of the fuel probably remained at fairly low temperatures (<2000 K) relative to the peak temperature or was exposed to high temperatures for only a short time. This conclusion is based on the relatively unrestructured appearance observed for much of the fuel, even through there are attached regions of previously molten ceramics.

The regions of previously molten U-Zr-O usually contain at least some traces of non-fuel rod materials (aluminum, chromium, iron, and nickel). These elements often were observed at grain boundaries or in voids. For

some particles, they are a significant portion of the total particle weight. Control rod materials (silver, indium, and cadmium) were not as commonly found as structural materials. However, major portions of three particles are metallic silver containing nickel-tin inclusions, indicating that control rod materials (or at least silver) apparently had less of a tendency to mix or interact with fuel rod materials than did the structural materials.

Chemical Examinations

Elemental analysis of the core debris grab samples was performed by inductively coupled plasma spectroscopy (ICP) on the recombined bulk samples and the individual particles and aliquots. Elements for which analyses were performed were selected to characterize five groups of core components: (a) uranium fuel and zircaloy cladding; (b) Ag-In-Cd control rod materials; (c) poison rod materials (boron, gadolinium, and aluminum); (d) structural materials (stainless steel and Inconel); and (e) elemental tellurium.

Most elemental constituents of the core components were present in all recombined bulk samples, particles, and aliquots, suggesting that significant disruption, mixing, and relocation of these components has occurred. The analyses for uranium and zirconium indicate that significant depletion ($\leq$50%) of zirconium from the debris bed has occurred. Analyses for control rod materials with emphasis on silver indicate that as much as 90% of the silver has relocated from the debris bed. There appears to be a general increase in silver concentration associated with a decrease in particle size. The burnable poison rod materials, aluminum and gadolinium, were measured in most of the samples. The wide distribution of gadolinium is of particular interest, because only four fuel assemblies in the core contained gadolinium control material (13 kg). These fuel assemblies were located at four quadrants, about mid-radius in the core.

Aluminum is concentrated at the surface of the debris bed, suggesting that the debris bed may have functioned as a trap or retention zone for some core materials. Structural materials are well mixed in the debris bed in

concentrations similar to their original concentrations in the fueled portion of a fuel assembly. Elemental tellurium, which may originate from natural or fission product sources, is concentrated near the surface of the debris bed similar to aluminum.

Radiochemical Examinations

Radiochemical examinations were performed on the recombined bulk samples, particles and aliquots from all samples, and the ferromagnetic components of Sample 6. The examinations included gamma spectroscopy, fissile-fertile material ($^{235}U/^{238}U$) content, and ^{129}I and ^{90}Sr analyses. Examinations were performed to characterize radionuclides of expected high volatility (^{129}I and ^{137}Cs), intermediate volatility (^{106}Ru and ^{125}Sb), and low volatility (^{90}Sr and ^{144}Ce).

Comparison of the measured-to-predicted retention/release of these radionuclides in the core debris is shown in Table A-1 and approximately follows the expected volatility of the radionuclides (i.e., the most volatile materials, ^{129}I and ^{137}Cs, were most significantly released). The results shown are normalized to predicted core average concentrations and are usable for intercomparison purposes. Actual in-core fission product concentrations per gram of fuel may vary by a factor of two. However, the retentions of the low-volatility fission products (e.g., ^{90}Sr and ^{144}Ce) near 100% suggest that the listed retentions are accurate within 20 to 30%. The high concentrations of ^{144}Ce are probably due to the presence of localized zones of higher burnup fuel at the locations sampled. The ^{129}I content of the samples tends to increase with surface area for the small particle sizes and may indicate a surface area retention dependent mechanism. Also, a correlation was observed between the concentrations of nickel and the ^{125}Sb and ^{106}Ru concentrations, suggesting that nickel functioned as a scavenging material for these radionuclides in the debris.

TABLE A-1. RADIONUCLIDE RETENTION NORMALIZED TO URANIUM CONTENT
(% of core inventory)

Radionuclide	Calculated Core Average Concentration[a] (Ci/g)	H8 Samples		E9 Samples	
		Measured Average Retention[b]	Range[c]	Measured Average Retention[b]	Range[c]
^{90}Sr	8.12 E-3	94	91-102	92	79-100
^{106}Ru	1.41 E-3	49	35-74	63	52-86
^{125}Sb	4.53 E-4	28	19-37	28	18-38
^{129}I	2.81 E-9	24[d]	19-28	19[d]	10-25
^{137}Cs	9.32 E-3	19	18-21	24	6-32
^{144}Ce	3.37 E-3	121	114-128	107	90-130
^{235}U[e]	--	2.5	2.3-2.7	2.7	2.5-2.8

a. Calculated based on ORIGEN-2 analyses, decay-corrected to April 1, 1984.

b. Average measured retention for all samples.

c. Range of retention for recombined bulk samples.

d. Calculated based on particle and aliquot analyses. Uncertain is ~100%.

e. Uranium enrichment calculated from fissile and total uranium analyses.

Contributions to Understanding the TMI-2 Accident

This section describes how the results from the examination of the core debris grab samples contribute to understanding the condition of the TMI-2 core and accident scenario.

Metallurgical analyses of the large particles from the core debris grab samples indicate in some of the material that peak temperatures up to the melting point of the UO_2 fuel were achieved. However, a significant amount of material showed no restructuring, indicating temperatures below about 2200 K. There are indications of either a prolonged candling[a] sequence or multiple temperature excursions. Evidence of movement of molten material down the fuel-cladding gap was observed, and there is some evidence of strong interaction of the fuel materials.

Evaluations were performed to estimate the degree of mixing, physical relocation, and segregation of core materials. The examination results suggest that the molten core debris was mixed vigorously to produce the degree of mixing and homogeneity observed. However, the observed mixing may be localized phenomena at the locations sampled and may not be representative of the entire debris bed.

Evidence of physical relocation and mixing of the fuel assembly materials was obtained by comparing the original uranium enrichments of the H8 and E9 fuel assemblies with the measured enrichments of samples removed from these locations. No correlation exists between the original and measured enrichments, indicating that significant physical relocation of fuel at the H8 and E9 locations occurred.

---

a The term "candling" is used to denote melting, relocation, and resolidification, similar to that which occurs to the wax of a lighted candle as it is burned.

idence of significant relocation and segregation of some
terials (zirconium, silver, indium, cadmium, gadolinium, and
contributions of these material movements on understanding
on and accident scenario are:

examined portion of the core may have zones of heterogeneous
al composition with significantly different compositions
he debris bed samples.

lations of aluminum and tellurium at the surface of the
bed suggest that the surface of the debris bed functioned
rap for some structural materials. Several mechanisms have
uggested that would allow the observed segregation to have
ed (a) during the accident (vaporization and subsequent
sation on surfaces) or (b) during natural recirculation
the accident (deposition of AlO(OH) or Al_2O_3 powder on
rface of the debris bed).

ncentrations of silver tend to be higher for the smaller
μm) particle size fractions, suggesting either finely
nted silver or a retention mechanism that is dependent on
e area.

shows the normalized average retention of radionuclides in
es as percentages of the predicted concentrations contained
nium. Release of radionuclides from the fuel is in the
d volatilities of the radionuclides (^{129}I, ^{137}Cs,
Ru, and ^{144}Ce), with the exceptions of ^{125}Sb,
The retention of ^{125}Sb in the core debris grab
han expected and is similar to ^{137}Cs. No significant
ore inventory of ^{125}Sb has been measured outside the core
data suggest that a large fraction of the core inventory
ide may have been transported to lower regions in the
ted mechanism for this transport is by reaction with

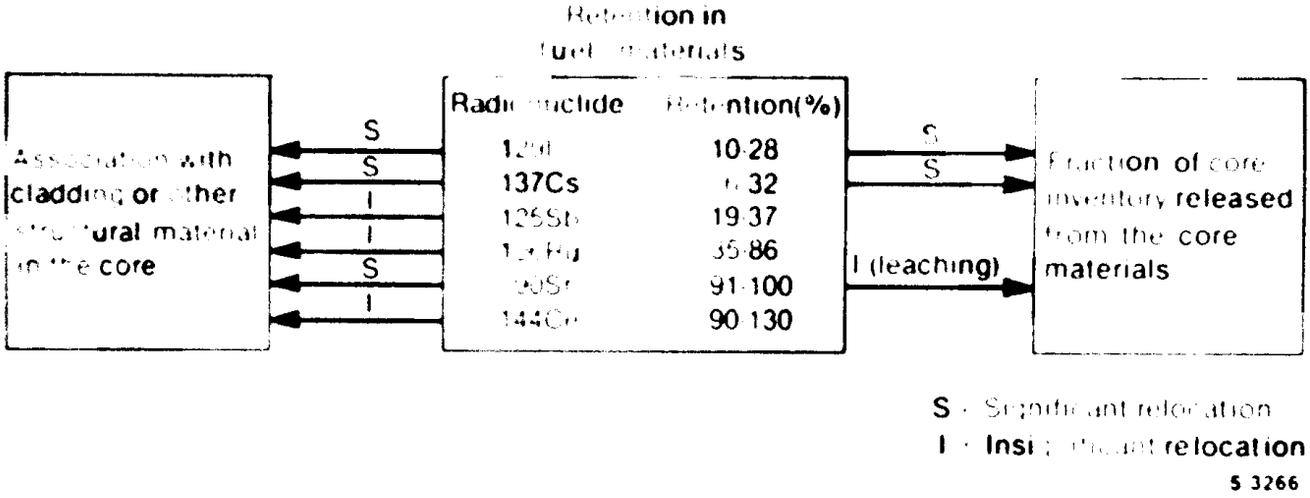

Figure A-3. Schematic showing the behavior (retention/relocation) of various radionuclides in the TMI-2 core.

als which were transported out of the debris bed.
enging of ^{125}Sb by structural nickel was observed for
.

was retained to a greater extent and ^{106}Ru to a lesser
xpected based on the volatility of the elements. The
ntion in the samples may be attributable to the formation
involatile oxide of strontium. The greater release of
understood at this time. The formation of highly
e unstable oxides, RuO_2 and RuO_4, would require much
potentials than likely existed based on the most probable
ratios over most of the high-temperature portion of the
$H/H_2O < 1$).

ained from analysis of the core debris grab samples suggest
n of the lower regions of the core might be significantly
at observed in the debris bed. The data also suggest that
ht be present as accumulations or that there may be
lower in the core.

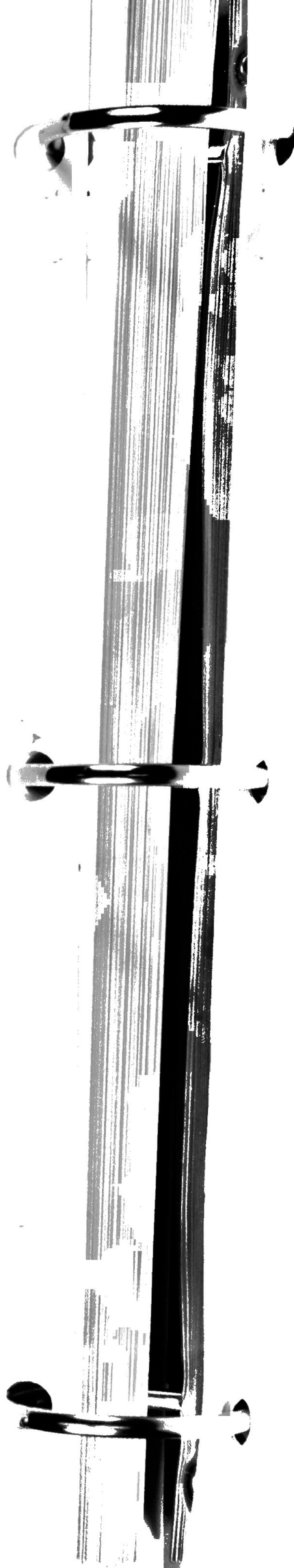

APPENDIX B

SUMMARY OF CORE BORE LOCATIONS AND MAJOR INSPECTION RESULTS

APPENDIX B

SUMMARY OF CORE BORE LOCATIONS AND MAJOR INSPECTION RESULTS

The principal information necessary to complete our understanding of the mechanism controlling the progression of core damage includes (a) the end-state visual characterization of the damage to the lower half of the core, the core support structures below the core, and the reactor vessel lower head, and (b) samples of the degraded core materials for studying the important physical and chemical interactions that took place during the accident and that allow closure to be made relative to the distribution of fission products.

A comprehensive Sample Acquisition and Examination Project[B-1] is under way to visually characterize the core damage via closed-circuit television and to obtain the necessary physical samples of the core materials as the core is being defueled. To provide samples from known locations of the core and lower plenum regions, a drilling unit was designed to drill through the degraded core material. The drill unit was modified using available mining/geology equipment and technology to provide (a) precise positioning over the reactor vessel; (b) a microprocessor for operational control and safety interlocks; and (c) recorded drilling parameters (torque, load, etc.). The machine drilled "core" samples approximately 2.5 in. in diameter which were enclosed in slightly larger casing tubes. The encapsulated samples were then removed from the core region. The resulting hole provided access for video inspection. The drill samples will be gamma-scanned, sectioned, and radiologically and metallurgically examined to determine fission product retention, material composition, and prior peak temperatures.

The core bore machine was used to acquire ten samples from those fuel assembly positions shown in Figure B-1. In four of the locations, drilling extended to below the core region into the core support regions. In two of these locations, the drilling and sample acquisition extended through the core support structures into the fuel debris resting on the lower reactor vessel head.

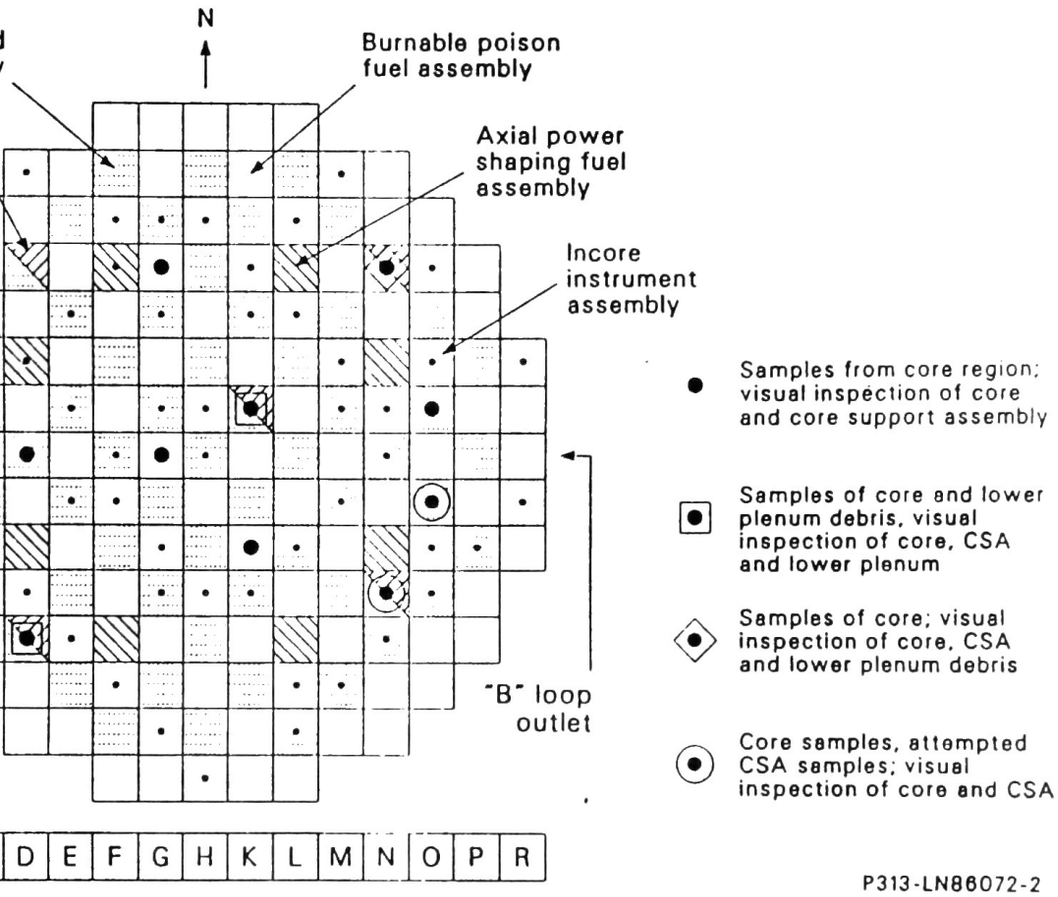

Figure B-1. TMI-2 core bore locations.

Video data characterizing each of ten drill locations, along with the data characterizing the "drillability" of each location, have provided important information for interpreting the damage conditions of the lower core and core support structures. The data have also been helpful in identifying the core damage locations and evaluating the mechanisms leading to the core degradation and fuel migration into the lower plenum. Major findings include the following:

- The central two-thirds of the lower part of the core generally consists of two distinct regions:

  (a) An upper region of previously liquified ceramic and structural materials, starting approximately 5 ft above the lower end fittings, forming a convex lens-shaped layer roughly 3 ft thick near the core center and tapering to a foot near the outer edge;

  (b) A region of intact rod stubs (in some cases, oxidized) below the previously liquified materials.

- The migration path of the previously liquified material to the lower plenum is located near the core periphery.

- There appears to be no major damage to the lower core support assembly based on the limited video data.

- The fuel debris resting on the bottom vessel head near the center of the reactor vessel appears to be loose and relatively fine compared with the larger agglomerated debris existing near the edge of the reactor vessel.

Specific implications of the core bore acquisition data relative to our understanding of the core damage progress are discussed in Reference B-2. Examination of the core bore samples will further confirm our understanding of the mechanisms controlling the core damage progression and fission product behavior during the accident.

References

et al., TMI-2 Accidednt Evaluation Program Sample
and Examination Plan, EGG-TMI-7132, January 1986.

n and P. Kuan, "Implications of the Core Bore Acquisition
Understanding of the Core Damage Progression, Light Water
ety Symposium, October 1986.

APPENDIX C

CORE DAMAGE ZONE CROSS SECTIONS

APPENDIX C

CORE DAMAGE ZONE CROSS SECTIONS

The contour data to define the interfaces between the molten region and lower intact fuel rods (shown in Figure 7 of the text), with the contour data in Appendixes C and D to define the boundar upper debris bed, allow core damage cross sections to be drawn. cross sections through fuel assembly rows B through P are presente Figures C-1 through C-13.

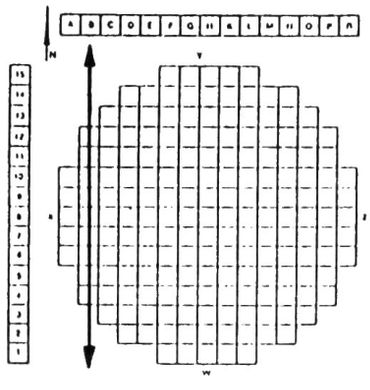

Section B

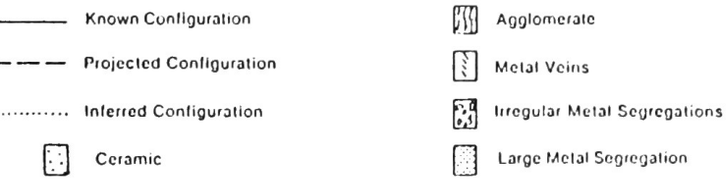

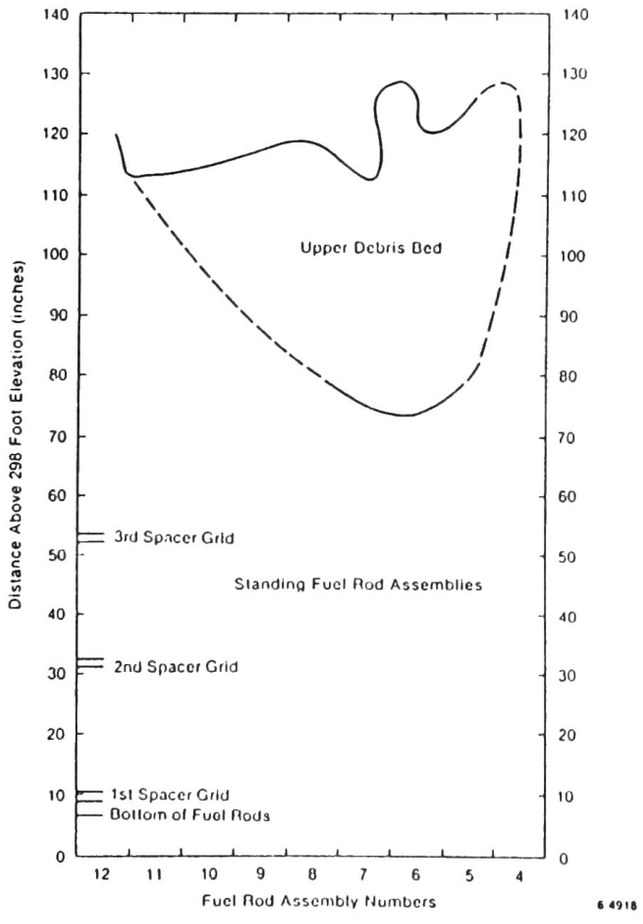

e cross section showing end-state damage configuration
ough B row of fuel assemblies.

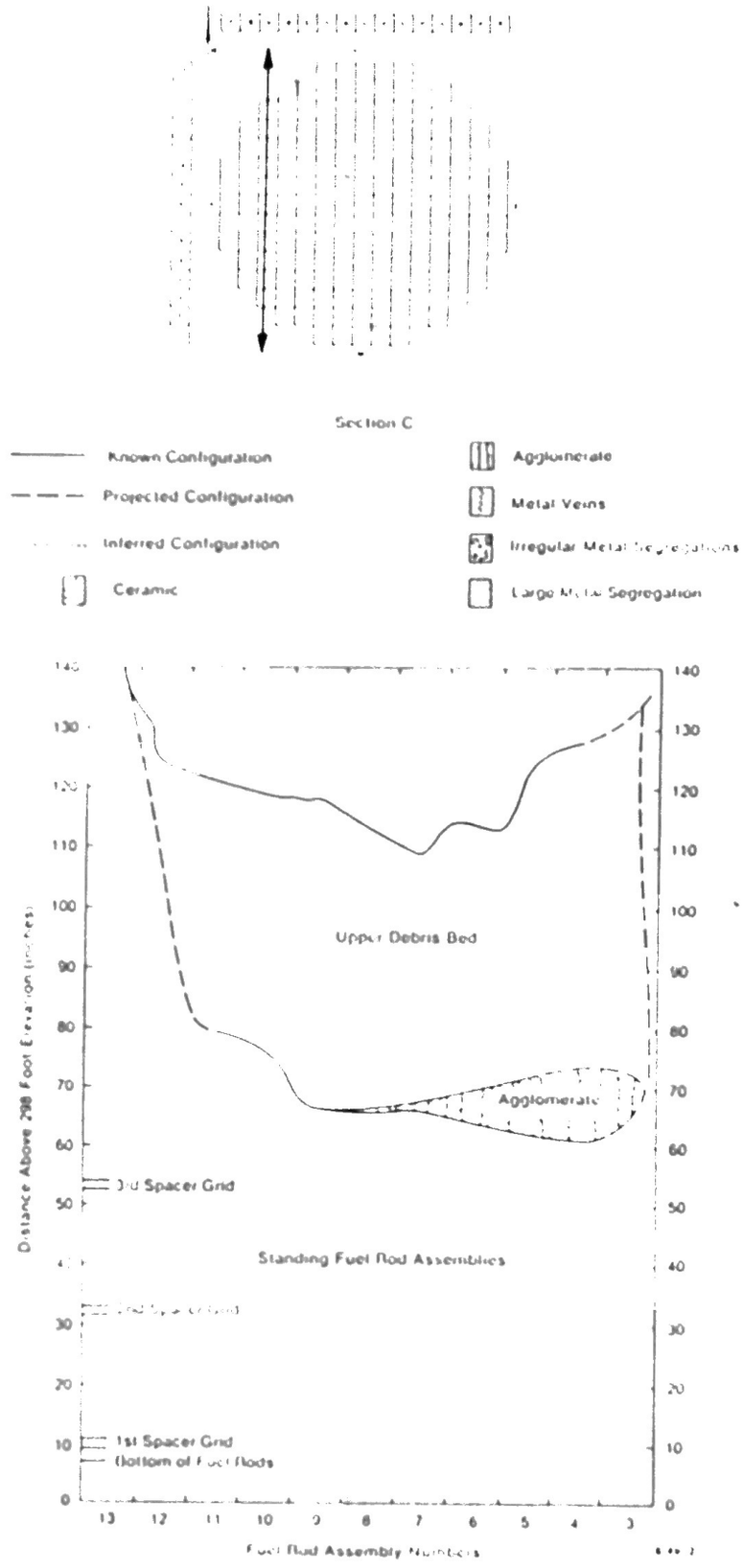

Figure C-2. Core cross section showing end-state damage configura through C row of fuel assemblies.

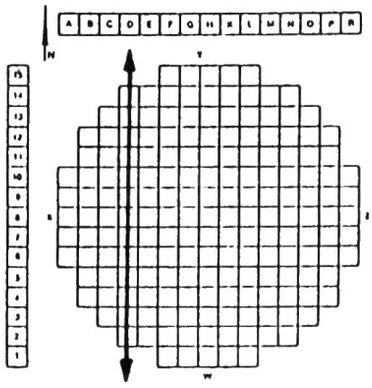

Section D

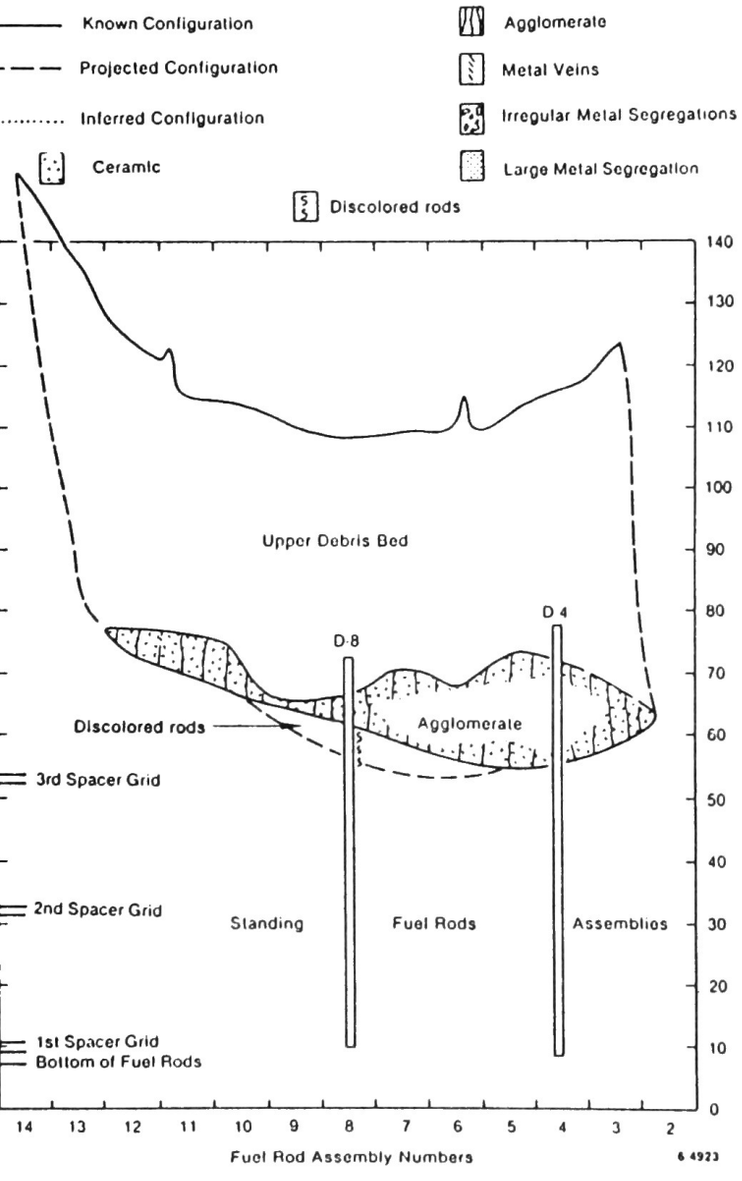

cross section showing end-state damage configuration
ugh D row of fuel assemblies.

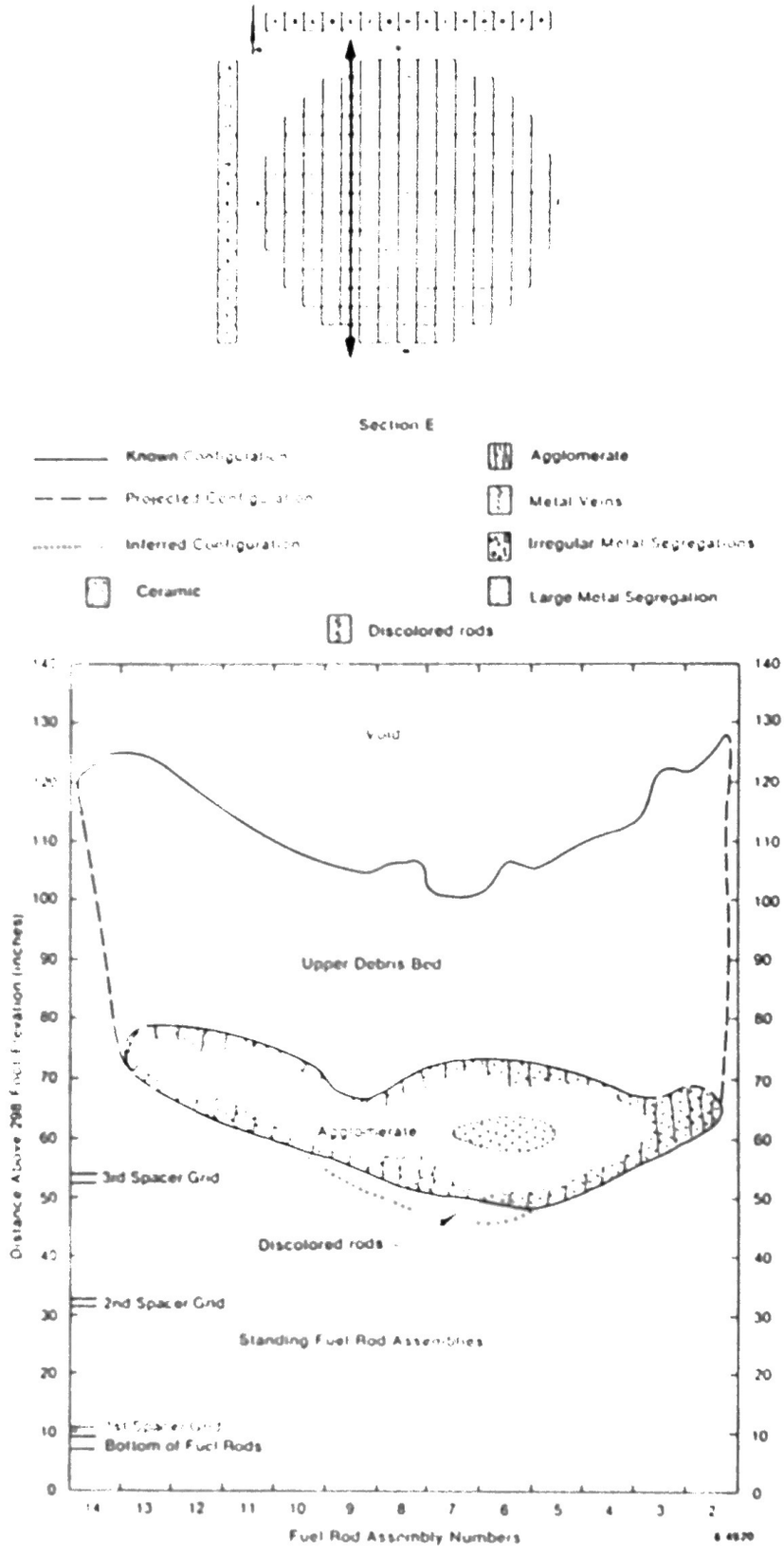

Figure C 4. Core cross section showing end-state damage configurati through E row of fuel assemblies.

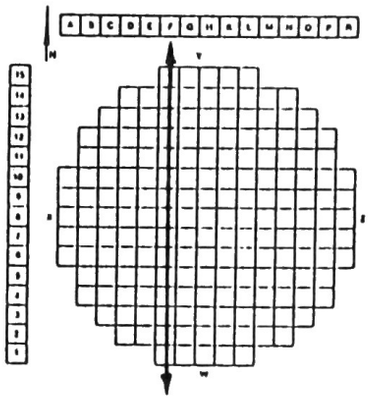

Section F

Known Configuration

Projected Configuration

Inferred Configuration

Ceramic

Agglomerate

Metal Veins

Irregular Metal Segregations

Large Metal Segregation

Discolored rods

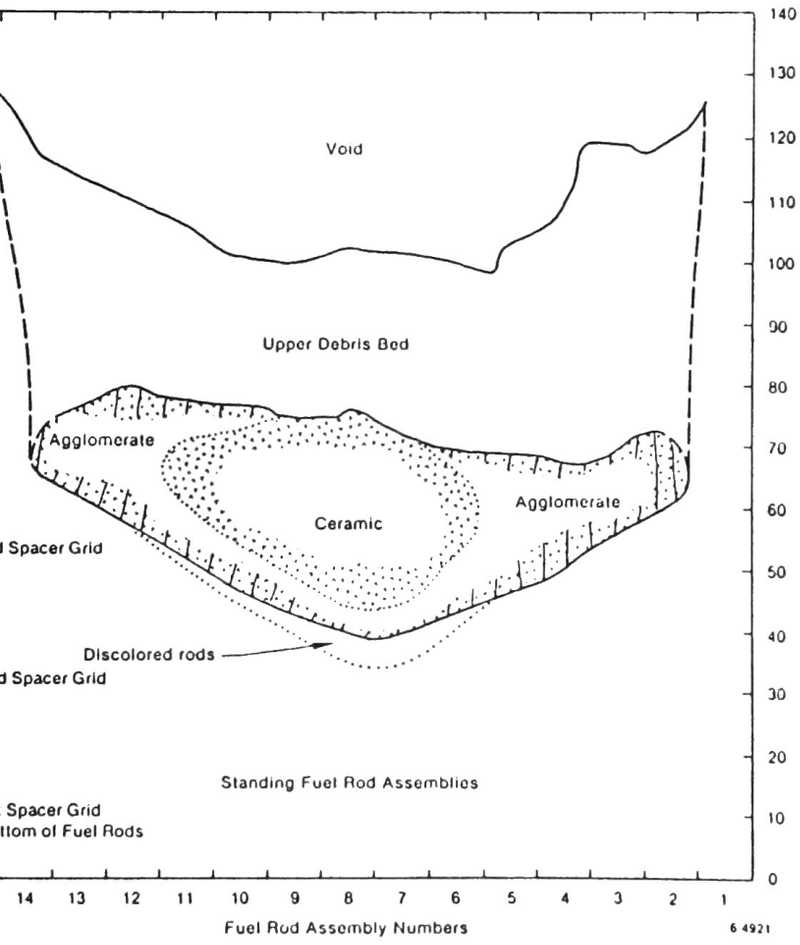

cross section showing end-state damage configuration
gh F row of fuel assemblies.

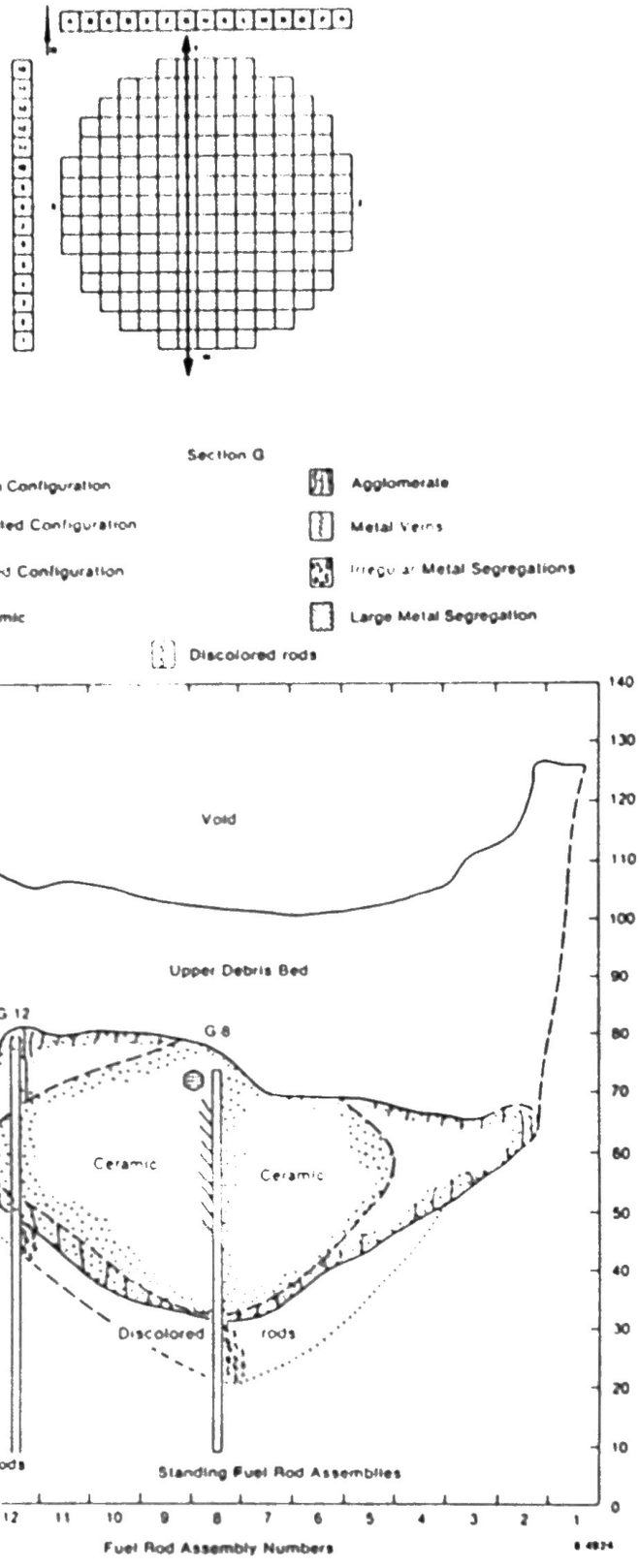

Figure C 6. Core cross section showing end-state damage configurati through G row of fuel assemblies.

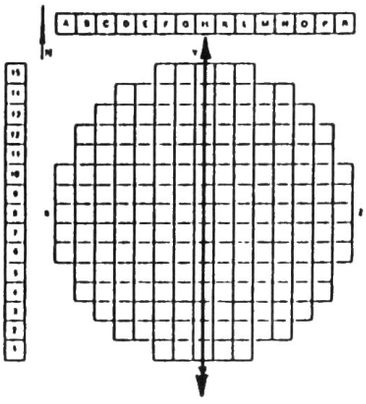

Section H

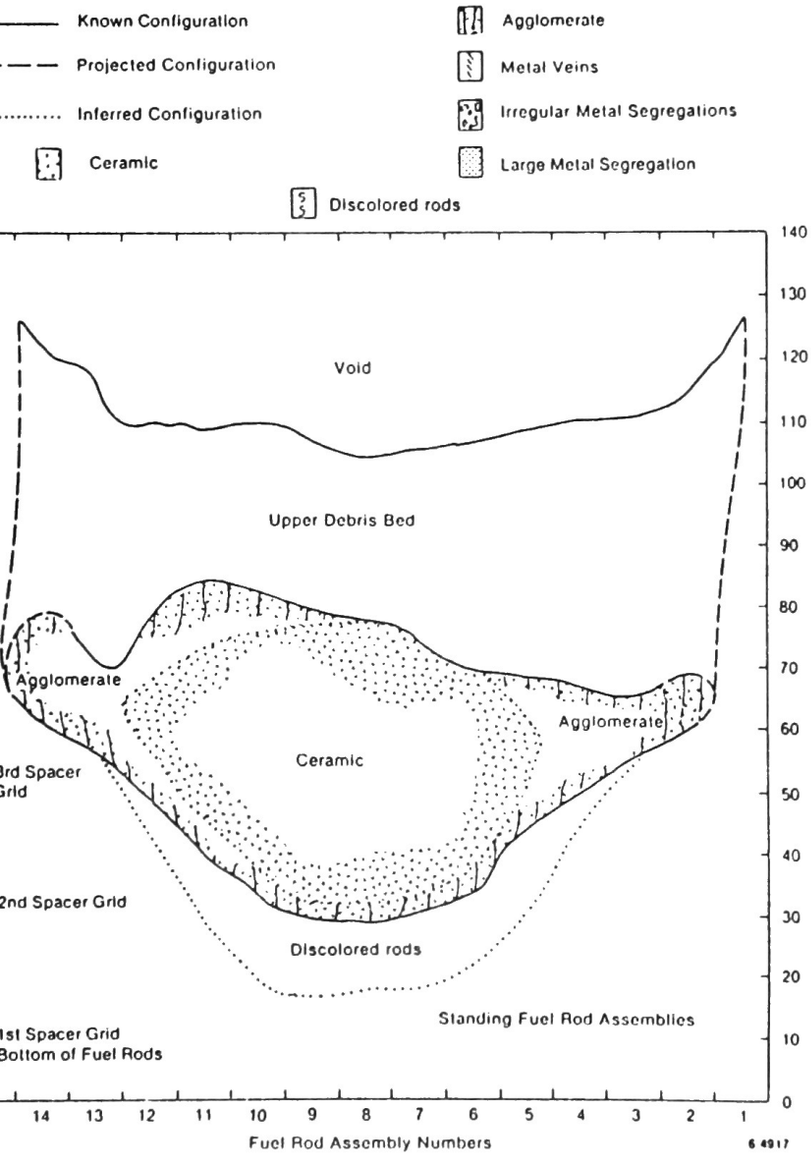

cross section showing end-state damage configuration
gh H row of fuel assemblies.

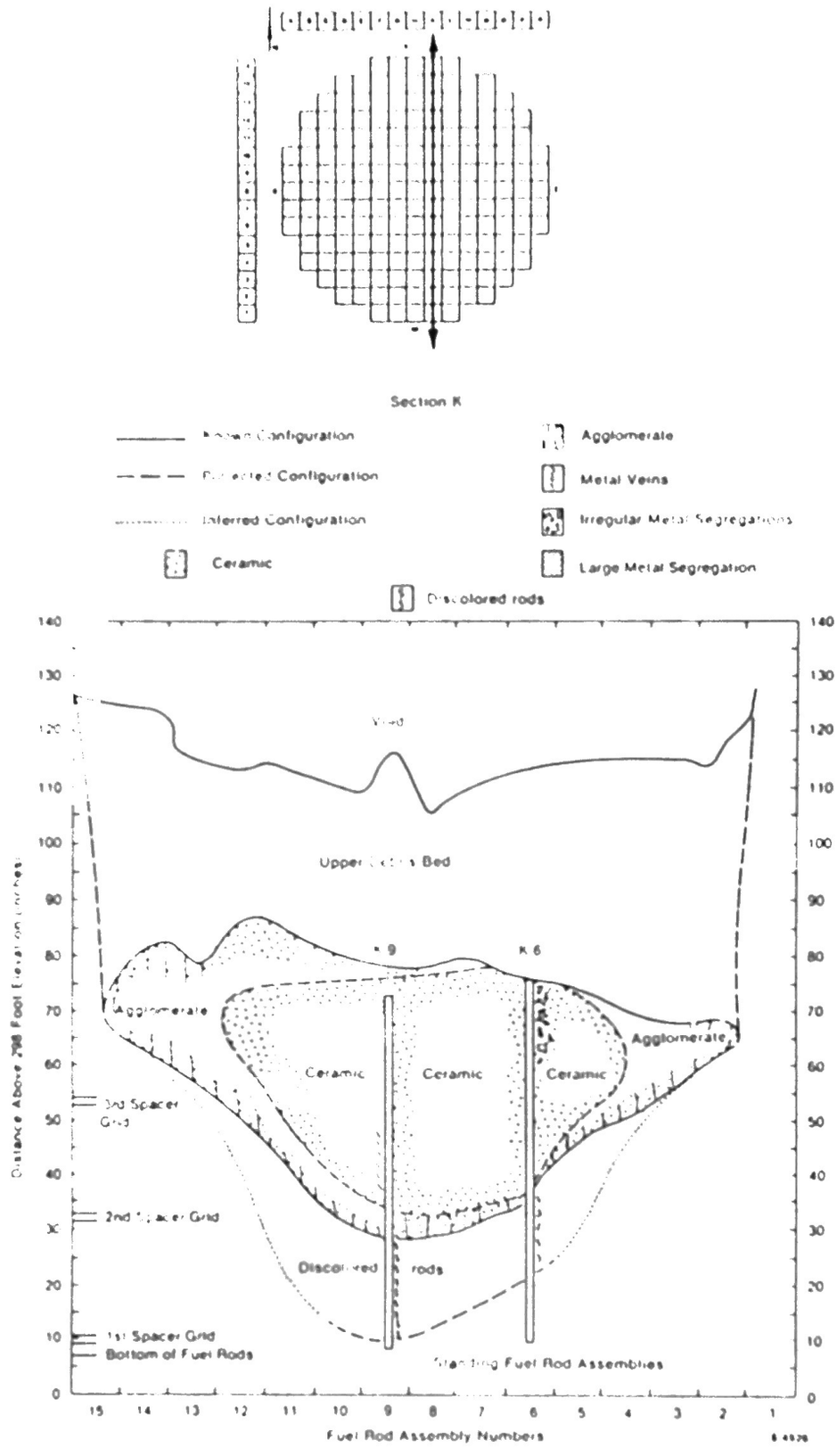

Figure C-8. Core cross section showing end-state damage configurati through K row of fuel assemblies

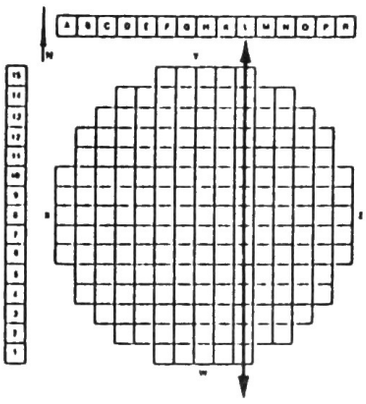

Section L

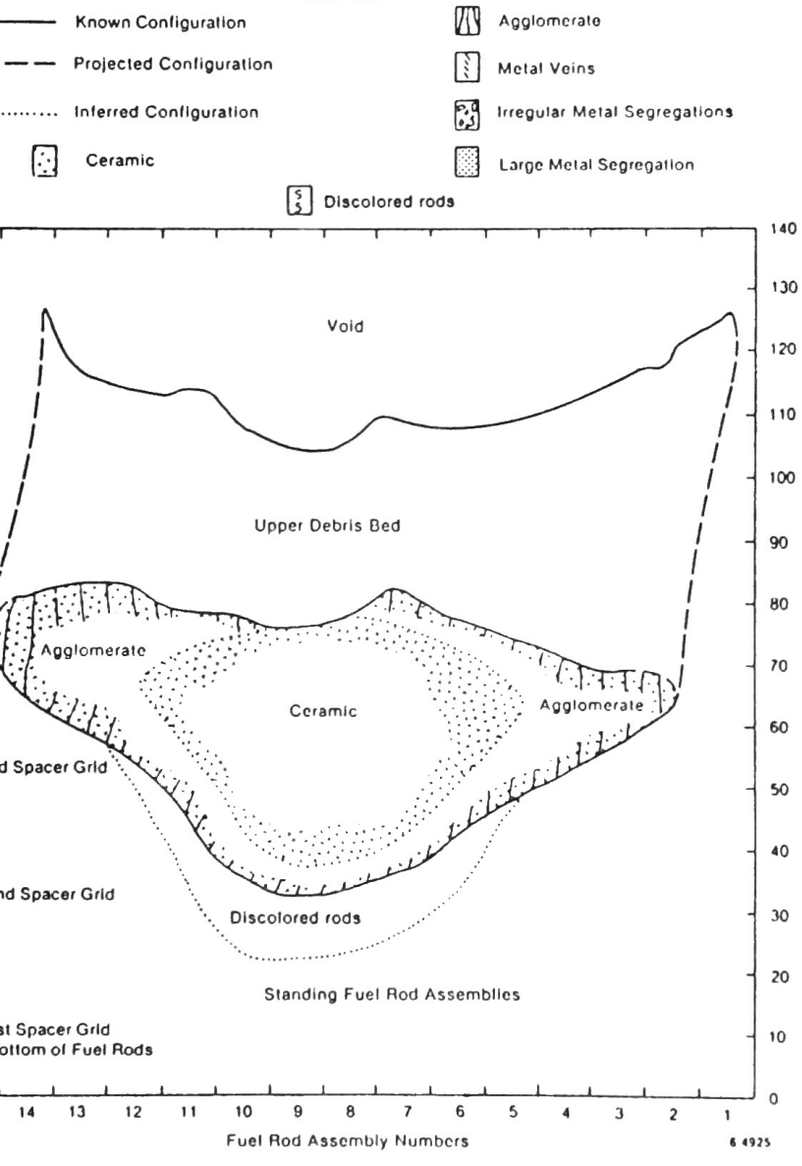

cross section showing end-state damage configuration
gh L row of fuel assemblies.

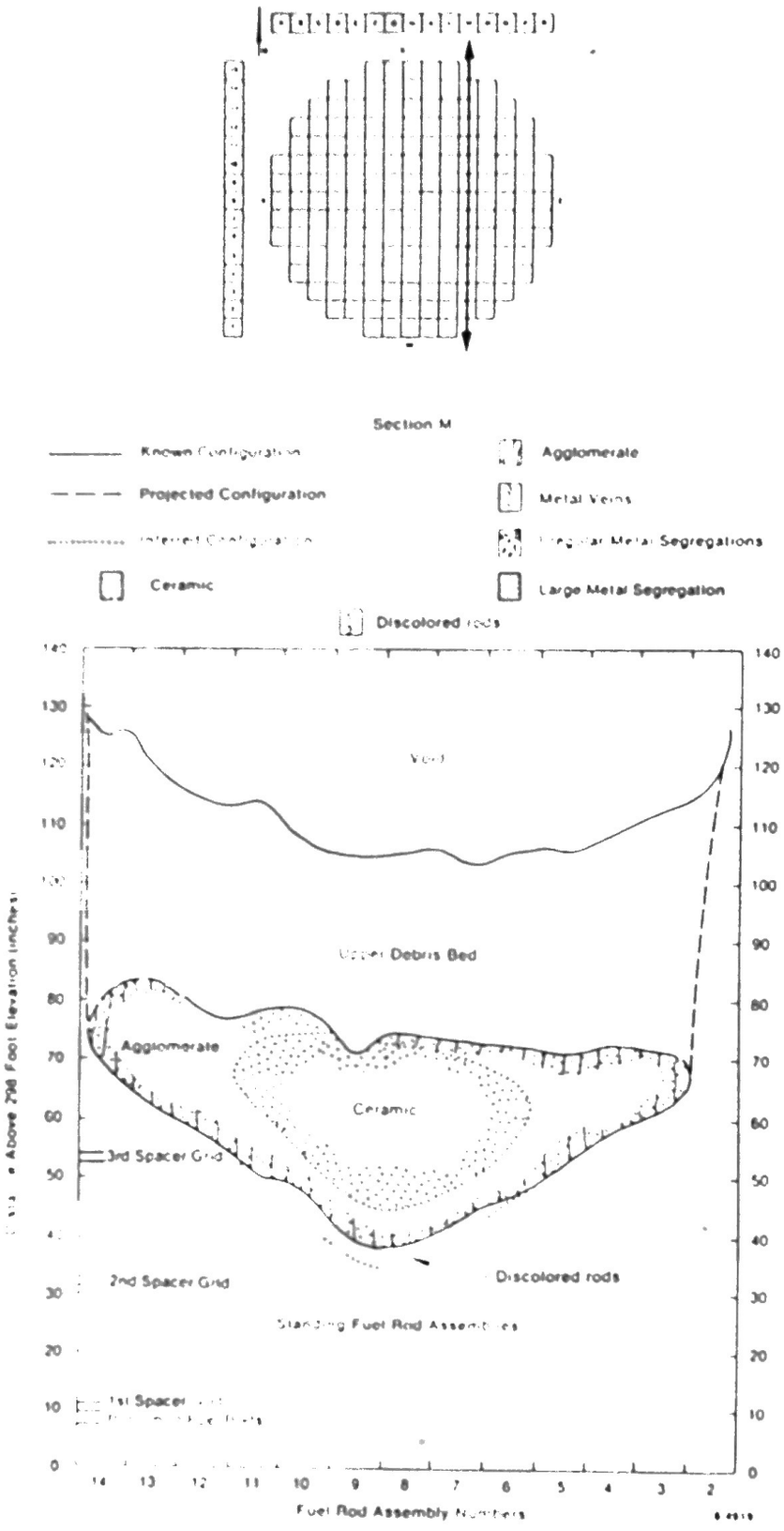

Figure C-10. Core cross section showing end-state damage configurat
through M row of fuel assemblies.

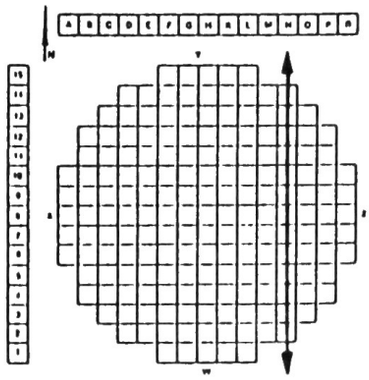

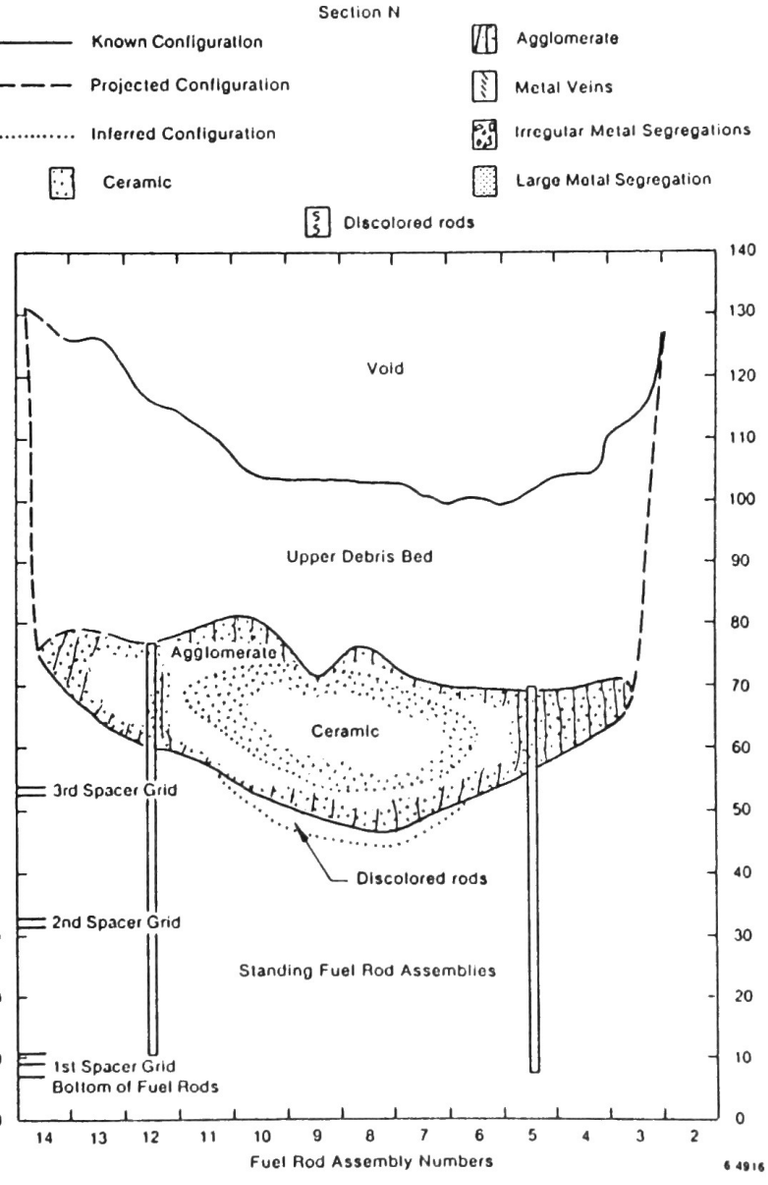

cross section showing end-state damage configuration
ugh N row of fuel assemblies.

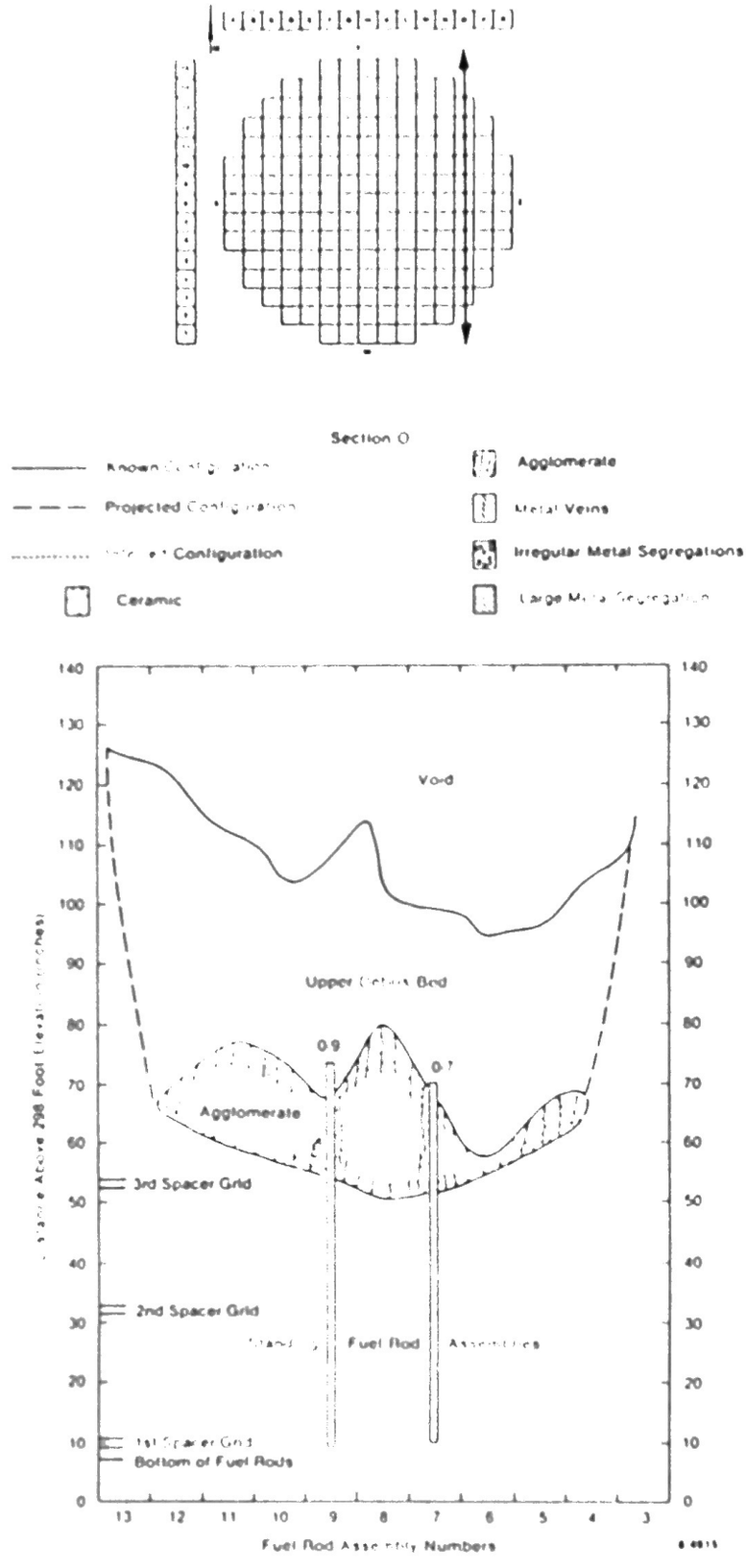

Figure C-12. Core cross section showing end-state damage configura through O row of fuel assemblies.

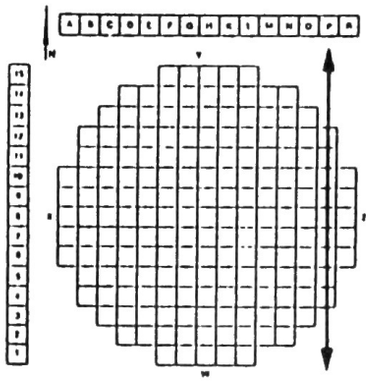

Section P

Known Configuration
Projected Configuration
Inferred Configuration
Ceramic
Agglomerate
Metal Veins
Irregular Metal Segregations
Large Metal Segregation

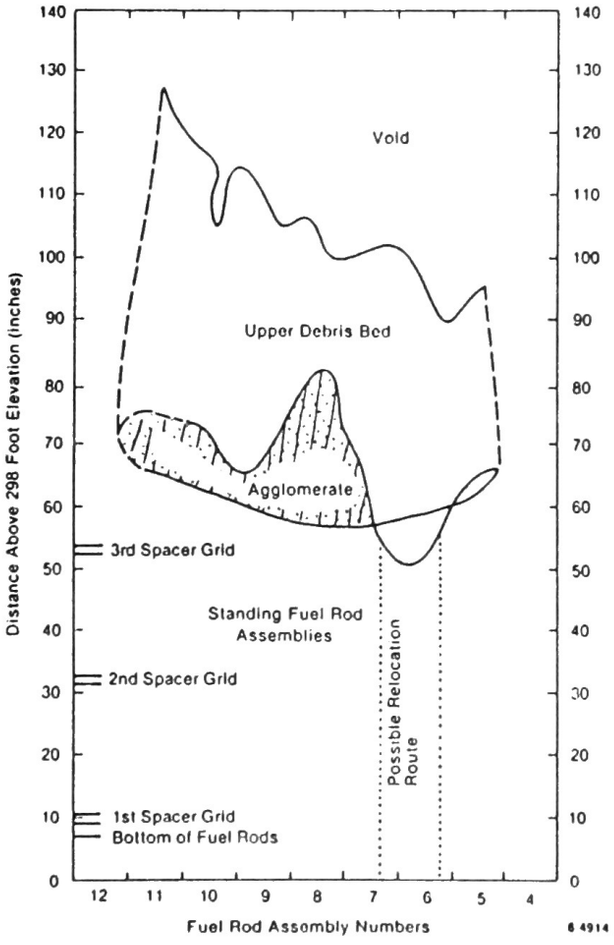

cross section showing end-state damage configuration
ugh P row of fuel assemblies.

APPENDIX D

CORE SUPPORT ASSEMBLY CONFIGURATION AND NOMENCLATURE

APPENDIX D

CORE SUPPORT ASSEMBLY CONFIGURATION AND NOMENCLATURE

The TMI-2 core support assembly configuration and nomenclatur
shown in figure D-1. The nomenclature shown in figure D-1 has be
throughout the report.

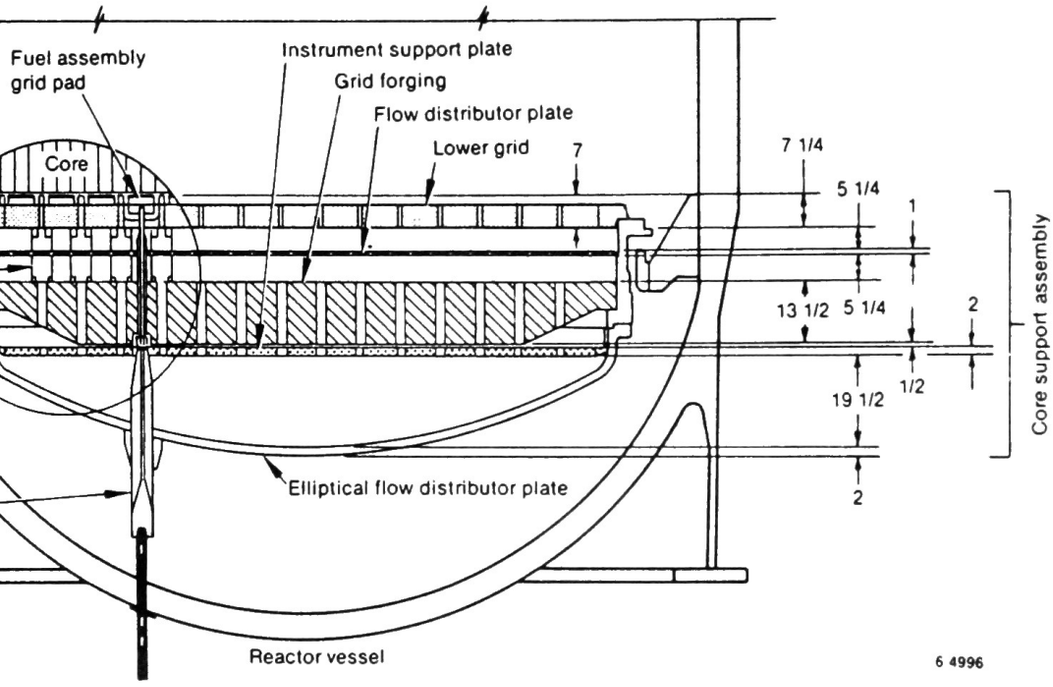

e D-1. TMI-2 Core Support Assembly configuration.

APPENDIX E

INTERPRETATION OF THE TMI-2 SOURCE RANGE MONITOR RESPON

APPENDIX E

INTERPRETATION OF THE TMI-2 SOURCE RANGE MONITOR RESPON

There were two TMI-2 source range monitors (SRMs) utilized t
the low level startup neutron flux. The SRMs were BF_3-filled pro
counters about 75 cm long and are mounted between the reactor ves
biological shield, as shown in Figure E-1. Only one detector (SR
recording continuous data (stripchart).

The SRM response data are important, since they are directly
the core and downcomer liquid levels and the configuration of the
measured output from SR NI-2 is shown in Figure E-2 for the first
TMI-2 accident.

The SR NI-2 data have been extensively analyzed via neutroni
to (a) estimate void fraction of the RCS coolant during the perio
were running (prior to 100 min) and (b) infer liquid levels in th
vessel after 100 min.[E-1] The original interpretation assumed an
core configuration. Table E-1 summarizes the original SPND inter
work (refer to Figure E-2).

More recent analyses are underway to evaluate the impact of
configuration changes (initial fuel relocation, melting and reloc
control rod materials, and global relocation of core material int
plenum) on the SRM response. These calculations show that (a) th
response is significantly affected by changes in core configurati
and control rod relocation) and (b) the accident scenario as pres
this report provides an improved interpretation of the changing SR
responses at 174 min (pump transient), 200 min (ECCS injection),
(core relocation).

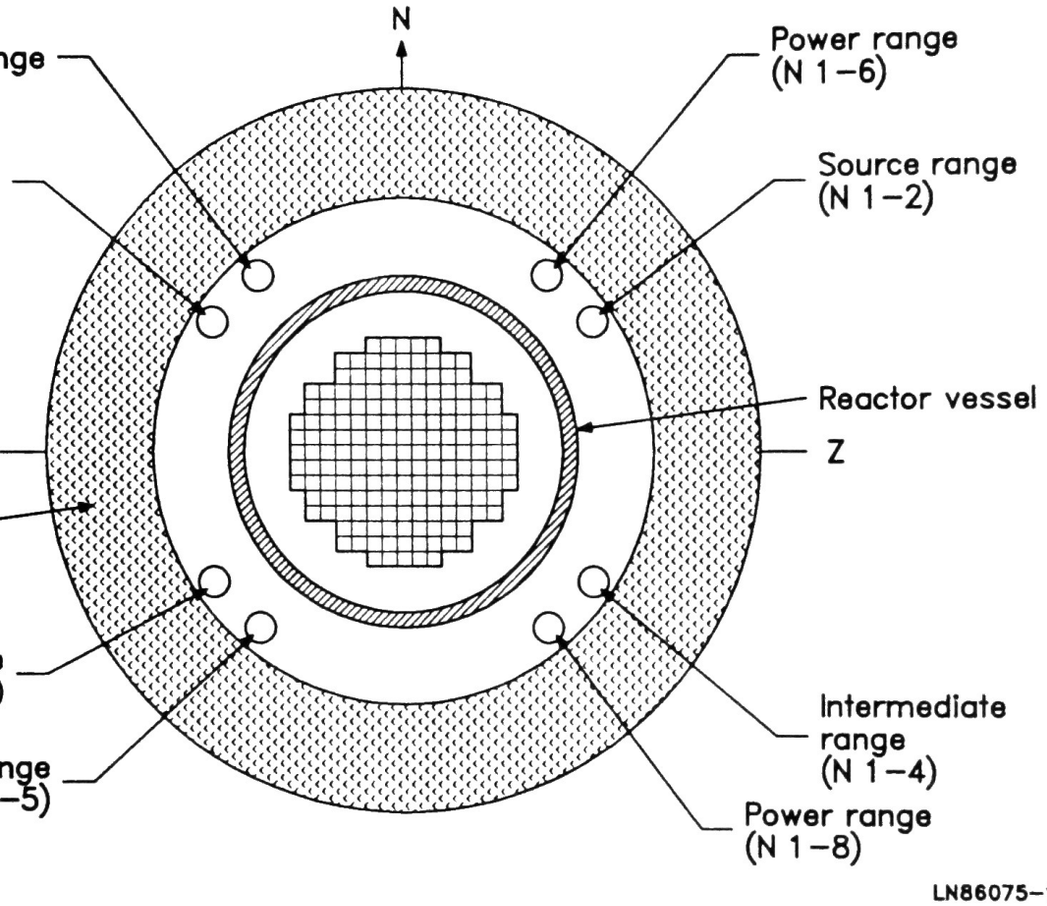

TMI-2 source, intermediate, and power range monitor configuration.

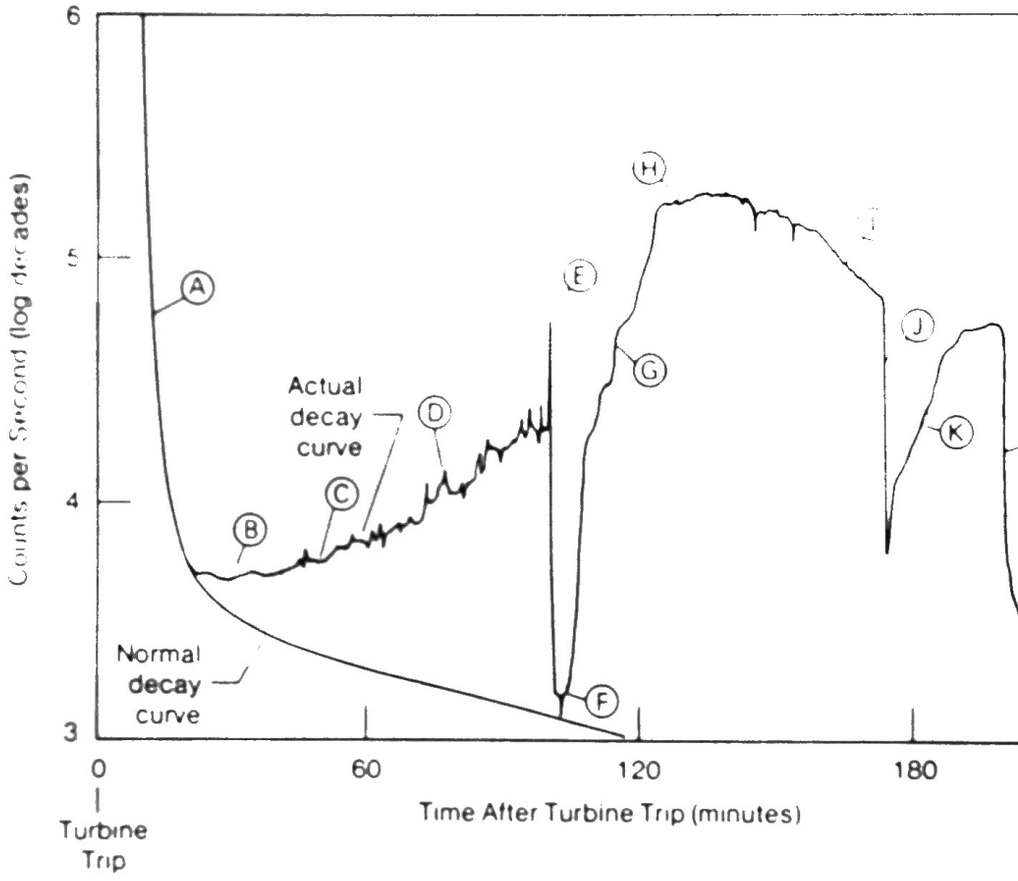

Figure E-2. TMI-2 SRM reponse during the first 4 h of th

irst 20 min, source-range instrument behavior was consistent
rmal, posttrip decay rate of about one-third decade per minute.

roximately 20 to 30 min, the source count rate should be
g through the 600 to 700-cps range. Instead, the curve
ut at about 5000 cps due to buildup of voids (steam bubbles)
wncomer and core regions. This is consistent with the fact
sure had reached saturation (approximately 6 min after turbine
net outflow through the open electromatic relief valve
to empty the system. Void formation is also consistent with
ved drop in reactor coolant flow rate because of the reduced
ead produced by two-phase flow conditions.

loss of coolant from the primary system leads to increased
nd increased detector count rates. The recording began to
oise, which is reflective of unsteady flow (pump surging) and
aration characteristic of "slug flow." This phenomenon
with time.

74 min, the B reactor pumps were secured by the operator.

n, the A reactor coolant pumps were secured. This caused a
sient and separation of voids to the upper regions of the
Voids rising to the top and coolant fill from the hot legs
a "solid" water condition seen at the detector. The detector
e abruptly dropped.

um count rate is suggestive of the fact that the downcomer
el was at or near the top of the active core level.

release of fluid out of the relief valve began to boil off
from the core and downcomer area. Makeup flow, assumed to be
ighborhood of 140 gpm, was not sufficient to maintain
water level. The core mixture came within better view of the
as the water levels dropped; the count rate increased.

l level continued to increase but at a slower rate as
variations began to be counterbalanced by the loss of neutron
.e., UO_2 being removed from the core region). In this
so, the rate of uncovery is believed to have slowed somewhat
oil-off tended to equilibrate with a relatively unchanging
ow rate.

period, the count rate was decreasing as the loss of neutron
d reduced neutron multiplication became predominant. The
nd in detector count rate can be interpreted either as core
continued uncovery. However, the weight of evidence from
ow estimates and other core instrumentation suggests that the
g count rate was in response to continued core uncovery.

TABLE E-1. (continued)

J.	The operator started reactor coolant pump 2B, sending a s water into the downcomer and essentially filling it.
K	Loop flow data indicate that the pump worked effectively brief period. This is corroborated by the abrupt turn-ar source range detector trace, as flow ceased and excess do moved into the core and was boiled off; equilibrium level re-established.
L.	High pressure injection flow was initiated at 200 min, 8 electromatic relief block valve was opened by the operato passed into the downcomer, filling it. Detector count ra sharply.
M.	Continued addition of high pressure injection flow began core. It is conjectured that the coolant first re-wetted region of the core, bypassing the hot center.
N.	Water entering the core eventually led to an unstable the condition. It is speculated that major portions of the c may have been suddenly quenched with a resulting large am coolant flashing to steam, accompanied by possible core a rearrangement. The jump in detector counts may be due to displacement of fuel and/or sustained voiding of peripher regions.

Reference

Interpretation of TMI-2 Instrument Data, Nuclear Safety
enter (NSAC), Electric Power Research Institute (EPRI), Palo
March 1980.

APPENDIX F

IN-CORE INSTRUMENT CONFIGURATION

APPENDIX F

IN-CORE INSTRUMENT CONFIGURATION

The nuclear core of the IMI-2 reactor (3.66 m long x 3.20 m diameter) contains 177 fuel bundles. There are a total of 52 in assemblies throughout the core, as shown in Figure F-1. Each as contains seven self powered neutron detectors (SPNDs), one gamma-compensating background detector, and one Type K core exit thermocouple with all leads exiting out the bottom. Figure F-2 cross section of an individual instrument assembly. The seven S spaced axially about .52 m apart along the active length of the Level 1 transducer is 0.270 m above the bottom, and the Level 7 is 0.273 m below the top of the active core (see Figure F-3).

Figure F-4 illustrates the cross section of the active segm typical SPND. An individual SPND consists of:

- A rhodium emitter, 4.57×10^{-4} m diameter x 0.121 m lo
- Alumina insulation (99.75% pure)
- A zircaloy-2 center conductor lead wire, 2.79×10^{-4} m diameter x 39.01 m long
- An Inconel 600 oversheath 1.59×10^{-3} m OD x 1.08×10 x 39.01 m long

The eighth element of the spool is the gamma-compensating s is identical to the SPND except that is does not have the neutro rhodium emitter

The ninth element of the thimble is a Type K chromel-alumel thermocouple which has alumina insulation and an Inconel 600 out

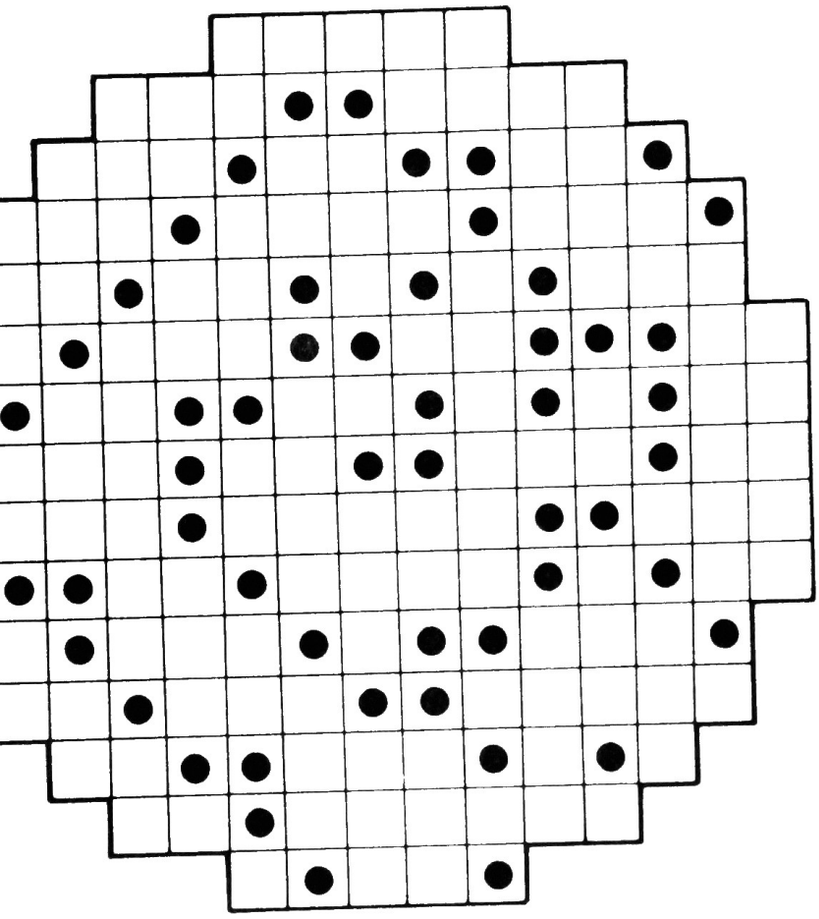

Figure F-1. TMI-2 core map.

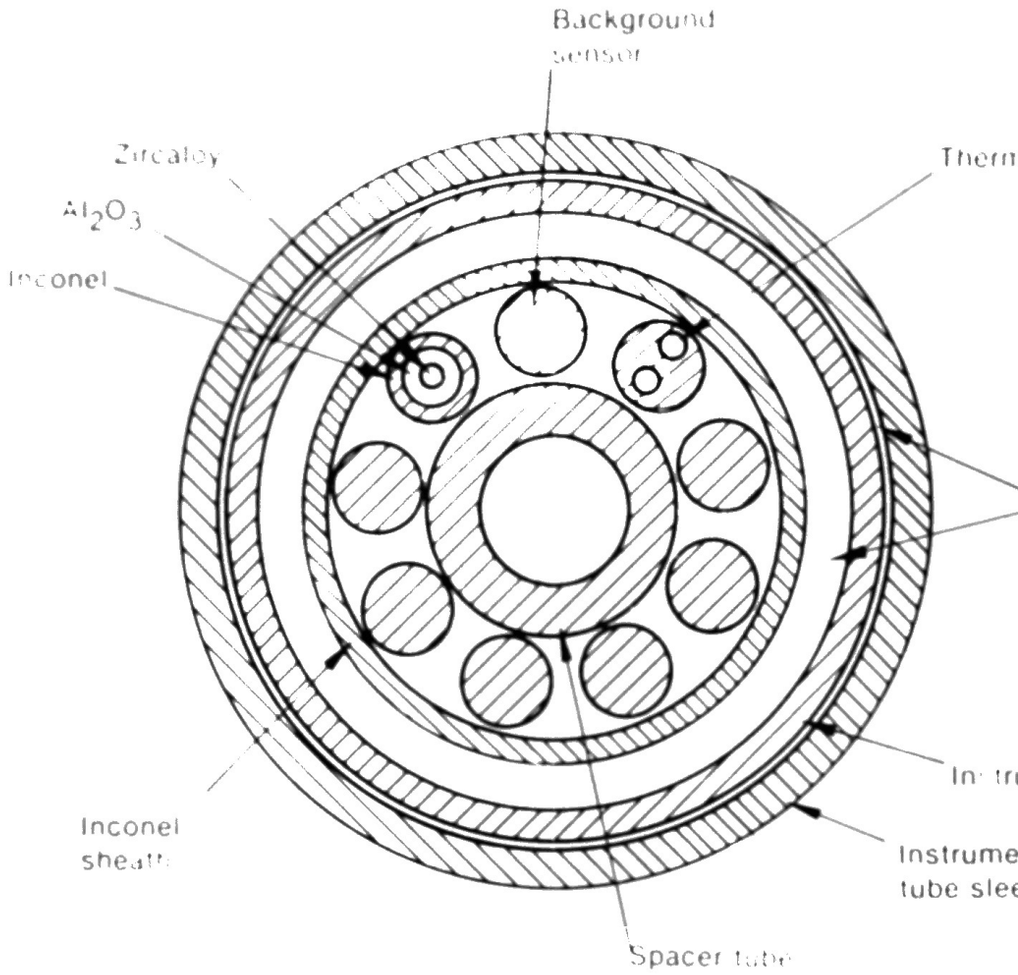

Figure F-2 Cross section of Individual IMI-2 Instrument

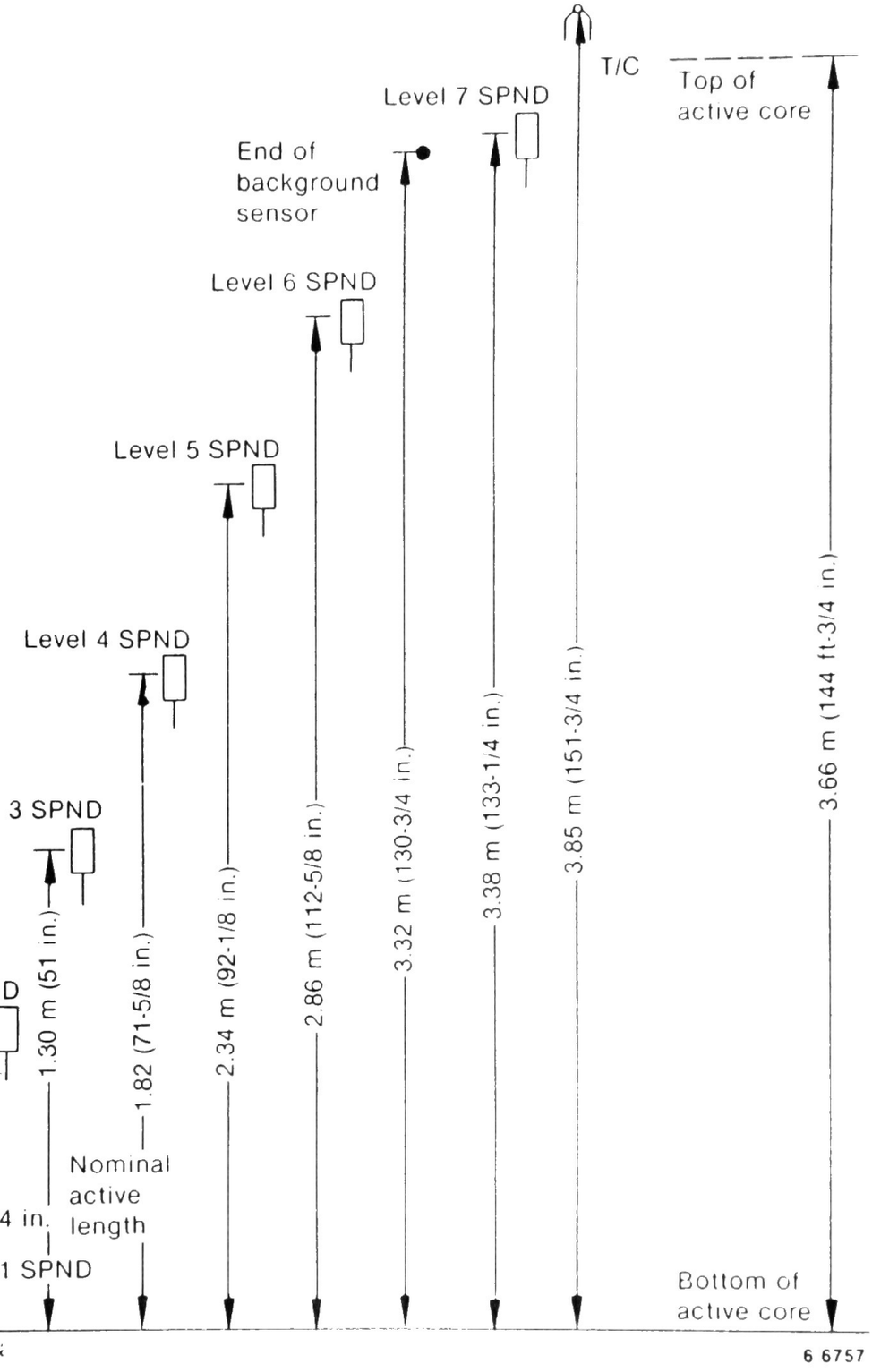

F-3. Axial configuration of TMI-2 in-core instruments.

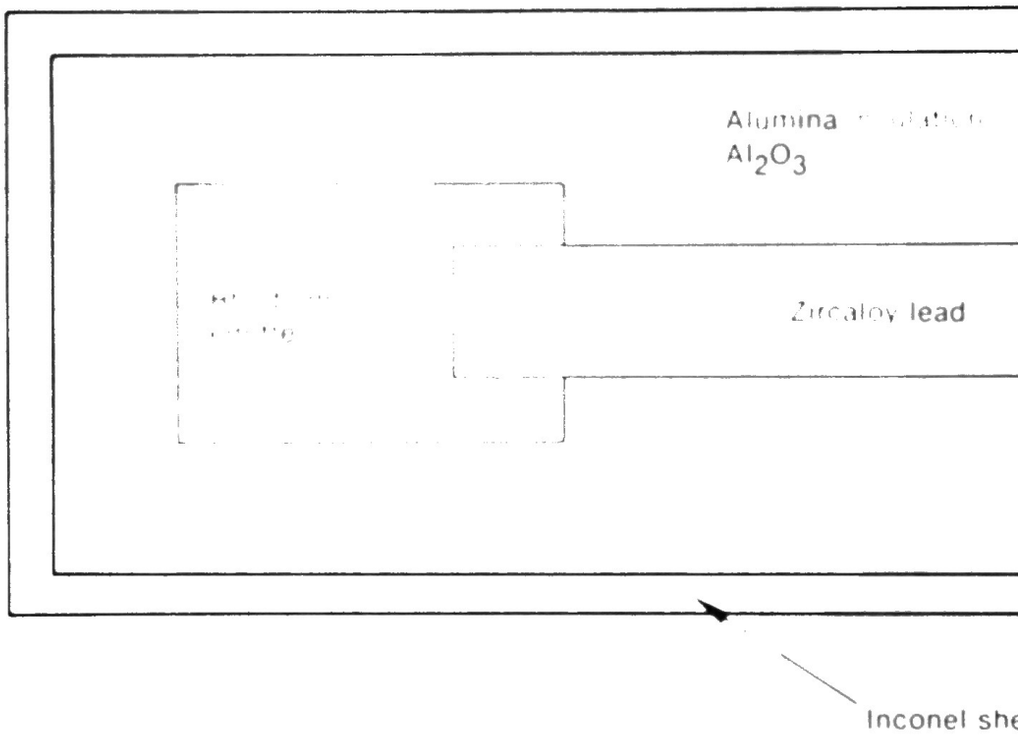

Figure F-4. Cross section of the active end of a typical IMI-2 neutron detector.

nent assembly is routed up through the core from the bottom
vessel. This routing scheme is very important in
e accident sequence through the in-core instrumentation

ata sources include the following:

lant computer output SPND data during the first day of the
ent (28 March 1979)

lant computer output SPND data of 30 March 1979

ackup multipoint recorders which monitored 36 selected SPNDs

and background detector resistances measured by Warren in
1979

background detector, and thermocouple resistances measured
ncey in 1981

s briefly discussed below.

Plant Computer Data Sources, 28 March 1979

computer system at TMI-2 used a Bailey 855 computer linked
NOVA computer to form an integral system. The principal
computer system was to monitor plant parameters
3000) and to display them along with any related calculations.

ermanent computer record of the in-core instrumentation was a
n two plant printers, the utility and the alarm. They are
printers; if either fails, its output is automatically
the other. The utility printer writes data only when
alarm printer writes data when an unusual occurrence has
as a parameters exceeding an alarm setpoint or changing

states. For the SPNDs, it printed a status report only when t
changed from on-scale to off-scale or when it returned to on-s
signal setpoint limits for being off scale were currents less
and greater than 2000 nA. The computer would interrogate each
SPNDs once each minute; and, if the instrument had changed sta
previous time, it would print an alarm. The magnitude and pol
signal were printed when the SPND alarmed on-scale, and a seri
questions marks was printed when it alarmed off-scale.

The TMI-2 accident started at about 4 a.m. on 28 March 19
74 min into the accident, there were no alarms from the in-cor
except for one thermocouple reading which was thought to be sp
data queue was waiting to be printed on the alarm hard-copy un
there was considerable automatic activity in the plant. The l
queue of data waiting to be printed increased, so that at 167
accident the alarm printer was about 93 min late. At this poi
contents of the memory buffer in the computer were erased beca
operators needed timely information. Thus, all of the alarm d
167 min after turbine trip were irretrievably lost. The initi
and uncovery occurred during this time interval.

Plant Computer Data Sources, 30 March 1979

On 30 March 1979, the SPND computer program was modified
sign and magnitude of the generated signals could be recorded.
from each of the 364 SPNDs and 52 background detectors were re
alarm printer. The results were:

- 305 SPNDs (83.8%) were generating negative currents
  to -2000 nA
- 30 SPNDs (8.2%) were producing no currents
- 29 SPNDs (8%) were producing positive signals in the
  2000 nA

Backup Multipoint Recorders

ion to the plant computer, 36 selected SPNDs were monitored on
ltipoint recorders (18 channels on each recorder). These two
tained SPND data taken during the time interval in which the
were lost. Only three (2, 4, and 6 levels) of the seven SPND
ecorded on the multipoint recorders.

oint for each channel was printed every 2.5 min (24 per hour).
ntification number was printed adjacent to its data point once
4 data points). This method of recording proved to be
ring the accident, because the channel identification number
associated easily with the printed data point. Because of this
SPND multipoint recording data were not used for the initial
he TMI-2 accident. Recently most of the strip chart data on
er No. 1 have been decoded, tabulated, and placed in a data
Recorder No. 1 could be decoded because the data points of the
annels had a distinctive and characteristic shape which allowed
n of individual data channels. Backup Recorder No. 2 could not
cause the pens were not inking properly.

up multichannel recorder data show that just before the
n the reactor at 97% power, the SPND signals ranged between
nA. At the start of the accident, the reactor was scrammed.
onded with their signals dropping to a few nanoamps after
The first anomalous signals were produced 135 min into the
at least two SPND channels went negative (currents less than
e first backup recorder. Beginning at 155 min into the
t of the SPND signal channels became positive, some in excess

In-Core Instrument Resistance Measurements

ren and Yancey have measured the resistance of the in-core
and these resistance measurements were used to diagnose the end

state of the SPNDs. A high resistance (R greater than 10^8 ohm
an intact or operational SPND, whereas a low resistance (R le
10^5 ohms) indicated a failed SPND

APPENDIX G

SCDAP CODE FEATURES

APPENDIX G

SCDAP CODE FEATURES

SCDAP has been developed under the sponsorship of the U
Regulatory Commission, Office of Nuclear Regulatory Research
designed to model the progression of damage in single fuel p
rods, experimental bundles, or full reactor cores. The code
to help understand the phenomena that control core behavior d
accident, to help quantify uncertainties in risk assessment a
support planning and interpretation of severe fuel damage exp

The first version of the code, SCDAP/MOD0, was completed
1982. Assessment of SCDAP/MOD0 and subsequent versions of th
demonstrated its ability to accurately simulate the early pha
progression in small integral experiments. The TMI-2 analysi
important step in assessing SCDAP models for a full reactor e

Table G-1 contains a brief description of the important
considered in the analysis. The table also briefly defines h
the models representing those phenomena have been assessed.
models in SCDAP are based upon models that were developed ove
decade as part of the design basis accident research. Models
phenomena such as core hydrodynamics, core radiation, heat co
fuel rods, and zircaloy cladding deformation have been thorou
for design basis accident conditions (relatively intact geome
ballooning and rupture and temperatures below 1477 K). Other
treating phenomena such as control rod behavior, high tempera
liquefaction and relocation of core materials, and fragmentat
from the quench of embrittled materials have been developed s
accident and have limited assessment.

Although the experiments necessary to fully quantify the
in SCDAP calculations are still underway, limited code-to-dat
have shown the following results. Fuel rod temperatures, oxi

friction factors and fluid volumes. Changes in fluid properties due to hydrogen addition are considered. SCDAP includes both a detailed, two-fluid, nonequilibrium model taken from TRAC-BD1 and a simplified quasi-equilibrium drift flux model based on an approach proposed by Sun. The simplified model, which has shown good agreement with experimental and detailed model results for boil-off conditions, was used in current analysis.

Radiation heat transfer

Both surface-to-surface and surface-to-coolant radiation is considered. Radiation within representative bundles is modeled using detailed surface network exchange with absorption by the coolant. The bundle radiation model was taken from TRAC-BD1 and has been shown to give good agreement with experimental results.

Loss of bundle geometry

Loss of bundle geometry due to both extensive liquefaction and relocation or quench-induced fragmentation on an individual (representative) bundle component basis is modeled. However, once damage becomes extensive at a given elevation in the bundle, subsequent behavior for that portion of the bundle is modeled using SCDAP debris models based upon porous body representations. Because these models have not been assessed against experimental results, the SCRAP debris models were not used in this analysis.

Fuel rod behavior:

Nuclear heat generation

For this analysis, the decay heat was computed using the ANS 5.1 model including corrections for actinides, release of volatile fission products, and fuel relocation. The prior operating history, which is also used to establish the initial fission product inventory, was taken from Reference 16. This basic model has been extensively assessed, although assessment of corrections due to fission product release and fuel relocation is limited.

Oxidation

Oxidation of the zircaloy cladding is modeled using Cathcard-Pawel (<1850 K) and Urbanic parabolic rate equations. Oxidation limiting processes modeled include steam starvation, hydrogen blanketing (based on the work of Chung), zircaloy consumption, and freezing of external crusts. Oxidation of liquefied Zr-U-O mixtures is included, assuming zircaloy kinetics are applicable. Oxidation kinetics below the melting temperature of zircaloy are well established. Experimental data on Zr-U-O or molten zircaloy are nonexistent.

Heat conduction

Radial heat conduction from the fuel to cladding is modeled using a finite elements approach. The effects of burnup, fuel axial and radial relocation, in-situ liquefaction, chemical reactions, and cladding deformation are included. Applicability of the finite element approach is well established. Models to treat burnup, etc., have been qualified through comparisons to the FRAPCON and FRAP-T codes.

Cladding deformation

Cladding deformation is based on both models developed as part of the FRAP-T code. Both models use strain rate dependent cladding constitutive equations. The ballooning model uses cladding anisotropic material properties. These models are based upon first principles and have undergone extensive assessment as part of FRAP-T.

Fission product release

The release from the UO_2 matrix is based on the PARAGRASS model developed at ANL which has undergone extensive assessment as a stand-alone code and as subcodes in FRAP-T and FRAPCON. The PARAGRASS model has been modified by ANL to treat both noncondensible and volatile fission products and release enhancement mechanisms associated with UO_2 dissolution or fragmentation. The release from the gap to the coolant is based on the experiments of Lorenz and includes the identification of the chemical form of the fission products. The treatment of volatile fission products, release enhancement, and chemical forms has undergone only limited assessment.

TABLE G-1. (continued)

Effect	Comment
Liquefaction and relocation	Melting of zircaloy, dissolution of UO_2 by molten zircaloy, breach of an outer ZrO_2 layer by the liquefied material, and relocation of liquefied mixtures are modeled. The changes in material properties due to changes in mixture composition due to oxidation and Zr-U interaction are considered. Oxidation of flowing Zr-U-O mixtures and frozen crusts is considered. Axial relocation of solid UO_2 due to ballooning or void formation is considered. Comparison of this model with the limited data currently available indicates that this model tends to underpredict the amount of UO_2 that relocates due to zircaloy melting.
Fragmentation	Fragmentation of the UO_2 and cladding is based on the embrittlement criteria of Kassner and Chung in conjunction with thermal-hydraulic calculation of quench front movement. The debris formed is assumed to have a size distribution based on in-pile experiments resulting in fuel fragmentation. Comparison with the limited experimental data indicates that both the embrittlement criteria and particle size distributions that were established from design basis accident conditions are inadequate for more severe conditions. These results indicate that assuming the fuel rod shatters when the cladding is embrittled may, in many cases, be incorrect.
Control rod behavior:[a]	
Oxidation	Oxidation of both zircaloy guide tubes and stainless steel cladding is modeled using parabolic rate equations including the limiting processes described above.
Heat conduction	Same as above for fuel rod except that irradiation and deformation effects are not considered.
Liquefaction and relocation	Separate melting and relocation of absorber, stainless steel cladding, and zircaloy guide tubes is modeled.

a. No data currently exist for LWR conditions other than TMI.

uction rates, ballooning and rupture, noble fission gas
the onset and location of Zr-U-O_2 liquefaction and freezing
icted for a "TMI-like" heatup up through zircaloy melting at
ve 2200 K or once the fuel rods are quenched, the degree of
agreement is uncertain because of increasing scatter in the
, the release of noble fission gases during cooldown, the
dissolved or disintegrated following zircaloy melting, and
flow channel blockage are underpredicted by the code. The
on of the preceding processes is due in part to lack of
models to accurately describe the disintegration of UO_2 by
oy. Experiments and analyses necessary to remove these
re underway.